UPPER LIMITS ON

NEUTRAL ASSOCIATED PHOTOPRODUCTION

CROSS SECTIONS

Thesis by

Donald Gerald Coyne

In Partial Fulfillment of the Requirements

For the Degree of

Doctor of Philosophy

California Institute of Technology
Pasadena, California

1967

(Submitted 4 October, 1966)

ACKNOWLEDGMENTS

My wife, Lelia, in spite of the pressures of her own gradu-
ate career, was able to give me much support and encouragement,
for which I am greatly indebted.

Dr. J. H. Mullins was the director of research and my
advisor for this experiment, doing a superb job of treading the thin
line between dominance and neglect of his neophyte. I want to thank
him especially for serving me as a fine example of the balance be-
tween intuitive and quantitative thought that should characterize a
physicist.

My colleague in the Bubble Chamber group was Dr. L. J.
Fretwell, Jr. His efforts in pioneering most of our techniques and
willingness to pass on the information about them have made my task
incalculably simpler. For this and his personal friendship I am
grateful.

Dr. R. L. Walker was Deputy Director of the laboratory
during most of my tenure. His constant support in the face of early
setbacks, and his patience with an incredible time scale, have been
of great value to me. He also aided me by suggesting the area of
study eventually leading to this experiment.

Besides Dr. Mullins, my directors and instructors in the
early days of this project were Drs. J. M. Teem and E. D. Alyea, Jr.,
who exemplified the enthusiasm that this field can generate in those
who want it.

willingness to assume and discharge responsibility as needed lightened my burden considerably. The compatability of diverse personalities in our group attests to her skill of organization.

I would like also to thank the other members of the permanent nucleus of our scanning group. Mrs. Marcia Morris and Messrs. Fred Beuger and Percy Anderson contributed large amounts of scanning, as well as cooperating in other side projects. Mrs. Judith Tincher and Mr. William Peterson were our measurement specialists, and each processed the entirety of the data. The latter individual was also very helpful with computer checkouts and various calculations, as was Mrs. Betty Berzens.

The major side project referred to above was a utilization of the multiple scattering information for momentum determination. This project was coordinated by Mrs. Phyllis Nilsson, who constructed the entire computer analysis thereof. She was also of aid in various computer-related projects.

The huge amount of help with formal details, contributed by Mrs. Beatrice Hall and Miss Cherry Carter throughout my stay, and by my typists Miss Bette Brent and Miss Yvonne Dawson, is completely appreciated.

To my friends:

"...So we'll go no more a'roving

    so late into the night,

    though the heart be still as loving

    and the moon be still as bright...."

ABSTRACT

A search for events of the type $\gamma + n \rightarrow K^0 + \Lambda^0$ or $\gamma + n \rightarrow K^0 + \Sigma^0$ has been made. Photon energies up to 1530 MeV were available. The technique used was to observe the region near the interaction point using a heavy liquid bubble chamber, with the liquid surrounding a central tube containing deuterium gas. About 14,000 pictures were multiply scanned and analyzed by techniques developed especially for these reactions. The most probable conclusion is that no events of the above types were seen. The meaning of this result in terms of limits on the average cross sections for those interactions is given, and the significance of the result with respect to previously published theories and experiments is discussed.

TABLE OF CONTENTS

LIST OF FIGURES

LIST OF TABLES

I. MOTIVATION FOR EXPERIMENT

Extension of the study of the photon-nucleon interaction to include all the channels

$$\gamma + N \longrightarrow Y + K$$

Y = strangeness - 1 hyperon

K = strangeness + 1 meson

poses a number of problems, both experimental and theoretical. The experimentalist must cope with small count rates, short-lived particles leading to multi-body final states, and with added background processes (at these high thresholds) which simulate the same final states. The theoretician must consider a large number of relatively unknown intermediate states, and must use dynamical or symmetry approximations known to be incorrect. Aside from the residual curiosity for observing something new, does knowledge of these reactions merit the trouble that the quest for it generates? Two "generations" of answers are discussed below.

1. Early Motivations and Prior Experiments

At or near the time this thesis experiment was proposed, the primary interest in associated photoproduction was to obtain fundamental constants characterizing the interacting particles. Calculations[1-3] indicated that the differential cross sections, excitation functions and polarization resulting from these reactions would be sensitive to the relative parity of the KY system, the spin of the $K^{*}(891)$, the coupling constants $g^2_{K\Lambda N}$ and $g^2_{K\Sigma N}$, and

the anomalous magnetic moments of Λ^O, $\Sigma^{\pm, O}$ (including the

transition moment implied by $\Sigma^O \rightarrow \Lambda^O + \gamma$).

The reactions

a) $\gamma + n \rightarrow K^O + \Lambda^O$

b) $\gamma + n \rightarrow K^O + \Sigma^O$
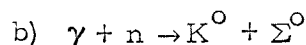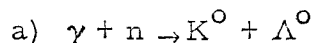
were considered particularly suited for this purpose because of

the limited types of interactions (see Part I-2-B). The present

experiment was not conceived to generate any of the detailed data

necessary to answer these questions, but to see if the average

total cross sections of the reactions a) and b) were large enough

to make these reactions useful for further exploitation. Some

ideas of the combined effect of these parameters, plus a rough

comparison with the interesting[4] strong interaction

c) $\pi^- + p \rightarrow K^O + \Lambda^O$
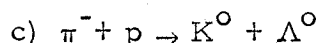
could hopefully be obtained.

The prior experiments consisted of counter data on the

excitation function plus very limited angular distributions of

$$\gamma + p \rightarrow K^+ + \Lambda$$

$$\gamma + p \rightarrow K^+ + \Sigma^O$$
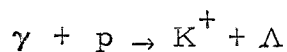
with scanty polarization data on the former.[5-8] Also available

was the result of a bubble chamber exploratory experiment of

E. D. Alyea[9] giving the average cross section for

$$\gamma + carbon \rightarrow K^O + hyperon$$
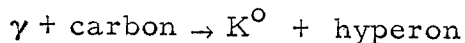
The results of this experiment, when combined with the later results of the A. D. McInturff[10] measurement of

$$\gamma + \text{Polyethylene} \rightarrow K^o + \Sigma^+$$
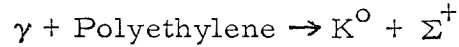
gave the expected results for the reactions a) and b) above:

$$\sigma_\Lambda = 6.9 \pm 5.1 \ \mu b \ (\text{if } \sigma_\Sigma = 0)$$

$$\sigma_\Sigma = 9.8 \pm 7.3 \ \mu b \ (\text{if } \sigma_\Lambda = 0)$$

$$\sigma_\Lambda = \sigma_\Sigma = 4.0 \pm 3.0 \ \mu b \ (\text{if equal})$$

This result obviously warrants a more direct measurement.

As a starting point for the design of an experiment to detect a) and b), the Born approximation calculations of Capps[2], and of Kawaguchi and Moravcsik[1] were fit to all existing cross section data with variation of the unknown parameters allowed. While these calculations are limited to a few terms (no K^* or other resonances included), fairly self-consistent fits were obtained. The nominal excitation function for $K^o + \Lambda^o$ throughout this experiment is the one predicted by the formulae of the latter authors, using the best parameters. The $K\Sigma^o$ cross section was sensitive to the parameters used, and was thus taken equal to the $K\Lambda$ but displaced to the proper threshold energy. These are shown in Figure 1.

2. Present Status of Associated Photoproduction

Most of the motivations mentioned in 1. have disappeared,
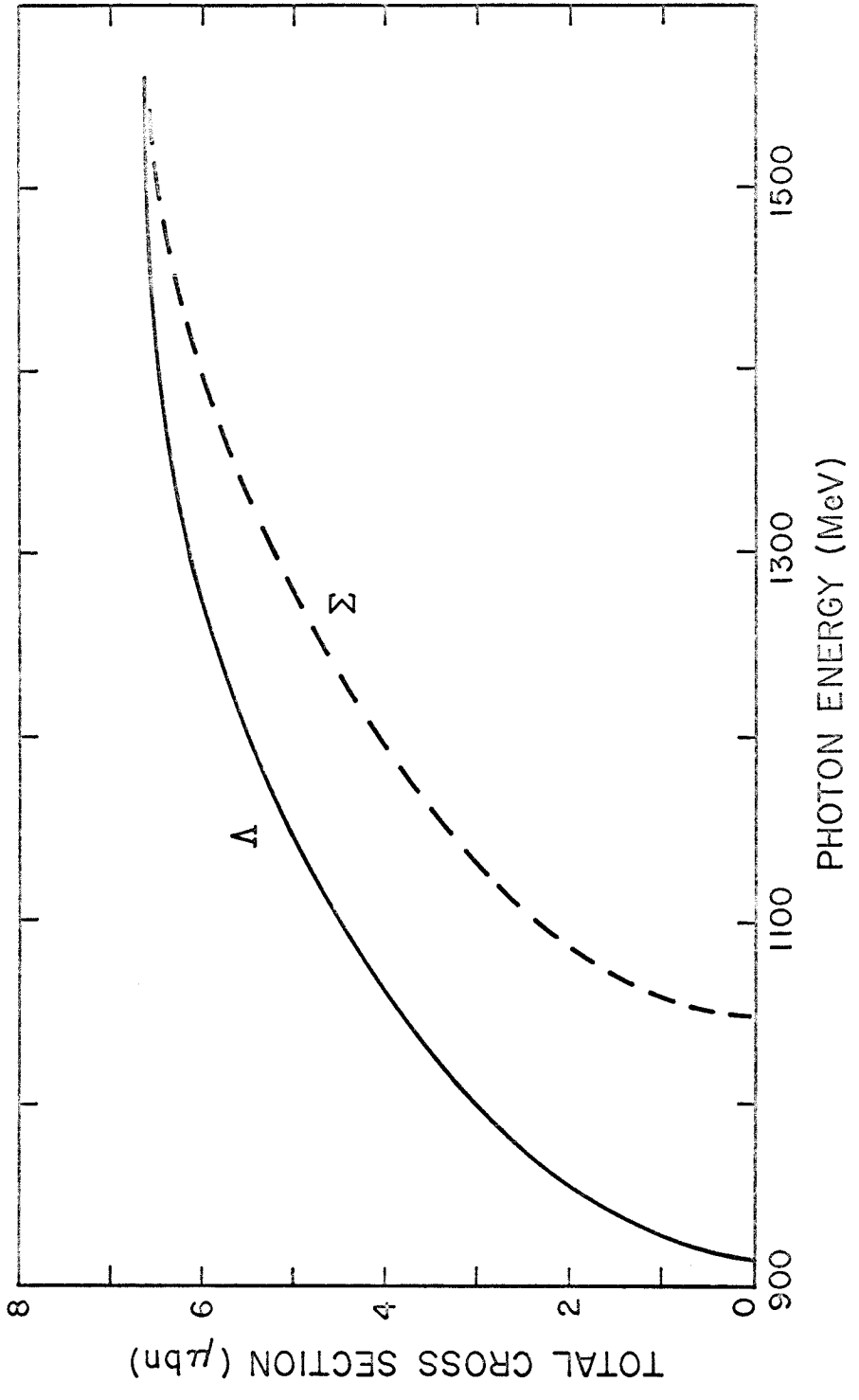
FIGURE I: NOMINAL CROSS SECTIONS

largely because of direct measurements of these parameters,
or inference from strong interaction processes. The central
problem at present appears to be how to predict the details of
each reaction using dynamical calculations and symmetry schemes,
preceded, as usual, by a phenomenological analysis to determine
the important states contributing. The paragraphs below summa-
rize the present state of confusion.

A. KΛ System in Strong Processes

Because there is no simple connection to strong
processes as for π photoproduction (e. g. , the Watson theorem),
at most we can hope that the similarity of final states will induce
similarities in behavior. Even for the best-known reaction (c),
however, the picture is cloudy. The observed excitation function,
Figure 2, and polarization data[4] have led to assorted conclu-
sions. Whereas the bump at total energy 1690 MeV is remi-
niscent of the $N_{1/2}^{*}$ ($F_{5/2}$, 1688) resonance, the angular distri-
butions do not show evidence of higher partial waves, and can
be fit reasonably well by a model incorporating a $P_{1/2}$ resonance
(due to Kanazawa[11]). This resonance may be in either the πN
system or unique to the KΛ system, and with its inclusion the
model fits the observed polarization everywhere except just at
the "bump" in the excitation function.

Hoff[12] has constructed a model using both $P_{1/2}$ and
$F_{5/2}$ resonances, but with the position and the width of the $F_{5/2}$
as parameters. The model then fits all data quite well, but
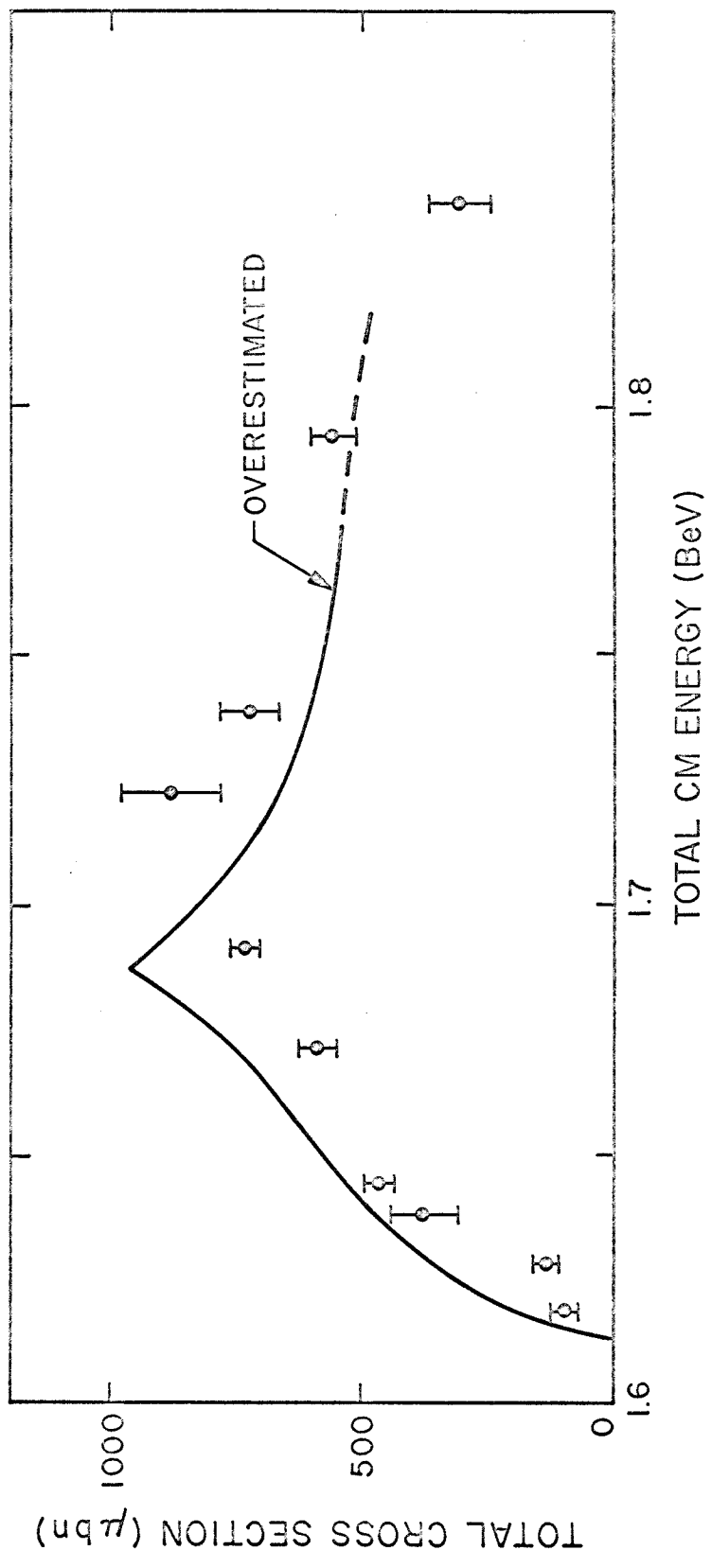
FIGURE 2: EXCITATION FUNCTION FOR $\pi^- + p \rightarrow K^\circ + \Lambda^\circ$

predicts that the $F_{5/2}$ resonance is centered at 1650 MeV and has a full width < 10 MeV. (In contrast to the $N_{1/2}^{*}$ (1688, $5/2^{+}$) with full width ~ 80 MeV.) This would sound like parameter juggling except for the experiment of Kuznetsov, et al.[13], possibly revealing a narrow (< 7 MeV) resonance (Z_1^{*}) in the K system near 1650 MeV. This resonance is not found by some others.

To complete the permutations, a model without either $P_{1/2}$ or "new" $F_{5/2}$, but using the standard third πN resonance is claimed to also fit all data if other partial waves are suitably adjusted.[14] Usually the experiment of Wrangler, et al.[15] is presumed to have seen

$$N_{1/2}^{*}(1688) \rightarrow K^{o} + \Lambda^{o},$$
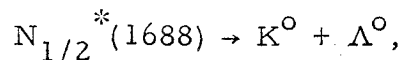
but their peak at ~ 1675 might be either the $Z_1^{*}(1650)$ or the $P_{1/2}$ resonance. These experimenters state that the very weak effect in

$$\pi N \rightarrow N \pi \pi \pi$$
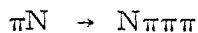
at 1675 tends to rule out the result usually attributed to them.

Finally a very early result of Adair,[16] arriving before most of the data, indicates that the excitation function (at least) can be roughly explained with an s-wave amplitude only. The "strange" peak near 1700 is then thought to be the cusp induced by the ΣK threshold at 1690.4 MeV. His prediction, shown by the solid line in Figure 2, can also account for the presence of p-waves if the ΣK is in a p-state somewhat near

threshold.

B. <u>Results of Models in ΛK^+ Photoproduction</u>

Whereas any model seems to work reasonably well for the strong process, all seem to fail when applied to the totality of photoproduction data. These models[17-21] are discussed in more detail by D.E. Groom[22], and C.W. Peck[23] in their presentation of data on the polarization and K angular distributions of $\gamma + p \rightarrow K^+ + \Lambda$. The predominant features of these data are quadratic angular distributions, a smoothly saturating excitation function, and a bump in the polarization at ~ 1700 MeV.

The figure below shows the Feynman diagrams for the Born terms and those for exchange of various resonances.

(a)   (b)   (c)
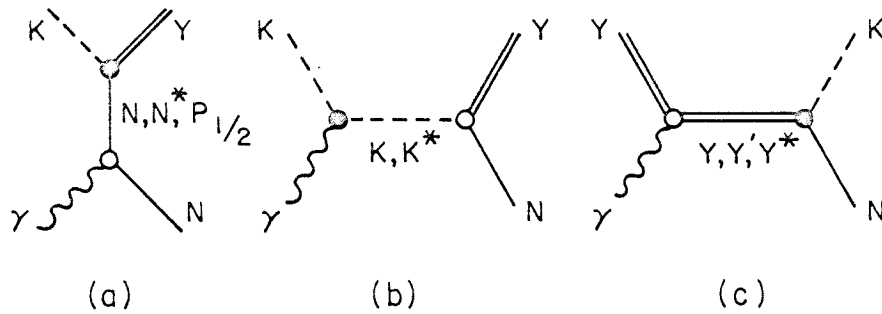
The open circle represents two choices: interaction with the charge or with an anomalous moment. Models such as that of Kuo[17] include diagrams (a) (with N, $P_{1/2}$) and (b). These

predict the wrong sign for the polarization. At the opposite

extreme, models such as that of Gourdin and Dufour[21] include

all diagrams except the $P_{1/2}$ resonance of (a) and the Y^* of (c).

They include both the second and third πN resonances. When their

parameters are varied, they can fit either angular distributions or

polarization, but not both simultaneously. The model of Fayyazuddin[20]

includes the first πN resonance but no other. He fits cross-section

data well but does not comment on polarization. No model has been

proposed including both $F_{5/2}$ and $P_{1/2}$ resonances found necessary

by Hoff. The Adair cusp analysis should give similar results as

when used in the strong process, but no evidence is present for any

cusps in the excitation function.

C. Predictions for Neutral Associated Photoproduction

In view of the above difficulties, skepticism is warranted

over any predictions made by these models, for $K^0 \Lambda^0$, $K^0 \Sigma^0$ systems.

In his study of the behavior of the models, Groom[22] has commented

that even the partial agreement with the data seems to be the result

of a delicate balance between large terms, leaving a small result.

Extrapolation to other energies then makes the result divergent.

For the $K^0 \Lambda^0$ or $K^0 \Sigma^0$ system, the interaction proceeds via the

anomalous moments only (see Feynman diagrams with N = neutron,

$Y = \Sigma^0$ or Λ^0, $K = K^0$) and without the K exchange term at all. If

Groom's contention is correct, one would expect all predictions to

be too large.

The absence of K exchange terms is of prime importance. Since this term contributes to all partial waves, the effects of resonances on the angular distributions can be masked when it is present. Thus the $K^o \Lambda^o$ production is the closest analog of the strong process, and except for experimental difficulties, the most amenable to analysis.

Of the various models listed, only Fayyazuddin has predicted the cross section for reactions with a K^o present. He finds $\sigma_{K^o \Lambda} = 4.5 \mu b$ at 1003 MeV, $\sigma_{K^o \Sigma^o} = 1.9 \mu b$ and $\sigma_{K^o \Sigma^+} = 14.3 \mu b$, both at 1157 MeV. The first two are roughly comparable to the values shown in Figure 1, but the latter value is at least three times the experimental result.[10]

The most direct prediction of approximate higher symmetry schemes is the SU(3) relation on the amplitudes:[24]

$$A(\gamma + n \rightarrow n + \pi^o) - \sqrt{3} \; A \; (\gamma + n \rightarrow n + \eta)$$

$$= \sqrt{3} \; A \; (\gamma + n \rightarrow \Lambda + K^o) - A \; (\gamma + n \rightarrow \Sigma^o + K^o) \; ,$$

which because of the four terms does not lead to a useful inequality. If additional assumptions are made, stronger predictions are available.[25] If the reactions of interest proceed mainly through the first πN resonance,

$$\sigma(\Lambda K^+) = \sigma(\Lambda K^o) = 0$$

$$\sigma(\Sigma^o K^o) = \sigma(\Sigma^o K^+) \qquad .$$

If the reactions are dominated by the intermediate state $N^*_{\frac{1}{2}}$ (1688), then there is an arbitrariness due to the unknown ratio of D to F type couplings[45]. Since the amplitudes are quite sensitive to this ratio, and large factors are also introduced by symmetry-breaking terms[46], experiments relating total cross sections are not likely to be particularly informative in deciding if $N^*_{\frac{1}{2}}$ (1688) predominates. The results of Holloway and Fujii[25], together with a D/F ratio given by $\alpha/(1-\alpha)$ give

$$\sigma(K^o\Sigma^o) : \sigma(K^+\Lambda) : \sigma(K^o\Lambda) : \sigma(K^o\Sigma^+)$$
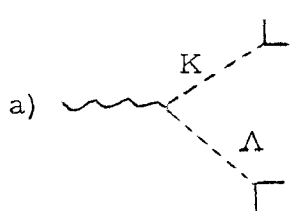
$$= 324 : 147 : 108 : 2$$

if α is taken to be 2/3 as might be speculated from SU(6) results. No additional constraints are given by the SU(6) symmetry as quoted by Tripathy[26].

II. EXPERIMENTAL SYSTEMATICS

Whereas the charged analogs of $K^O Y^O$ production are suitable for study by counter techniques, the neutral modes lead to a 4-body final state, with analysis more tractable by visual methods. Described below are the basic features of the kinematics of these reactions and the experimental method used to realize and exploit these features.

1. Kinematics

Given the cascading reactions:

a) $\gamma + n \rightarrow K^O + \Lambda^O$
$\quad \rightarrow \pi^+ + \pi^- \rightarrow \pi^- + p$

b) $\gamma + n \rightarrow K^O + \Sigma^O$
$\quad \rightarrow \pi^+ + \pi^- \rightarrow \Lambda + \gamma'$
$\quad \rightarrow \pi^- + p$

which in a visual detector manifest themselves as a vee-pair, we claim that knowledge of the geometric location of the incoming photon beam, identification of the final state particles and measurement of their spacial angles exactly determines the kinematics of a) without knowledge of the neutral masses (assuming the original reaction is two-body with the neutron at rest). Furthermore, if m_Λ and m_K are assumed, then b) is exactly determined without knowledge of m_Σ or any information about γ' except its mass. The counting of unknowns is diagrammed below, where the stated result becomes more transparent by breaking up the interaction into its sequential 2-body interactions. When this is done, each interaction occurs in a plane, so

that only three variables are needed to describe each particle; similarly, only three constraints from momentum-energy conservation are available. Note that the point of original interaction (origin) is determined by the intersection of any decay plane with the beamline, except for accidental coplanarities. Any additional information about the event overconstrains it. Loss of one constraint occurs whenever both vees and the beamline are coplanar, and when either vee has incoming and outgoing particles colinear. If coplanarity of both vees and colinearity of one occur simultaneously, only one constraint is lost, since the colinear decay gives the origin while losing a transverse momentum constraint.

In the following description, "$\checkmark$" will denote a known variable and "?" will denote an unknown. For the primary interaction we have:

Particle	Mass	Momentum	Angle
γ	$\checkmark$	?	$\checkmark$
n	$\checkmark$	$\checkmark$	$\checkmark$
K	?	?	$\checkmark$
Λ	?	?	$\checkmark$

5 unknowns and 3 momentum-energy conservation constraints = 2 unknowns.

Each decay gives:

Particle	Mass	Momentum	Angle
neutral	?	?	$\checkmark$
π	$\checkmark$	?	$\checkmark$
π (or p)	$\checkmark$	?	$\checkmark$

4 unknowns and 3 momentum-energy conservation constraints = 1 unknown.

Thus each decay vee may have the momentum of the neutral expressed as a function of $m_{neutral}$. These two independent constraints then provide just enough information to determine the initial reaction.

b) K and Λ are completely determined since m_Λ, m_K are assumed. The 3-particle final state in three dimensions is then determined as shown,

Particle	Mass	Momentum	θ	ϕ
γ	✓	?	✓	✓
n	✓	✓	✓	✓
K	✓	✓	✓	✓
Λ	✓	✓	✓	✓
γ'	✓	?	?	?

leaving 4 unknowns and 4 momentum-energy conservation constraints, thus determining the problem.

2. Mechanics of Observation

The primary consideration governing the choice of experimental apparatus was that the CalTech 12" heavy liquid bubble chamber was extant. The design of this chamber was primarily based on the reasonable assumption that a high counting rate per picture is desirable for analysis by a comparatively small group with minimal automatic scanning and measuring equipment. This assumption naturally leads to the need for high beam intensities and a dense target. These

factors are mutually incompatible because the interaction of photons
with matter produces, in addition to desired events, large amounts of
forward-going electromagnetic cascades, obscuring not only the vi-
cinity of the origins of the events, but spreading out somewhat into
the detector medium (by virtue of multiple scattering). Use of a
magnetic field, desirable for additional momentum constraints, aggra-
vates this problem by reducing the natural geometrical separation
between high-momentum forward-going electromagnetic background
and lower-momentum wide-angle final state particles from reactions
under consideration.

The CalTech group[27] used a compromise design to reduce
these conflicts. The immediate vicinity of the beamline was con-
sidered lost, and was enclosed by a steel tube. The tube contained the
target material as high pressure gas, which reduced the divergence
of showers attributable to multiple scattering. The tube geometry
roughly conformed to the expected shower geometry, so as to contain
it. Use of a heavy liquid (CF_3Br) as detector around this tube tended
to regain information lost when the use of a magnetic field was a-
bandoned. Both range-energy information on stopping particles and
multiple-scattering determination of (momentum $\cdot$ velocity) thus became
available. The latter, combined with bubble density information on
velocity, permits the masses of particles to be qualitatively or
quantitatively determined. The beam was intended to be both narrow
and intense. This combination of parameters would then lead to an
optimization of the number of primary reactions per picture, without

undue chamber obscuration. Whether or not these would be useful events (seeable) depended on the chamber efficiency for a particular reaction. This bubble chamber is shown in Figure 3. For more discussion of its properties, see Part III-1.

Actual operation of the chamber under these conditions, both on a preliminary run, and the data run itself, confirmed all of these goals. The reaction rates (not including efficiencies) were at least ten times those attained by using a conventional H_2 bubble chamber with field and dilute photon beam, as mechanized by Pless et al.[28].

3. Limitations of the Experiment

Complications are imposed by our setup on the simple kinematics of Part II-1.

(a) The photon beam is not a line source of possible origins, but is a tube of diameter ~ 2 mm.

(b) The neutron is not at rest but has a Fermi momentum in the D_2 gas used averaging about 50 MeV/c.

(c) Not all vertices can be seen because of the presence of the tube. Paths of particles coming from such hidden vertices will be distorted by passage through the steel tube.

(d) Multiple scattering will distort the observed decay planes in either case.

(e) The detectable difference between $K\Lambda$ and $K\Sigma$ production may be obliterated by the effective loss in mass resolution caused by these effects.

Difficulties (a), (b) and (d) can be overcome by analysis
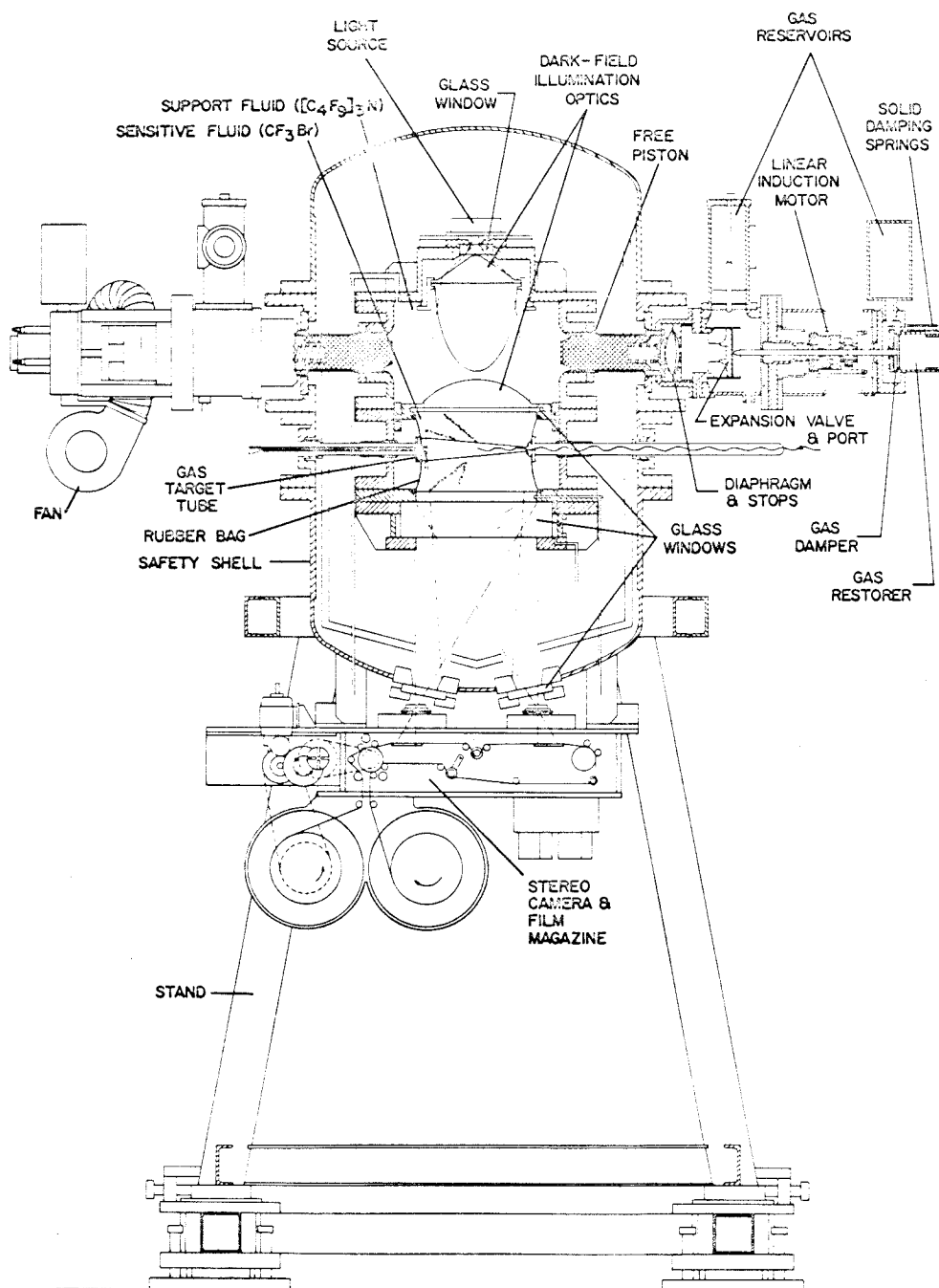
FIGURE 3: THE CALTECH 12 INCH BUBBLE CHAMBER

techniques described in Part IV and Appendix II. Difficulty (e) must
be taken as an ultimate limitation of the experiment, and is discussed
in Part IV. Difficulty (c) was thought to be surmountable, but was not,
and warrants further discussion here.

A preliminary estimate of the observable count rate, based on
crude calculations of chamber efficiency, and theoretical cross section
as described in Part I-2, gave an expected count rate of six events per
1000 pictures scanned (both $K\Lambda$ and $K\Sigma$). The majority of these events
(87%) would have at least one hidden vertex. It was believed that the
three-dimensional information contained in the stereo pictures would
be sufficient, at the scanning table, to select pairs of tracks emanating
from an off-beamline vertex, thus rejecting random combinations of
high-energy tracks. It was on this projected total number of counts
(300 for 50,000 pictures) that the experiment was planned[29].

The attempt to carry this out was abandoned at a later time
because of two new pieces of information. A careful (and long) Monte
Carlo calculation predicted that the chamber efficiency was about a
factor of two lower than expected, but that the completely visible 2-V
events constituted ~ 30% of what was left. This means ~ 1 count per
1,000 pictures will be a visible (i.e., vertices outside tube) 2-V event,
and 2/1,000 will be hidden in some respect. Concurrently, time esti-
mates and background estimates became available, indicating that there
would be something like ten "hidden pair" combinations per picture.
This came about because of the large number (50/picture) of high
energy tracks and the many close approaches of these tracks to one
another, which simulated vees slightly distorted by passage through

the beam tube. The scanning time also soared to about thirty minutes

per picture compared to four minutes per picture for visible V-pairs.

It was clear from these considerations that in terms of producing a

statistically significant measurement of a cross section, the experiment

could not succeed. Thus it was decided to use only the events most

easily recognized and analyzed, and to scan a subset of the original

50,000 pictures. The rest of this thesis will be devoted to the

explanation of this revised procedure only.

III. EXPERIMENTAL DATA RUN

This experiment was run in parallel with the 2π photoproduction experiment of L. J. Fretwell, Jr. , simply by interchanging D_2 gas for the H_2 target gas of that experiment. The techniques of beam alignment were pioneered by Fretwell in an earlier trial experiment, and perfected by both of us in two major runs. Whereas another complete description of the chamber and associated apparatus, beam alignment, and data run would be redundant with that given by Fretwell,[30] a summary is given here for the sake of completeness.

1. <u>Bubble Chamber</u>

In order to obtain the physical characteristics described in Part II-2, a heavy liquid (Freon) bubble chamber, originally designed by Teem et al.[27] and later modified and perfected under the supervision of J. H. Mullins, was used. This chamber employs a resonant pressurization system [31] which insures excellent hydrodynamic and thermodynamic properties. Referring to Figure 3 , its operation proceeds as follows: The internal fluids are depressurized by the sudden opening of the expansion valves, whereupon the chamber becomes sensitive. Before the outgoing pressure wave can bounce against the gas reservoir, the beam is passed through the chamber, bubbles form and are photographed by the dark-field system of light source, lenses and stereo camera. The returning pressure wave obliterates these bubbles, and is arrested at its maximum by the closing valves, which themselves have been timed to bounce back

in synchronism with the natural cycle of the chamber. This process
is repeatable every third second, the major limitation being heating
of the engines moving the expansion valves. This system performed
with superb reliability throughout our runs, producing pictures such
as the sample shown in Figure 4 . The only feature needful of im-
provement in a future design would be the nonuniformity and limited
nature of the chamber illumination.

2. Beam Alignment and Monitoring

In the data run of concern to this thesis, the CalTech electron
synchrotron was operated an an endpoint energy of 1530 MeV. The
photon beam generated by letting such electrons strike the internal
tantalum target was collimated to .022" diameter, "hardened"
(photons < 10 MeV removed) by lithium hydride in a pulsed field, re-
collimated to .032", fed into a vacuum tube and swept by 6.5 Kg-m
of field to remove non-neutral components, peripherally scraped by
a lead collimator, and finally introduced through a mylar window
into the deuterium gas target. This sequence is shown in Figure 5,[30]
which shows all important features of the experimental layout.

Alignment of this system was first accomplished by x-ray
photography to pass beam through the system, with final lineup being
done by maximization of flux through each element, using an ion
chamber as the quantitative element. All collimators were alignable
with micrometer accuracy (.002"). A compromise between premature
beam dump and vertical blowup of the beam fixed both the synchrotron
fundamental frequency and the radiator position. The chamber itself
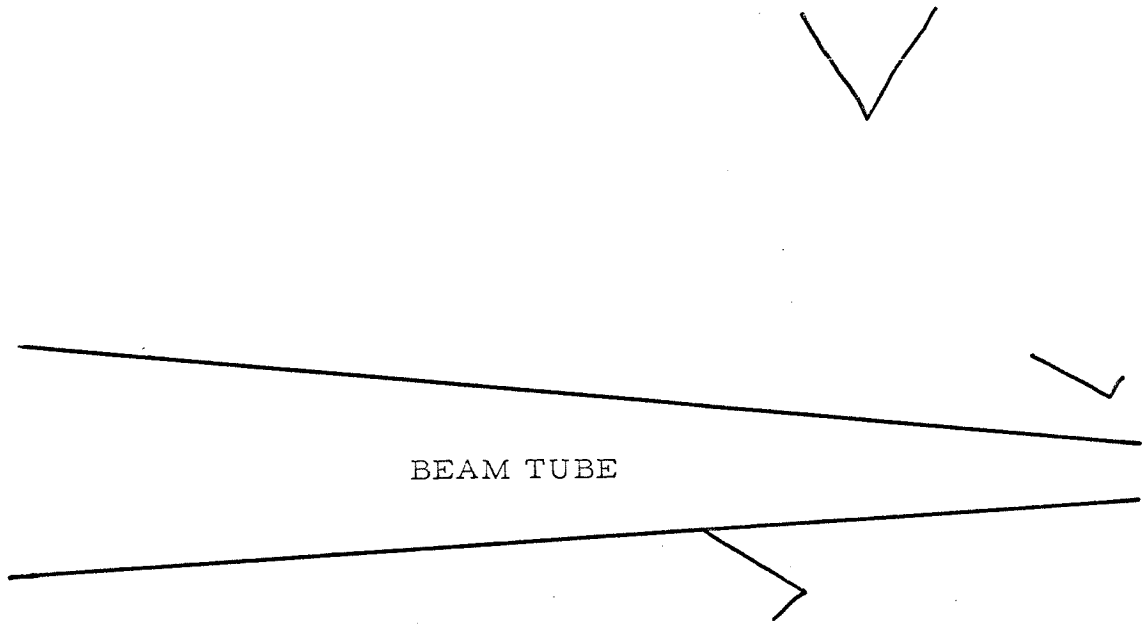
Figure 4

Typical chamber picture with three single vee candidates or two double vee candidates (all failed pre-analysis tests).
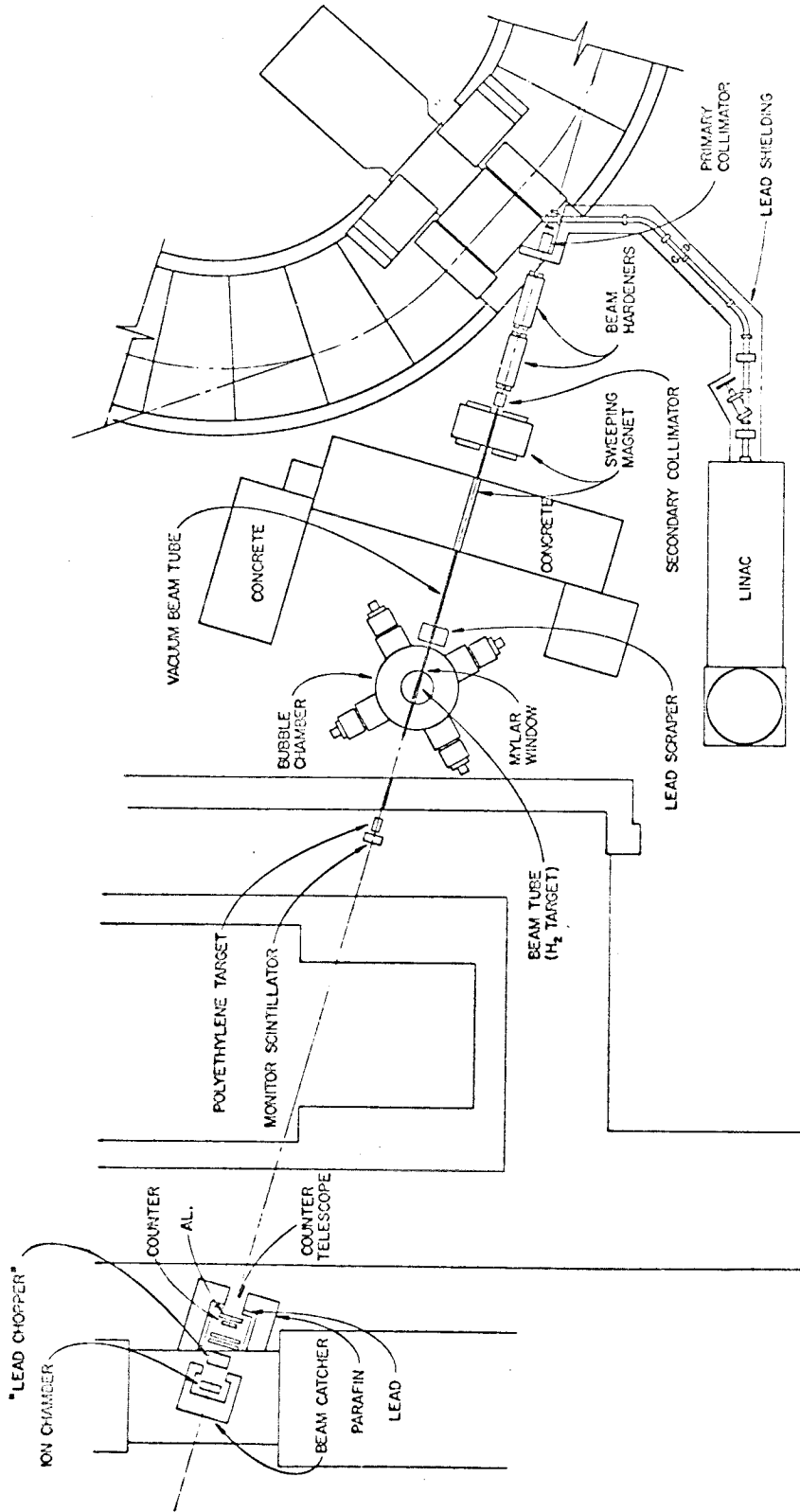
FIGURE 5: EXPERIMENTAL ARRANGEMENT AND BEAM AREA

was aligned by a sequence of x-ray pictures allowing the chamber beam tube to be accurately (.003") centered around the pre-aligned pencil beam.

Monitoring of the beam intensity was carried out by a counter telescope system due to Fretwell and Mullins. This telescope, viewing particles created by the photon beam hitting a polyethylene target as it exited from the bubble chamber, is necessary because saturation (of an otherwise indeterminable amount) takes place in ordinary ion chambers and quantameters when used with the intense, fast-dumped beam necessary for the bubble chamber. The counter system was continuously cross-calibrated with an ion chamber by using at least two slow beam dumps between each fast dump intended for a bubble chamber exposure. The typical beam intensity monitored was a total integrated energy of $.5 \cdot 10^9$ MeV of photons dumped in ≈ 100 μs. This total flux is but a tiny fraction (.00001) of the original energy of the electrons in the synchrotron. The extensive neutron, γ and charged particle shielding shown in Figure 5 was to deal with the chamber obscuring background, both beamline associated and from general room sources, caused by the dissipation of essentially all of the original energy of the electrons.

IV. DATA PROCESSING

The only certainty in an experiment of this nature is that the background of pseudo-events will be enormous compared to the real production rate. Therefore many screening tests are required to purify the sample. Whether a given test is to be applied during a first or subsequent pass at the picture on the scanning table, or in the computer, or in the final data, is a question involving optimization of the factors of reliability, time efficiency, and cost efficiency. The following two sections describe the manner in which this problem was solved for this experiment.

1. Purification of Sample at Scanning Level

Seeing the characteristic double-vee signature of a KY production constitutes a suitable requirement only if the scanning efficiency on a single pass for such features is high. Since this was highly questionable, the requirement was made instead that only a single vee be detected, with eventual combination of all such vees found on multiple passes. Additional tests which are easily performed at this level are:

A. Unreal Origins

On the assumption that an observed vee is the decay of a beamline produced K or Y, then in a single view on the scanner, by conservation of momentum, the possible origins on the beamline are those included in the region of the beamline bounded by the backwards

projection of the directions of the decay particles (see the figure

below). This region must include the D_2 target area. Furthermore,

the regions deduced from both views must have a common region, or

the vee is self-inconsistent.
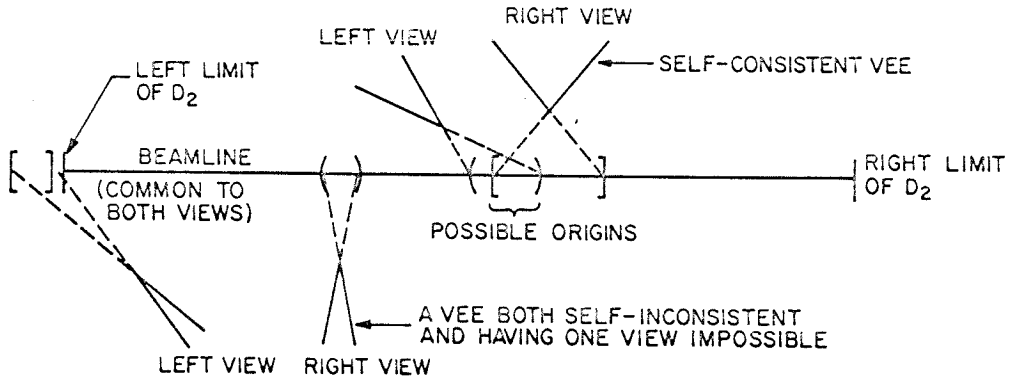
B. Fiducial Volume

From the Monte Carlo chamber simulation described in

Appendix I, a cutoff on the maximum allowable distance of 8 cm.

transverse to the beamline for which a decay vertex would be accepted

was set. The figure below shows the reliability of such a cutoff.
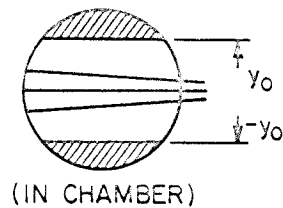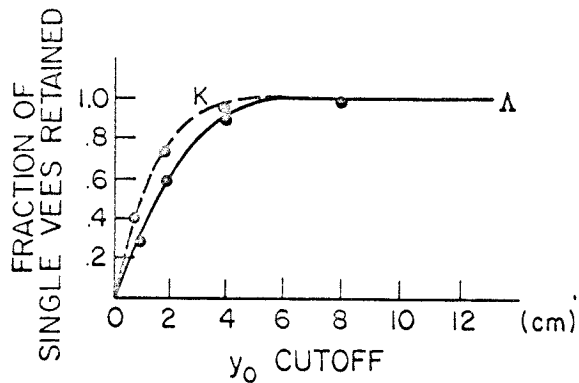
C. Large Opening Angles of Vee

Because a small-angle scatter closely simulates a large

angle decay, the chamber simulator was used to determine an upper

limit on the permissible decay angle. Interpreted in terms of the

two available views, it was demanded that the opening angle be

< 170° in at least one view, a limit shown to be safe by the following

figure:
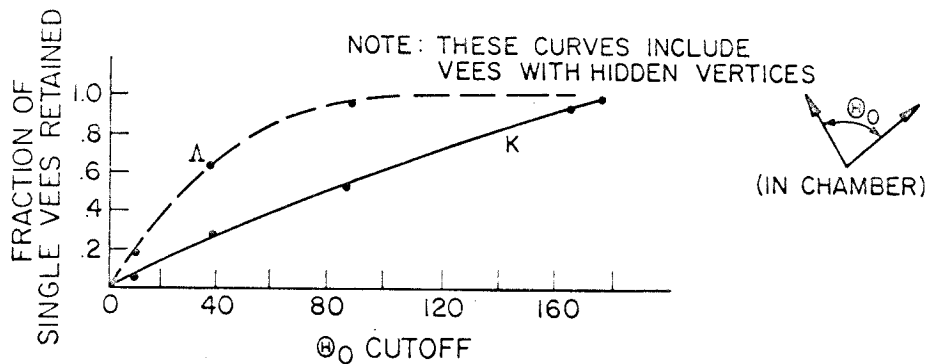
D. Small Opening Angles of Vee

Lambda particles often (10%) decay with opening angles less

than 5°, so no lower limit was imposed here. To help eliminate

electron pairs, the requirement was that if both particles were un-

ambigously electrons, and the opening angle was zero in both views

(over a distance of .5 cm) then the vee was rejected.

E. Additional Particle in Final State

A vee was not rejected if a track also emerging from its

vertex was a likely electron. This retains vees with knock-on

electrons.

These tests were applied on each of four independent scans (by different people) of the pictures. The surviving vees were then combined in all combinations for a given picture, subject to the condition that no pair appeared on the same side of the beamline. (The chamber simulator proved that the chance for a Σ-decay or transverse neutron to "bounce" the Λ across the beamline was negligible). The following tests then could be applied to a pair of vees:

F. Incompatible Origins

This test is the generalization of the test for unreal origins of a single vee. The common regions from the two views for each vee must themselves have a common region. Tolerances on this test were very loose, as on the former, since multiple scattering tends to obscure the result. In principle, it is possible to geometrically locate on the scanning table the location of the true origin. It was found that errors in lineup and multiple scattering make the answer so imprecise as to be useless, and this more exact test was abandoned.

G. Coplanarity

There also exists a simple geometrical test for coplanarity of the implied K, Λ, and incident γ. Physically the coplanarity is violated by the neutron Fermi momentum and the emitted γ-ray in Σ-decay to $\Lambda + \gamma$. The chamber simulator proved that this violation was small and that the test would still be useful. However, the geometrical test was perturbed by many factors such as lineup of the views, uncertainty in beamline position, and distortion of straight lines. The net result was that its rejection of background was so

small ($< 10\%$) and the test so time-consuming that it was eventually dropped.

H. Improbable Decay Vertices

When taken as a pair, there are considerably more restric-
tions on what a real event can look like on the scanning table, because
of the correlation between the two produced neutrals. The Monte
Carlo calculation simulating the chamber and events, discussed in
Appendix I, showed (below) that essentially all real events can be
gleaned if it is required that at least one of the vertices of the vees
is less than 7 cm. from the beamline (on the scanner).
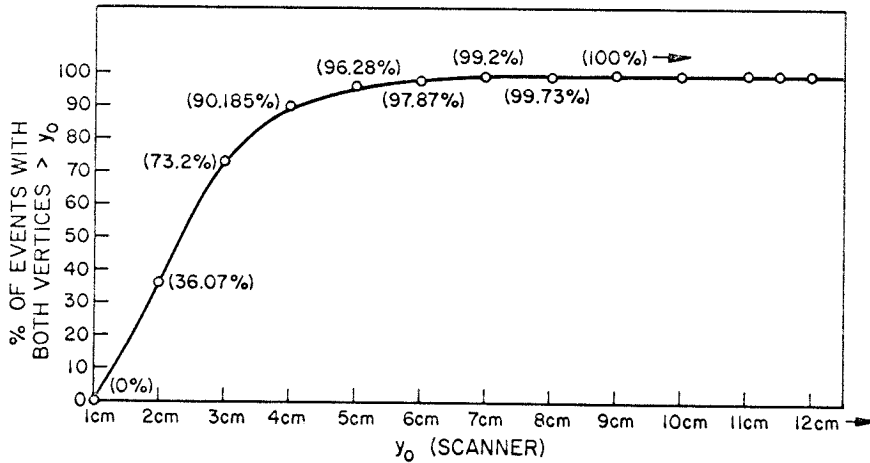
I. Improbable Decay Angles

Whereas once again no useful restriction can be placed on
small angles, the above-mentioned correlation has a dramatic effect
on the upper limit. The figure following shows the result that if
candidates having all four observed angles (2 vees, 2 views) $> 90°$
are rejected, no appreciable loss in real events is sustained.
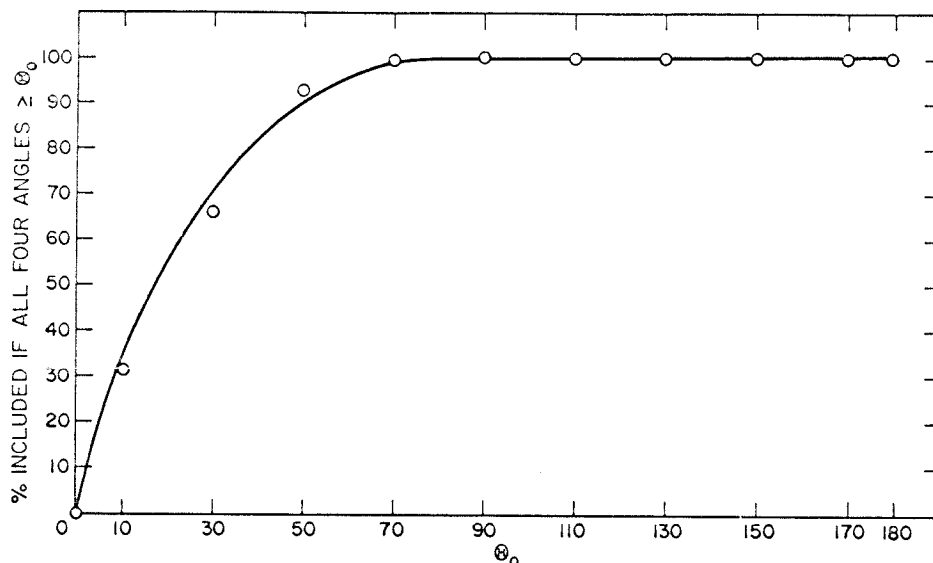
J. Backward-going Neutrals

The chamber simulator provided the result that the K and Λ are never (for practical purposes) so perturbed by the n or the decay γ from Σ that they emerge backwards (> 90° lab angle). Interpreting this on the stereo views, a calculation involving six pages of algebra shows that if both particles in both vees in both views go backwards, this guarantees that the "neutrals" went backwards and thus the event is discardable. This is a non-trivial result because the stereo views are point projections of the real event.

The results of this purification process, in terms of the background/foreground ratio and the attenuation of real events, is shown in Table 1. Some of the tests were not highly efficient, but these were retained because they were so easily done. No single test gave appreciable attentuation of the count rate, but the combined attenuation and uncertainty is non-negligible. This is the price paid for the extreme improvement in the purity of the sample.

Table 1

Purification of Sample at Scanning Table

Test	% Loss of Real Events (given by Monte Carlo calculation)	Background/Foreground (using predicted number of counts) After test at left:
All possible 2-vee combinations	(Limited by scanning efficiency)	45,000
Large Opening Angles	< .1%	7,200
Unreal Origins	negligible	4,200
Fiducial Volume (y_0)	< .1%	2,500
Electron Pairs	negligible	1,600
2v same side	1 ± 1% (KΣ only)	710
2v Origins Incompatible	negligible	530
Coplanarity of KY$_\gamma$	negligible	430
Backward-going Neutrals	0 ± .1%	320
Improbable Decay Angles	0 ± .5%	107
Improbable Decay Vertices	.8 ± 1%	100

2. <u>Purification of Sample at Analysis Level.</u>

A dual choice existed concerning the method of measurement and analysis. It was possible that all the physics contained in this experiment could be displayed through the use of simple measurements and trivial computer analysis. Evidence[32] was available, however, that such simple techniques did not give meaningful results in experiments with visual techniques. Thus the measurement scheme was constructed to be usable in either a complicated or simple analysis, the simple analysis was initiated immediately, and the complex analysis worked out in parallel to backstop the simple one should it fail. These systems are described briefly below and in detail in Appendix II.

A. <u>Measuring System</u>

The surviving double-vee candidates were measured on the analysis table devised and brought to a high state of perfection by Fretwell,[30] using essentially the exact scheme he describes for the data format and conversion to digital form. Furthermore, this author enjoyed the benefits of using <u>in toto</u> the chamber point reconstruction system developed and tested by the same colleague [30].

The nature of the measurements themselves was somewhat different from his experiment for which the system was developed. Recall that the event is kinematically determined by the observed angles of the decay particles. Since the vertices of the vees were visible, the entire development of multiple scattering of each track was evident. The precision of angle determination, using the vertex and a point out on the track, was thus enhanced if the track point was

chosen with discretion. However, if a single track point were used

and chosen incautiously, a large error could be incurred. The final

method used was to calculate (Appendix II) the best two points on each

track (beyond the vertex) to use such that the result would be rather

insensitive to human error in selection of the points. This optimum

selection depends only on the observed scattering, and can be quickly

carried out by the person measuring, as is demonstrated in the

following diagram. For all practical purposes, the angular precision

is always as good or better than use of a single point on the track.
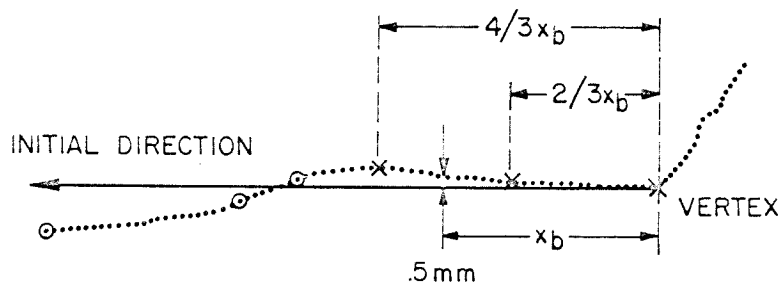
X = MEASURED POINTS FOR ANGLE DETERMINATION
O = MEASURED POINTS FOR RANGE DETERMINATION

The rest of the track was described by measuring points

along it until the particles disappeared, or stopped, or interacted.

Auxiliary information such as particle identification and nature of the

endpoint were included in the digitized information. The veracity of

both of these subjective quantities in our chamber has been verified[30],

even so, only an extremely conservative decision on whether or not a

particle stops has any quantitiative bearing on the results, as will be

discussed.

All candidates were measured twice by different operators to decrease the chance that an event would be lost through an error. Further, all measurements were required to pass the reconstruction program with an error assignment in reconstruction of less than .015 cm. (two-dimensional miss distance).

B. Rough Analysis System

Ideally, an event is determined by only six points: the two vertices of the vees and one point on each track. This neglects the neutron Fermi momentum, any decay γ from ΣK events, the finite beam size, and most important, multiple scattering. All of these effects lead to error and internal inconsistencies in the result. Nevertheless, the analysis is so simple that an IBM 7094 program was written to analyze all candidates. (Appendix II.)

To test this program accurately, a Monte Carlo event simulation program, including (a) scattering and (b) human measurement biases was needed. This program materialized at a much later time (see C. below), so a simpler program, not incorporating (b) at all and only a simple formulation of (a), was used. The simple analysis program was then run on these Monte Carlo events, and on a sample of generated "background" events (isotropically distributed vees which passed the preliminary scanning tests).

The quantitative results of this test were of course highly dubious, but many physically transparent results emerged.

(a) About 11% of real events is absolutely rejected (claiming momentum non-conservation, production from vacuum, etc.).

(b) About 86% of "background" is absolutely rejected.

(c) Of the accepted "events" in the absence of multiple
scattering, the KΛ or KΣ production will be cleanly
separated from background by examining the distri-
bution of the implied Fermi momentum of the neutron
(Fig. 6).

(d) In the presence of (approximately correct) multiple
scattering, the KΛ or KΣ peaks in (c) will be distorted,
but remain recognizable (Fig. 7).

(e) A 4-dimensional distribution in neutron momentum,
incident γ-ray energy, neutron lab angle with respect
to the incoming photon, and separation of the "origins"
implied independently by the two vees, produces a good
separation of background and real events (∼ 100%).
Figure 8 and Figure 9 attempt to show this result.

(f) KΛ and KΣ production cannot be distinguished from one
another.

The physics of results (d) and (e) is clear. Real events have
a photon energy between ∼ 900 and ∼ 1500 MeV, neutron Fermi
momentum ∼ 50 MeV/c and isotropic, and agreement between the
two origins implied by the two decay planes. Background events
generally have too large neutral angles and too large opening angles.
To get slow large angle neutrals, the C.M. system must be ∼ the lab
system, and the incoming photon must be of low energy. The almost
invariable result is for the neutron to go backwards with ∼ 500 MeV/c;
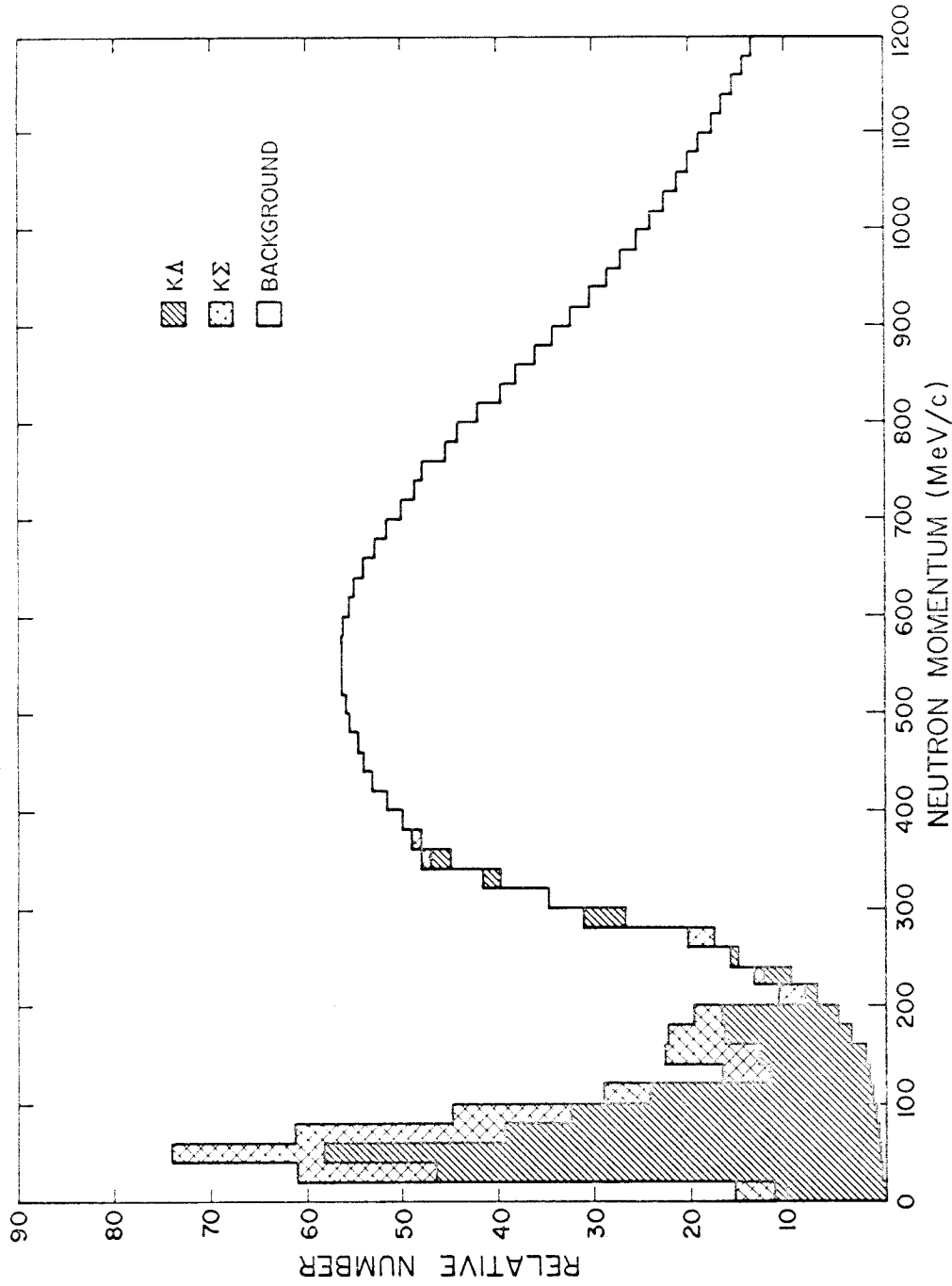
FIGURE 6: DISTRIBUTION OF NEUTRON MOMENTUM OF EVENTS AND BACKGROUND
FOR ROUGH ANALYSIS OF MONTE CARLO EVENTS
[WITHOUT MEASUREMENT ERROR OR SCATTERING]
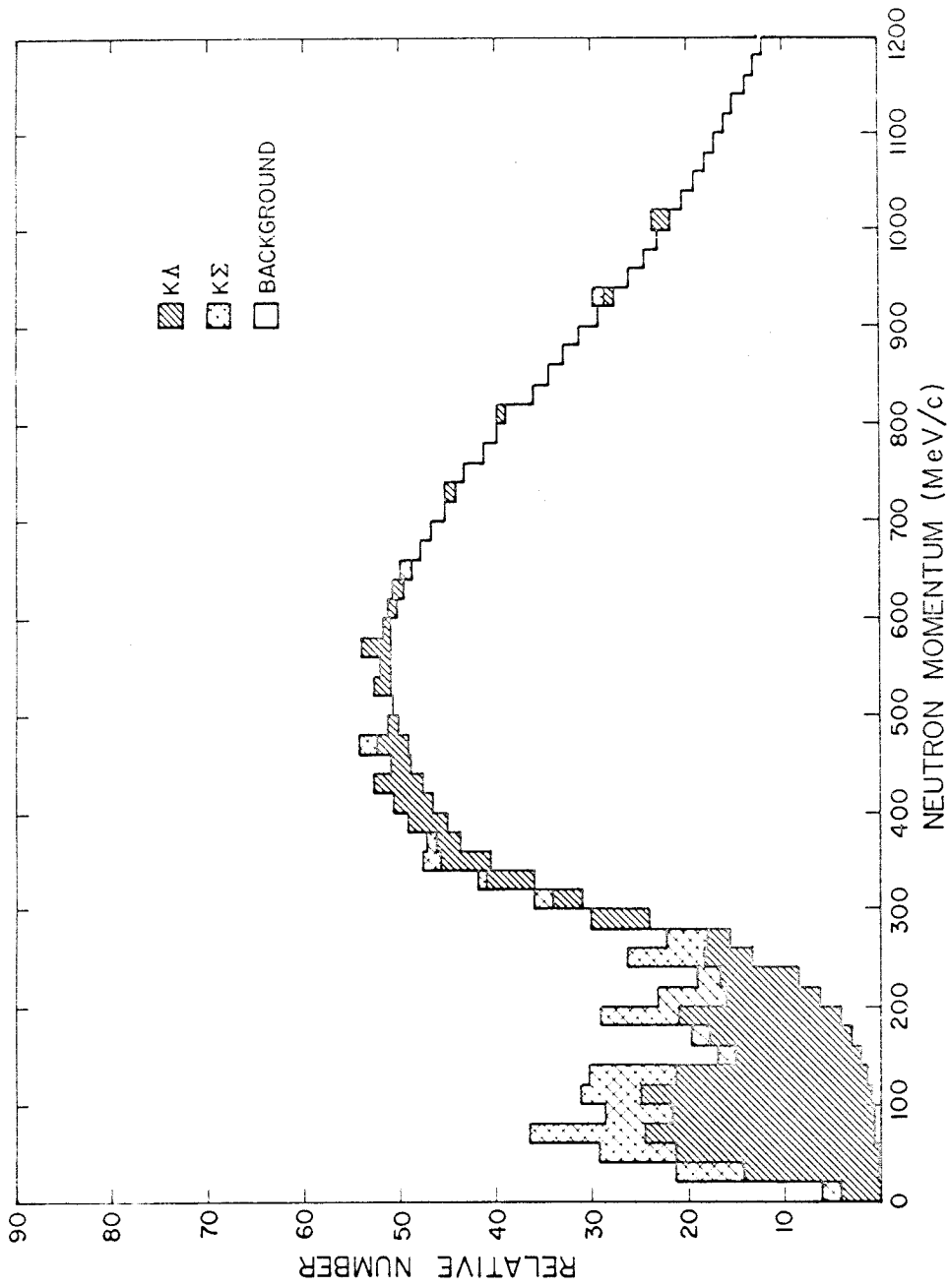
FIGURE 7: DISTRIBUTION OF NEUTRON MOMENTUM OF EVENTS AND BACKGROUND
FOR ROUGH ANALYSIS OF MONTE CARLO EVENTS
[MEASUREMENT ERROR AND SCATTERING INCLUDED]
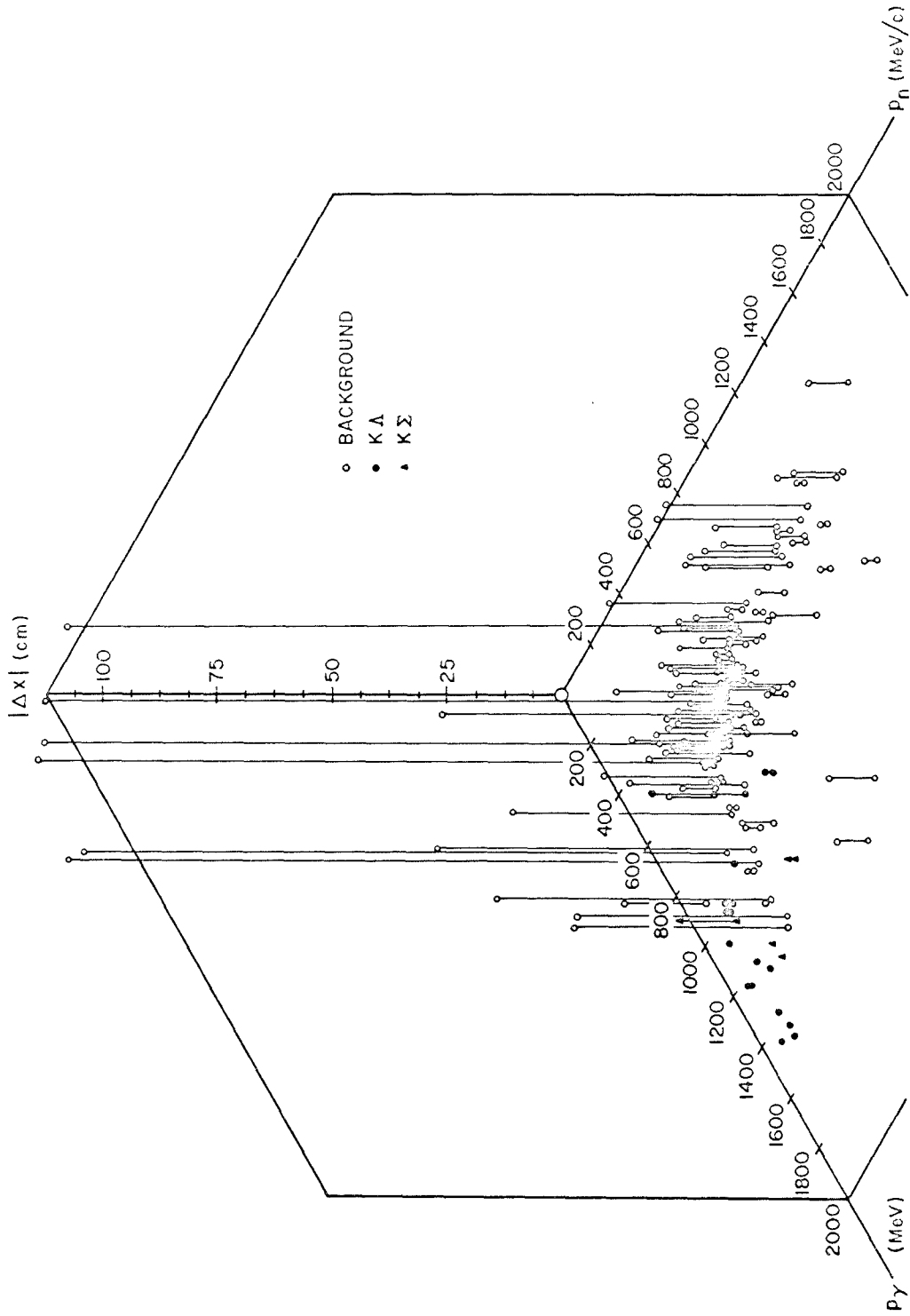
FIGURE 8: ONE 3-DIMENSIONAL SEPARATION OF MONTE CARLO
EVENTS AND BACKGROUND (ROUGH ANALYSIS)
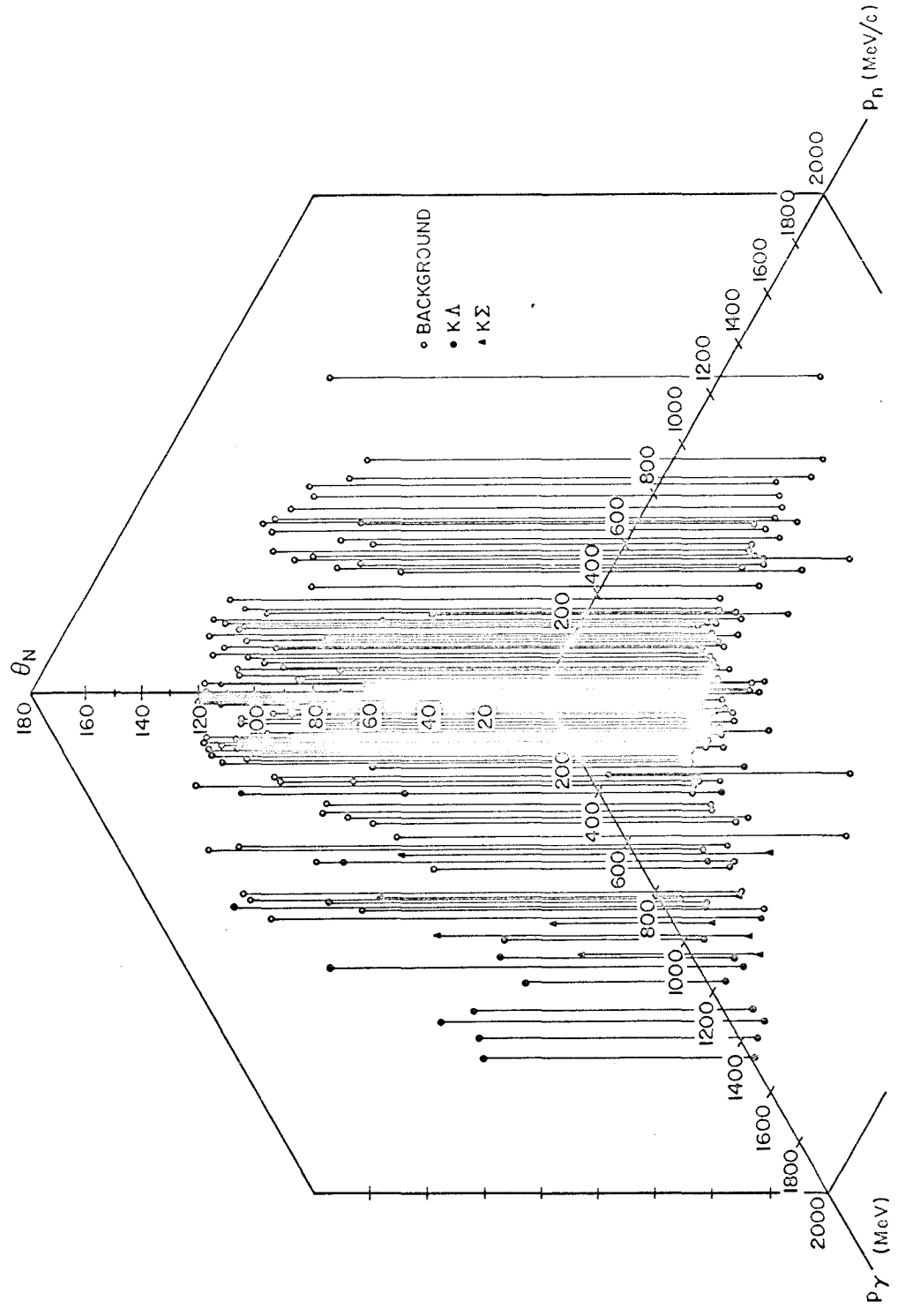
FIGURE 9: ANOTHER 3-DIMENSIONAL SEPARATION OF MONTE CARLO EVENTS AND BACKGROUND (ROUGH ANALYSIS)

the photon "slows down" to ≈ 700 MeV/c. The two origins are random
and tend to have large separations.

A later run on very accurate Monte Carlo events produced
analogs to the above graphs, but with poorer statistics. The peaks
and concentrations tended to smear into one another, making this
analysis system give results that are more ambiguous than before;
the skepticism leading to the construction of a more exact system was
justified.

C. Refined Analysis System

To try to assure that a negative result of this experiment
would be physical and not attributable to analysis, a fitting program
was written for the final analysis. Details of this calculation may be
found in Appendix II; a short synopsis is given here.

An event assumed to be a KΛ production, with final state
particles identifiable, can be described by 15 independent variables:

Spacial	Origin of event	3
	Decay lengths of K, Λ	2
	CM angles of a π in K, p in Λ	4
Energetic	3-momentum of neutron	3
	3-momentum of K	3
		15

If a likelihood function[33] is generated giving the probability that a
given set of 15 variables would lead to the physical measurement
made, and this probability is maximized with respect to the variables,
then one obtains the best possible estimate for those variables for

that measurement, and a χ^2 test for the significance of that result.

The exact likelihood function for this reaction could be written down, but was useless because the necessary lengths of computation exceeded all capacity, time and cost limitations.

As usual, discretion in making approximations to physical reality reduced the complexity to a manageable state. Proof that considerable pith survived the approximations may be shown by the physical ingredients and the test results, described below. The formulation included:

(a) Complete interdependence of all portions of the problem wherever possible.

(b) Inclusion of a priori knowledge of beamline position and distribution.

(c) Inclusion of a priori knowledge of neutron momentum wave function.

(d) Inclusion of a rough momentum measurement (multiple scattering) as a starting approximation, and a good momentum measurement (from stopping particles).

(e) Automatic restrictions against unreal conditions (particles with lower energies than implied by track length, or the unreal member of a double-valued solution).

(f) Inclusion of all point measurement errors due to digitizing error and point-reconstruction error.

(g) Use of the approximate multiple scattering distribution for two track points, with corrections for the correlation between the

points and modification in case two points were not available.

(h) Choice of all possible particle identifications consistent with
     KΛ production.

To insure that Monte Carlo events used to test the program
were precisely like real events might be, they were created in such
a way as to include the human biases usually present. After an event
was initially generated, it was plotted by the computer, using dots
like bubbles, in a manner simulating projection on the scanning
machine, and scaled accordingly (Appendix I). The same persons
who analyzed the real data selected the points on the tracks as they
usually did (not according to how they had been trained!). Measure-
ment and reconstruction errors, checked against the distributions
for real data, were then folded in.

The 15 + 1 - dimensional terrain of the likelihood function
(or more properly, its negative log) is extremely complex, ap-
parently containing both local minima at no physical solution and
considerable obstacles to convergence of the hapless event that starts
too far away from the true minimum. Thus the reliable manner in
which the analysis program converges on the events, given two in-
dependent measurements, is gratifying. This result is shown in
Table 2 , where it is seen that the program is about 98% efficient.
Further properties of the convergence are shown in the next series
of graphs. Figure 10 shows that the X^2/N distribution is quite reason-
able and sharp, but that all hope of distinguishing between KΣ and KΛ
is lost, since the KΣ distribution shows the same character. Figure 11

Table 2

Purification of Sample by Kinematic Fitting

Requirement	Surviving Fraction of Initial No. of Events		Background/Foreground (using predicted number of counts)
	$K\Lambda$	$K\Lambda$	
$\chi^2 \leq 100$	$98.5 \pm 1\%$	$98.5 \pm 1\%$	43
Origin, γ-Energy Physical	$96.5 \pm 1.4\%$	$93.6 \pm 2.2\%$	9
$\chi^2/N \leq 2.25$	$94.6 \pm 1.7\%$	$88.9 \pm 3.0\%$	1.8
[Include Pre-analysis Scanner Tests]	$93.7 \pm 2.5\%$	$87.0 \pm 3.5\%$	1.8
Neutron Momentum ≤ 200 MeV/c	$87.6 \pm 3.6\%$	$82.4 \pm 7.1\%$	.4
(Particle Identification)	$(73.1 \pm 4.0\%)$	$(68.9 \pm 8\%)$	(0)

shows that for $K\Lambda$ the derived photon energy is unbiased and good to about 3%, while for $K\Sigma$ (Figure 12) it is biased downwards by about 8% (the program tries to compensate for the energy carried off by the γ in $\Sigma^\circ \to \gamma + \Lambda^\circ$ by decreasing the all-over scale of energies. The mean γ has $\sim$ 90 MeV, so this is almost exactly right). Figures 13 and 14 show the basic correctness, but large uncertainty, of the neutron momentum. It is biased toward zero by the nature of the constraint. Figure 15 shows that the x-component (along the beam) of the neutron momentum is unbiased with respect to zero, an important result because background would be expected (as in the crude analysis) to show a strong bias toward large negative P_{n_x}. Figures 16 and 17 prove that the origins can be well located, justifying rejections of events produced in non-physical locations. Similar graphs, not shown, prove that the K energy and angle are good to within a few percent. Finally, the Monte Carlo analysis and results from Fretwell's experiment show that 16% of events will have particle identification mistakes because an alternate hypothesis looks better, and/or because of an incorrect subjective judgement.

The dot plot shown in Figure 18 really includes most of the aspects of the 5-dimensional background separation with respect to P_n, θ_n, W_γ, X_o and χ^2. If the restrictions are made, using the above graphs, that $\chi^2/N \leqslant 2.25$, $800 \leqslant W_\gamma \leqslant 1600$, $-17 \leqslant X_o \leqslant + 10$, and $P_n \leqslant 200$, then surviving events should be well separated from background. These physical restrictions let 86 % of Monte Carlo events survive.
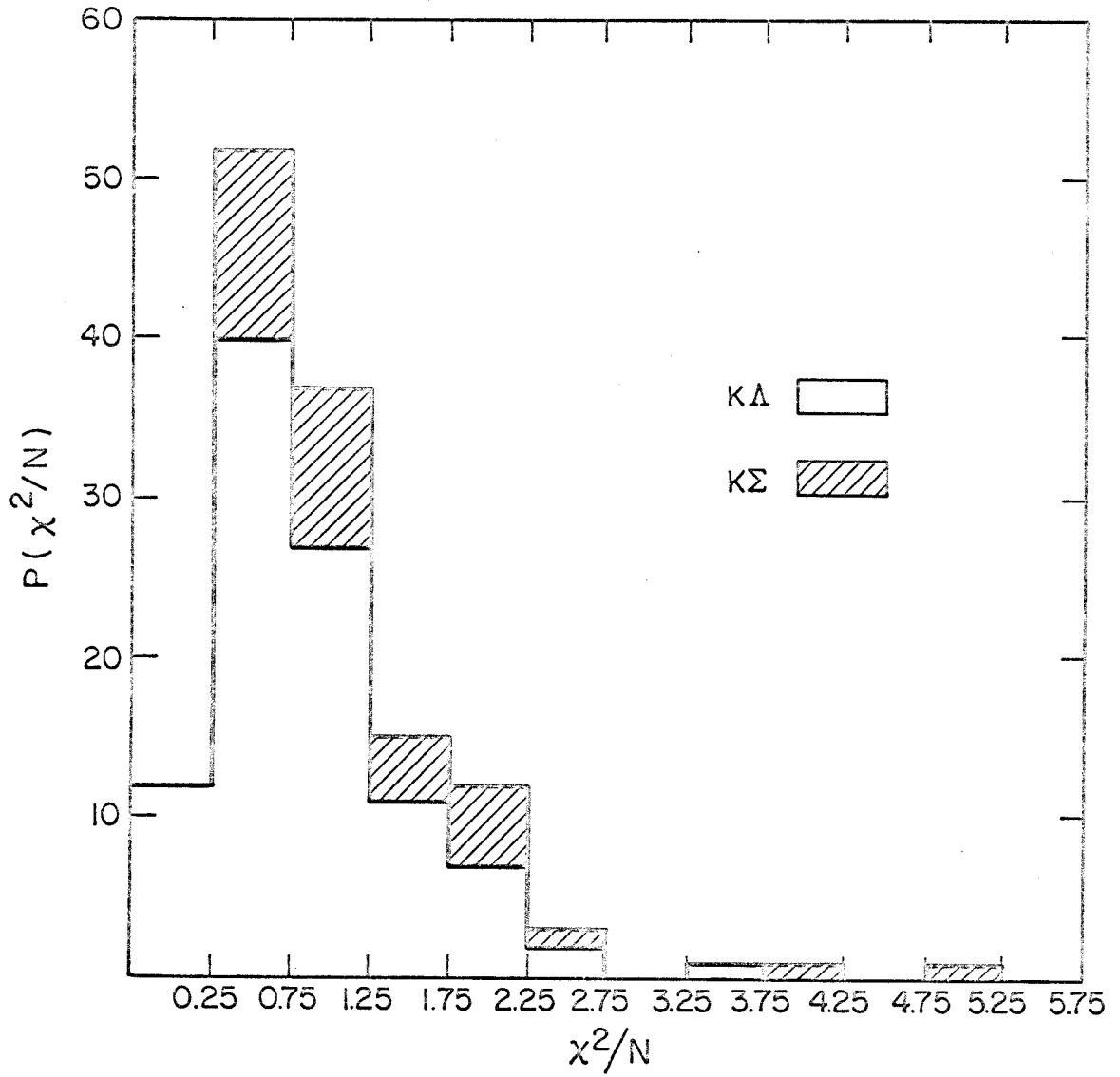
FIGURE 10: DISTRIBUTION OF (χ^2/DEGREES OF FREEDOM)
FOR MONTE CARLO GENERATED EVENTS
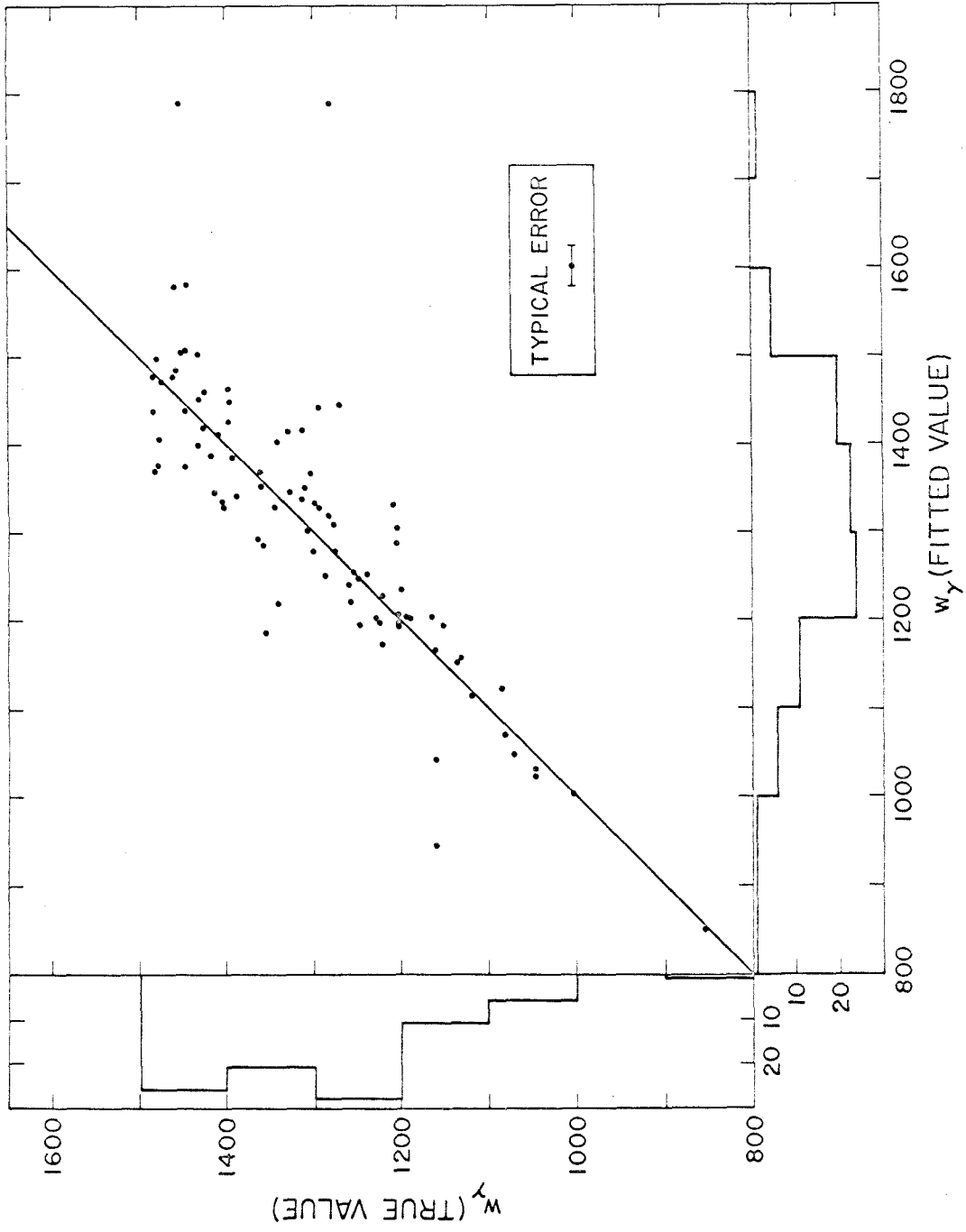
FIGURE II: PHOTON ENERGY DISTRIBUTION OF MONTE CARLO GENERATED KA EVENTS
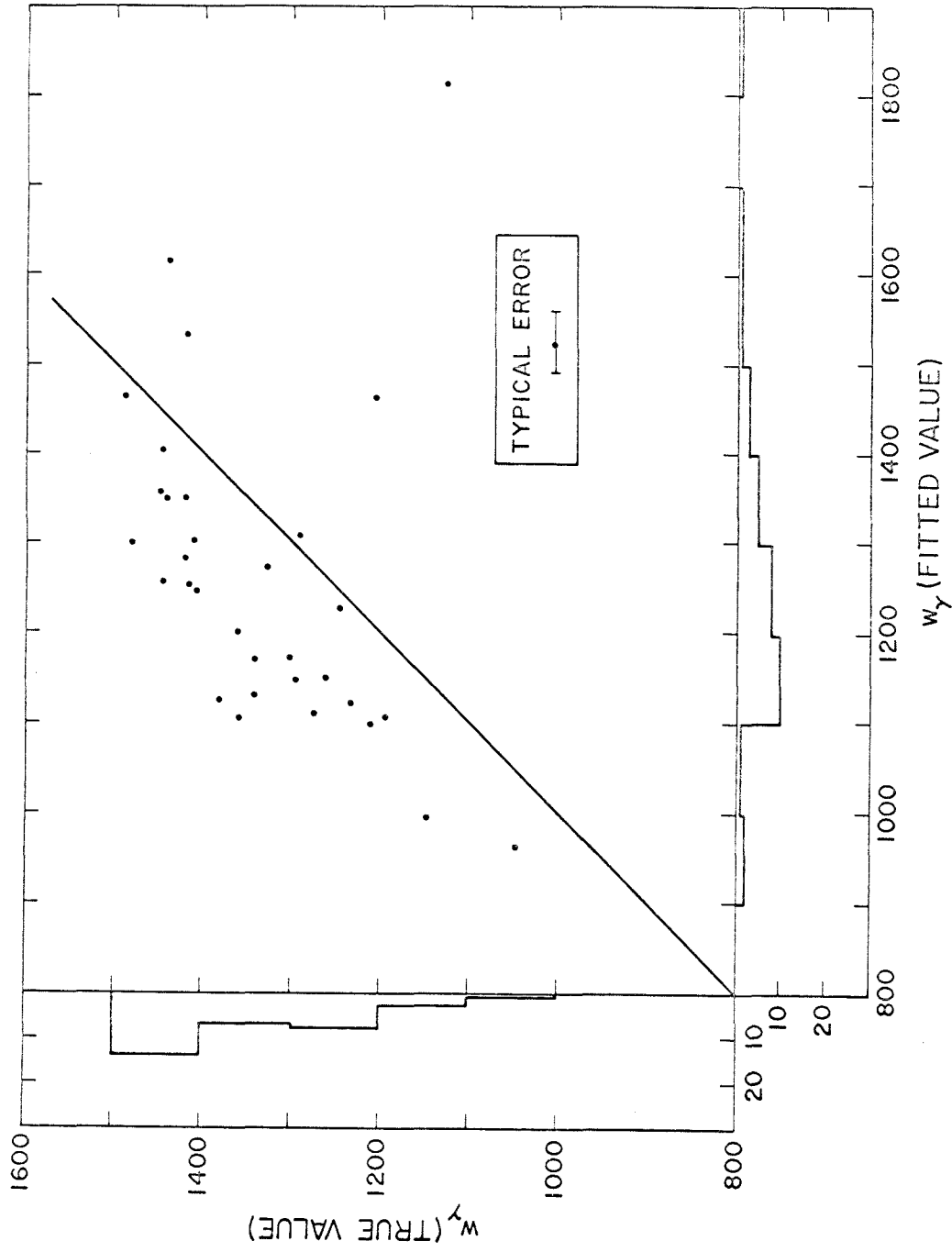
FIGURE 12: PHOTON ENERGY DISTRIBUTION OF MONTE CARLO GENERATED KΣ EVENTS
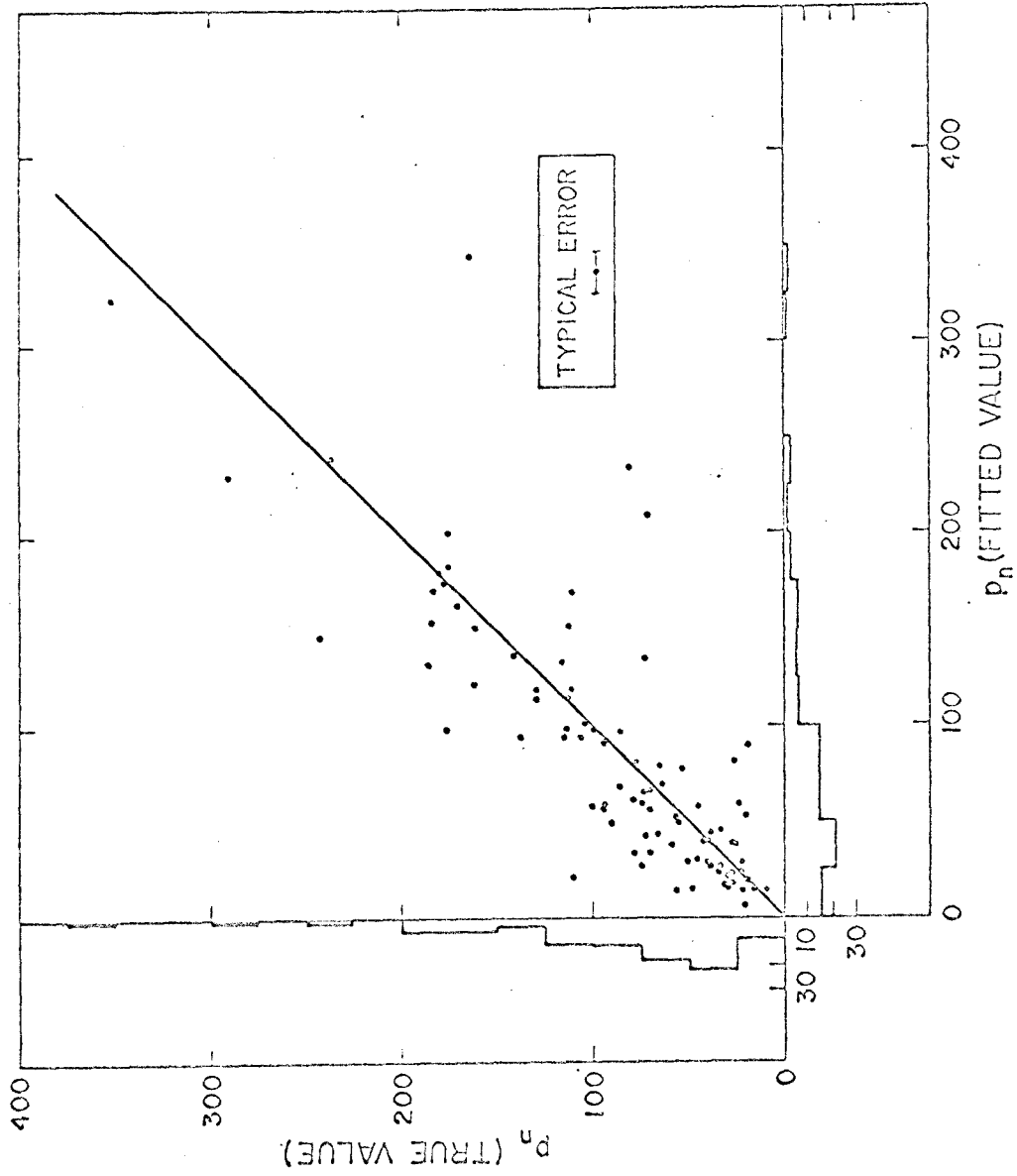
FIGURE 13: NEUTRON MOMENTUM DISTRIBUTION OF MONTE CARLO GENERATED KA EVENTS
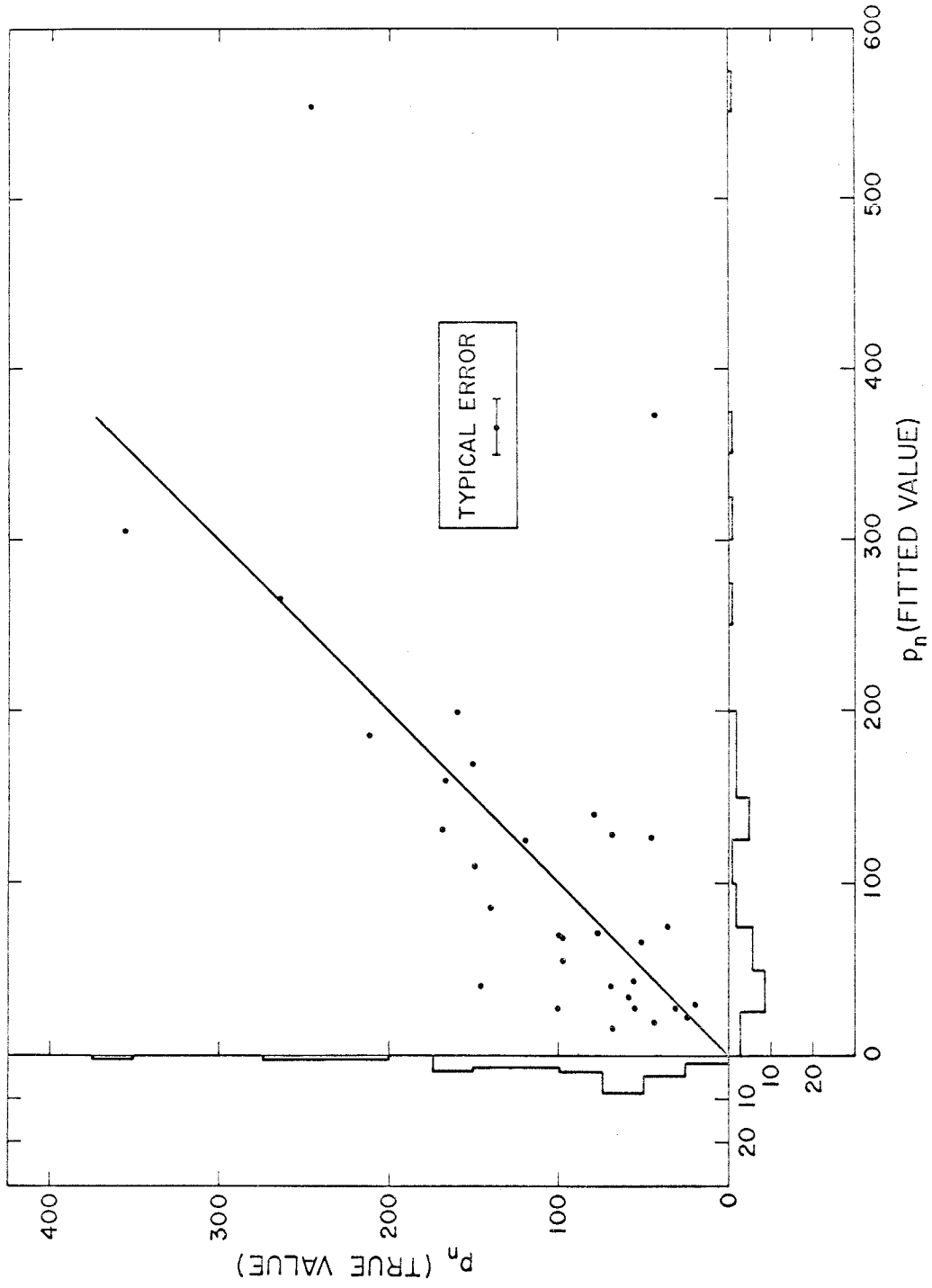
FIGURE 14: NEUTRON MOMENTUM DISTRIBUTION OF MONTE CARLO GENERATED $K\Sigma$ EVENTS
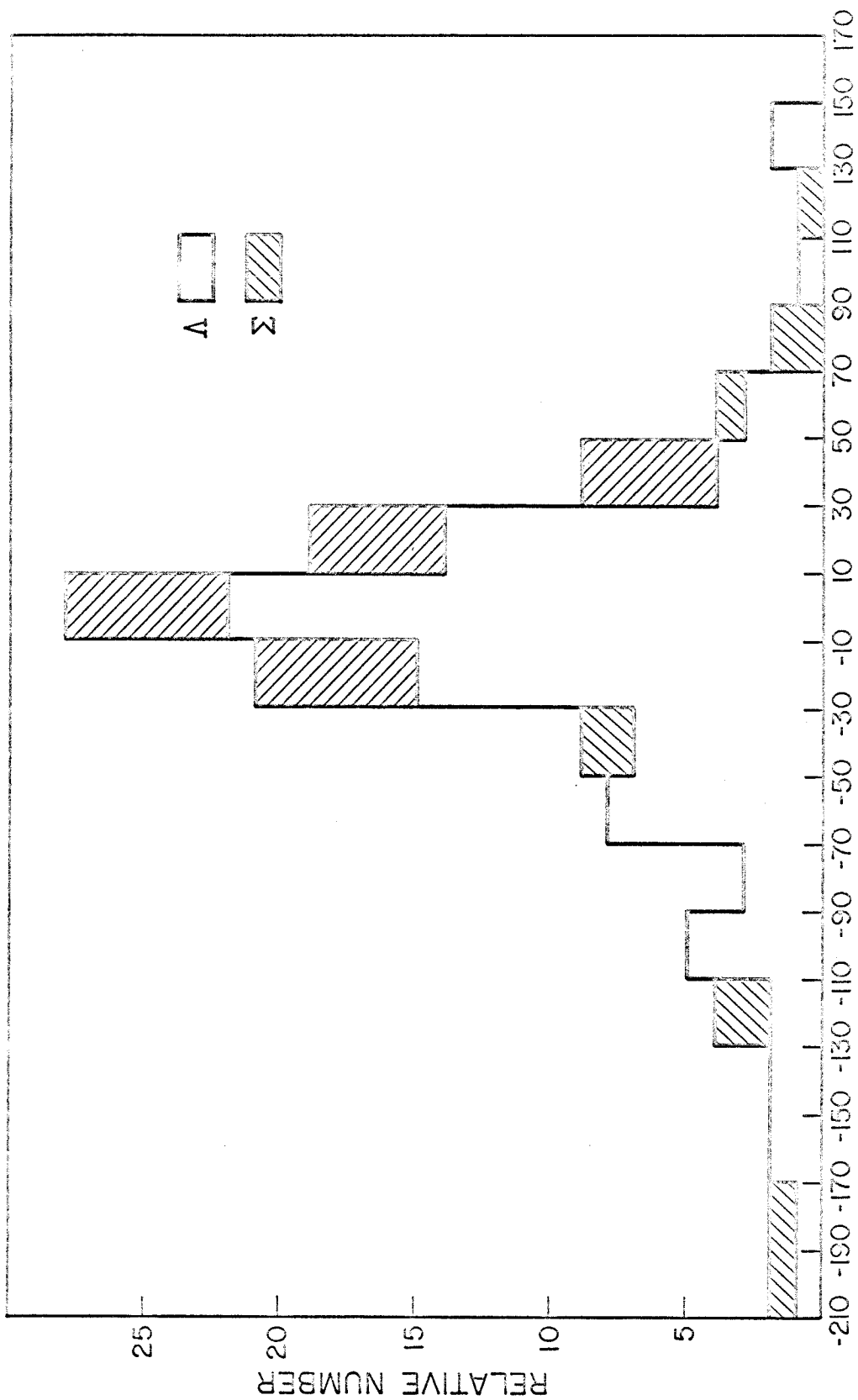
FIGURE 15: p_{n_x} DISTRIBUTION OF NEUTRON BEAMLINE COMPONENT OF MOMENTUM (MeV/c)
(MONTE CARLO EVENTS KINEMATICALLY FITTED)
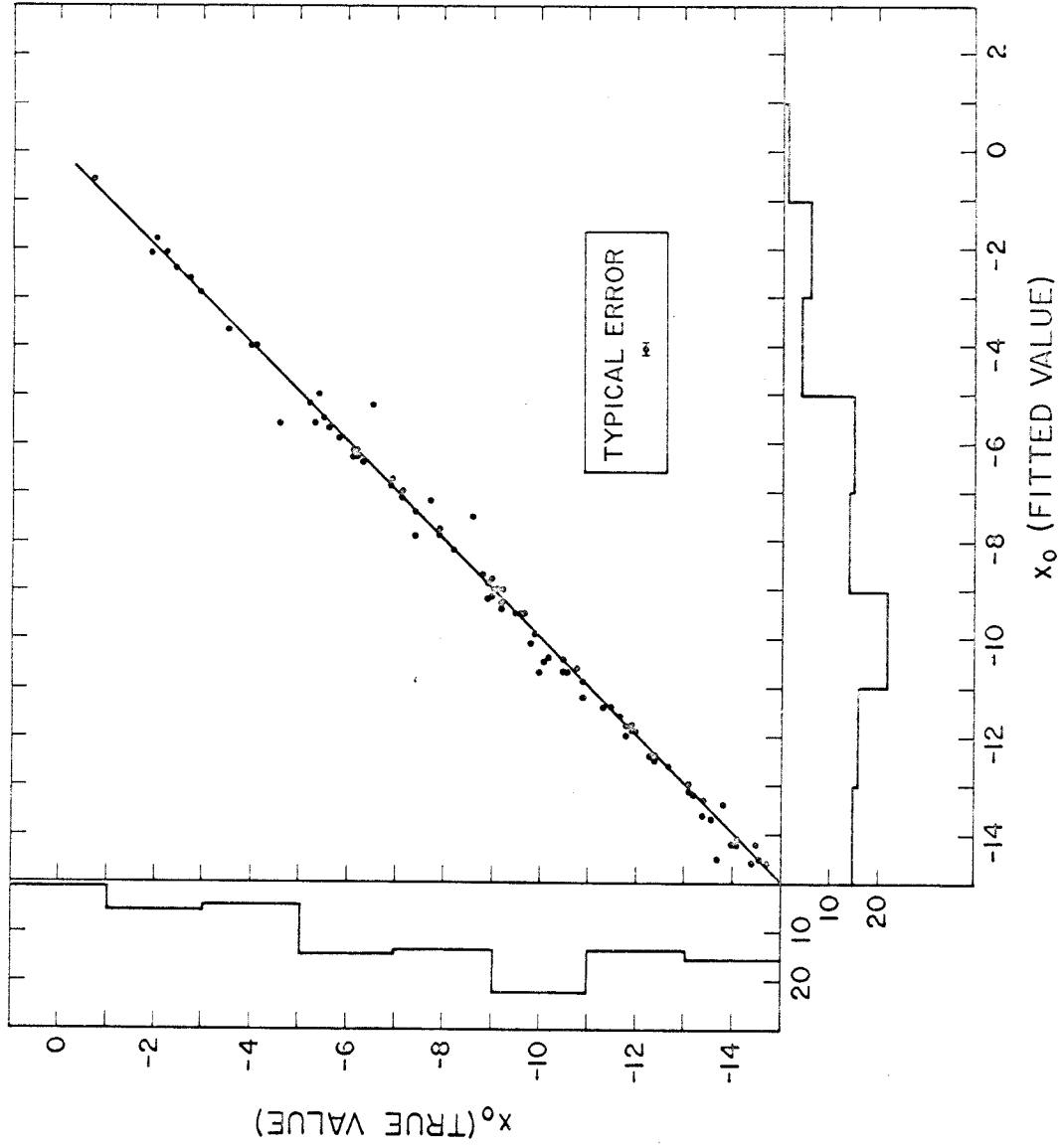
FIGURE 16: ORIGIN DISTRIBUTION OF MONTE CARLO GENERATED KA EVENTS
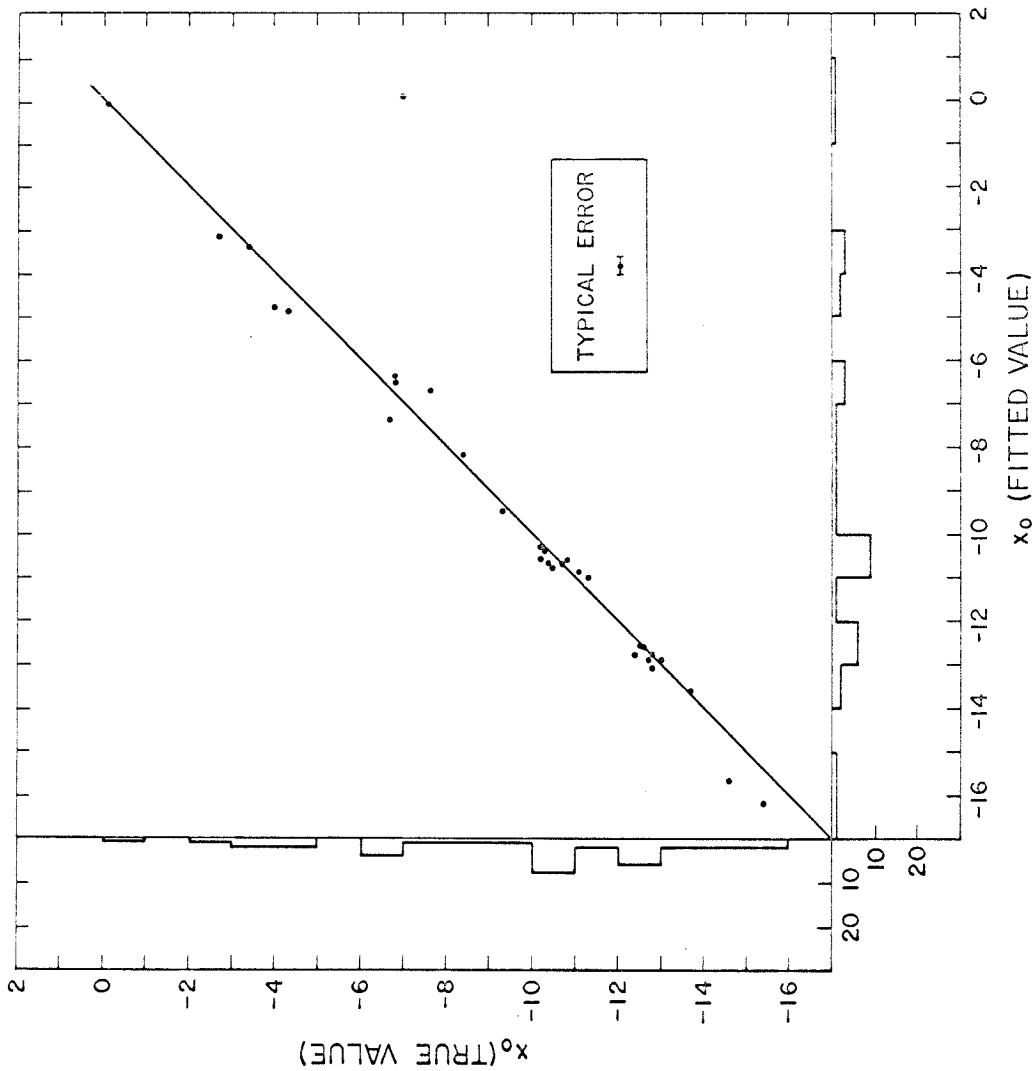
FIGURE 17: ORIGIN DISTRIBUTION OF MONTE CARLO GENERATED KΣ EVENTS
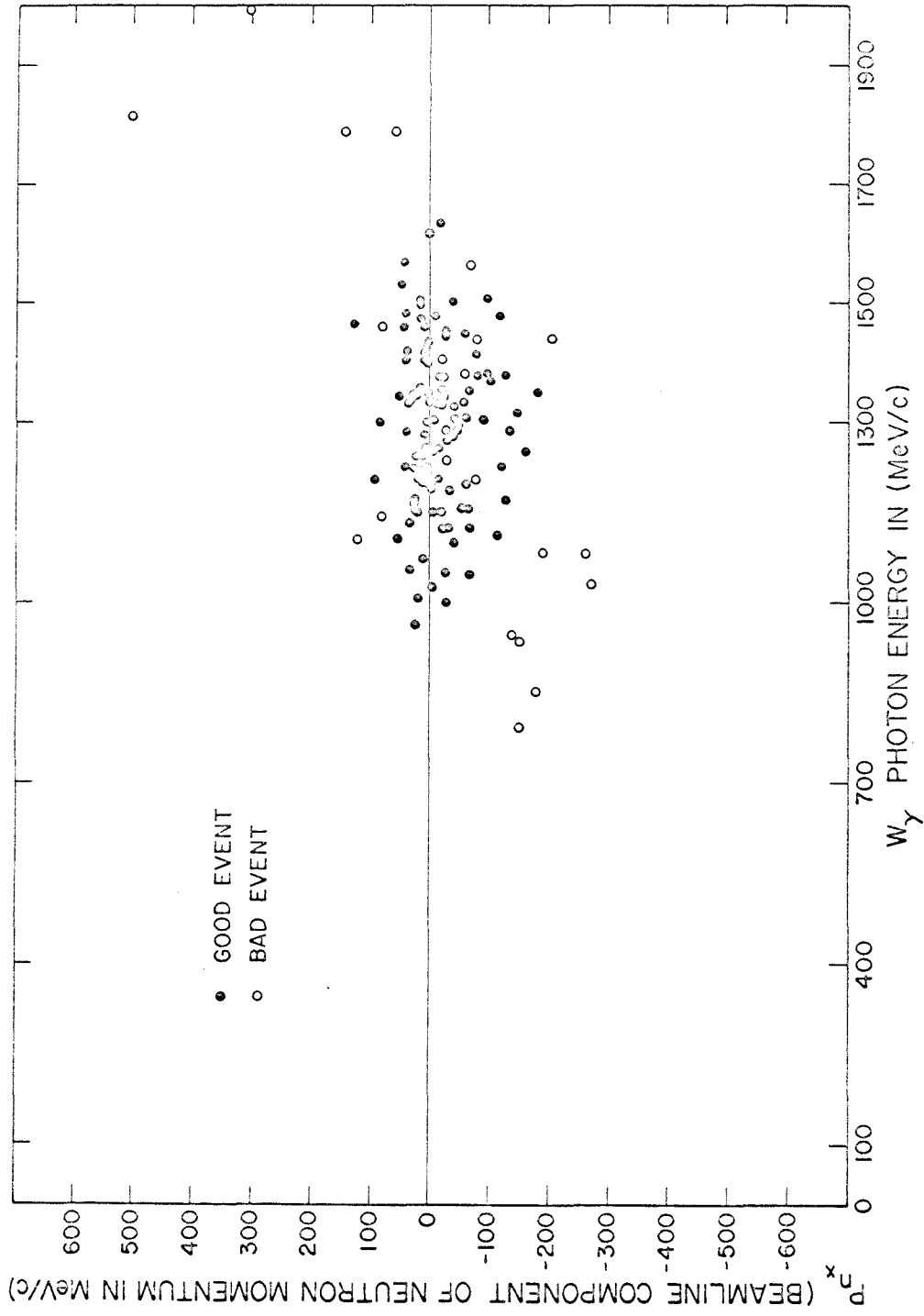
FIGURE 18: EFFECT OF MAXIMAL RESTRICTIONS
ON ANALYSIS OF MONTE CARLO EVENTS

No background calculation analogous to that for the simple analysis was attempted because the plethora of assumptions inherent in it would negate any result. Moreover, the real distribution of background is almost impossible to calculate, and the way in which the analysis program might treat background is impossible to calculate. The results of this experiment will mainly represent background events, and if the characteristic peaks and clusterings as seen in the foreground Monte Carlo results do not appear above background, then a null result (no experimental knowledge) must be accepted. If the background is also absent from these regions, a negative result (valid limits on the nature of the reactions) is obtainable.

V. RESULTS

1. Analyzed Events

A. Approximate analysis. The simple analysis program described in Part IV-2B was applied to all candidates gleaned from 13,832 pictures. The momentum distribution of the neutron (Figure 19) taken from the best hypothesis (for particle identification) of accepted events, shows no peak near 100 MeV/c, as expected from Figure 7. The multi-dimensional distribution of photon energy vs. neutron momentum vs. origin error, Figure 20, shows some indication of an event or two near the appropriate region (see expected behavior in Figure 8), but certainly no grouping in that region. As expected, this analysis gave an ambiguous result.

B. Detailed analysis. The various methods of displaying the results of the kinematic fitting are shown for two cases: a) all events regardless of acceptance (best hypothesis is taken to be lowest χ^2/N = degrees of freedom), and b) events passing the restrictions that $\chi^2/N < 2.25$, the event be produced in D_2 and not in vacuum, the photon energy be between 800 and 1600 MeV, and that the neutron Fermi montum be $\leq$ 200 MeV/c. The attenuation due to these factors is not large, as discussed in Part IV.

Figures 21, 22 show the distribution of χ^2/N. The background peak is near the region of interest, but both histograms indicate no peak or shoulder near χ^2/N = .75.
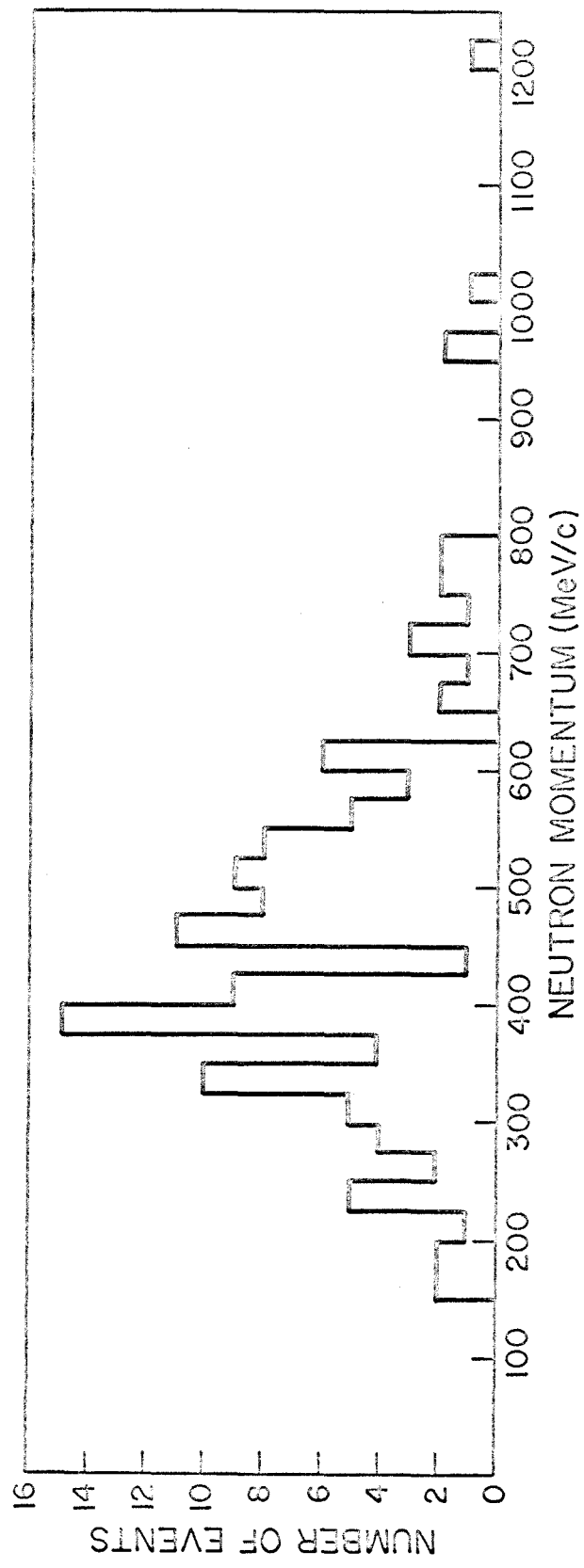
FIGURE 19: NEUTRON MOMENTUM DISTRIBUTION (ROUGH ANALYSIS OF DATA)
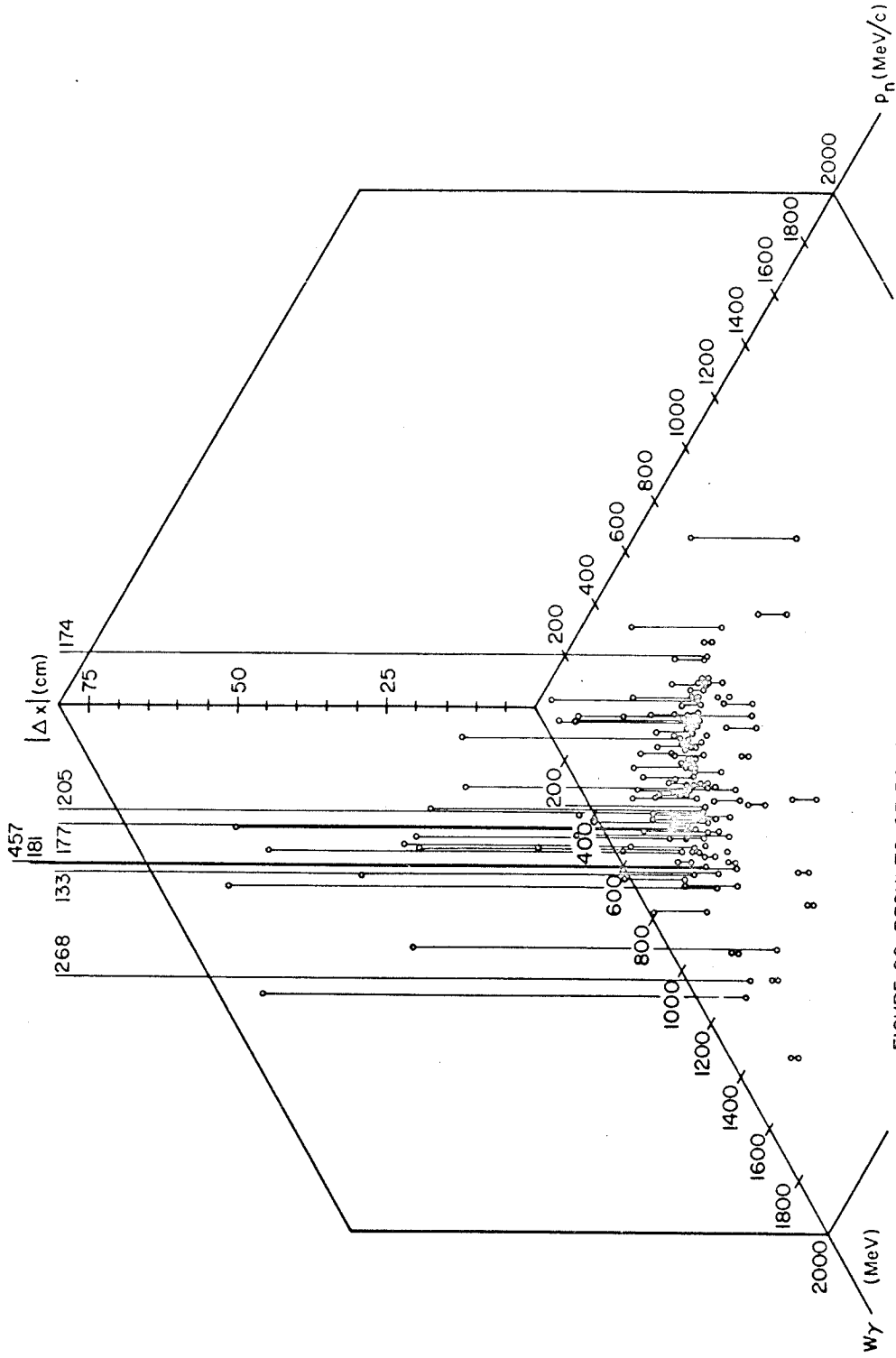
FIGURE 20: RESULTS OF ROUGH ANALYSIS SYSTEM OPERATING ON DATA
(3- DIMENSIONAL SEPARATION)

FIGURE 21: χ^2/N DISTRIBUTION (NO RESTRICTIONS)
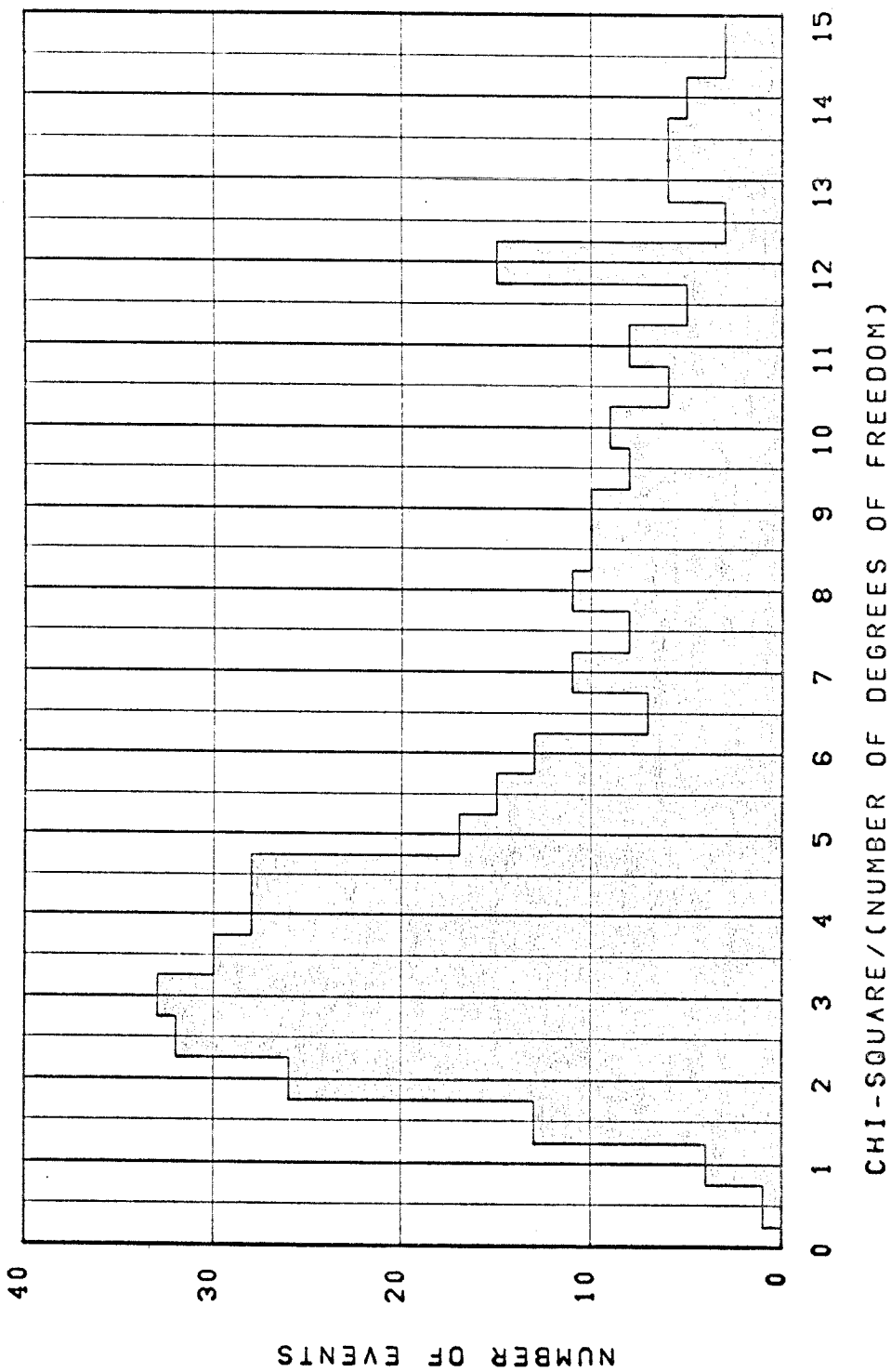
FIGURE 22: x^2/N DISTRIBUTION (ALL RESTRICTIONS)
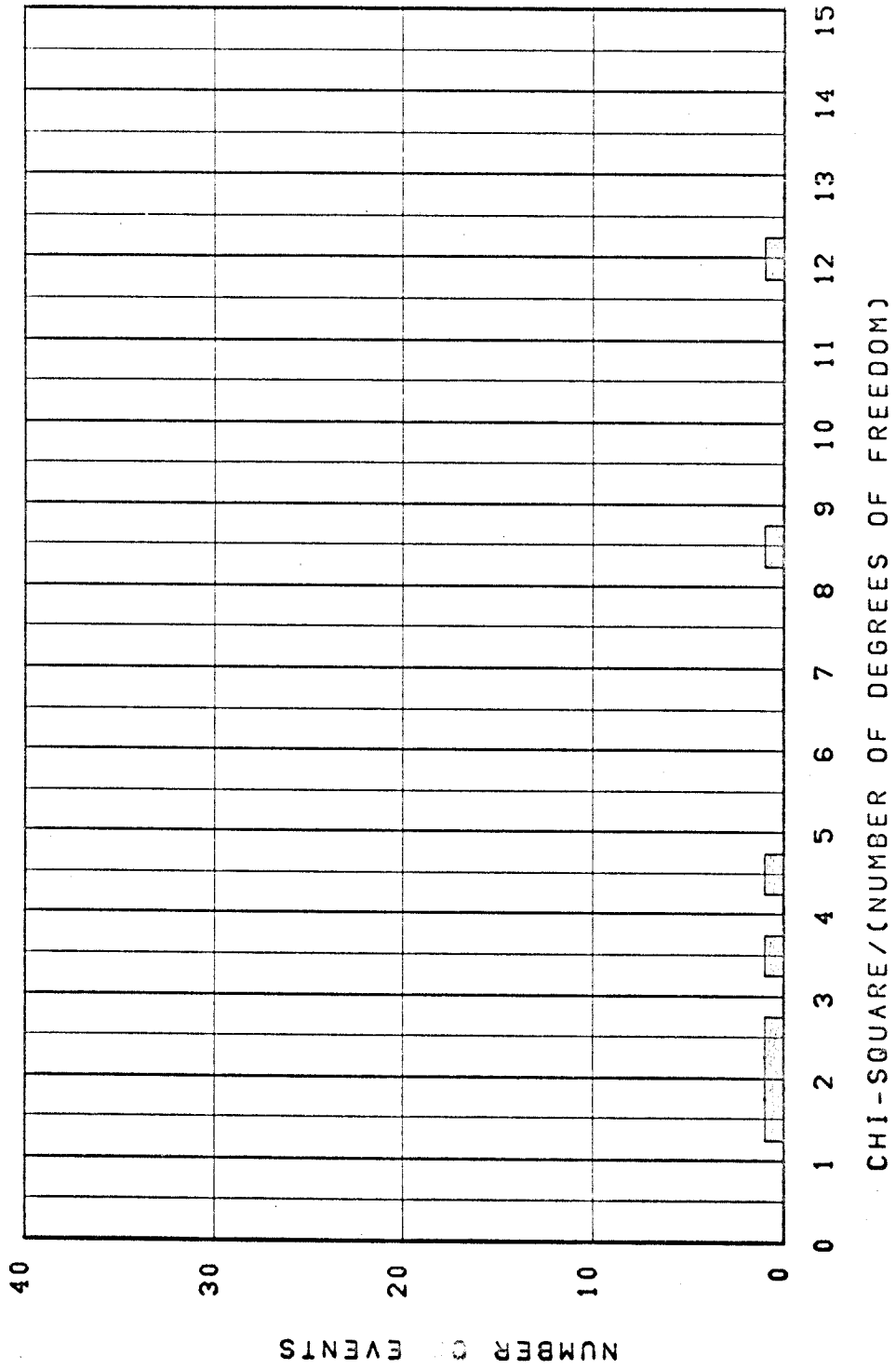
The neutron Fermi momentum distribution shows a great deal of background for all events (Figure 23) but the restricted set of events has practically no background at all, (Figure 24) and is particularly vacant near the expected peak (Figure 13).

No event in the restricted set had its particle identification consistent with a true KY event. Most of these had simply been assigned four pion tracks.

The plot of beamline component , of neutron momentum vs. photon energy (Figure 25) has many candidates in the physical region, but when the restrictions are applied, Figure 26 shows only two survive.

The surviving candidates of these tests can now be examined in detail. Since no candidate passed all the objective tests above (including particle identification), and since the background is sufficient (in the "tail" regions where these candidates occur) to account for their presence, subjective examination is required only to increase confidence in the results. Table 3 gives some of the characteristics of these "peripheral" solutions. One clue is the repeatability of the solution to successive measurements. While Monte Carlo events repeat as solutions to better than 90%, background events seem to have solutions characteristic of shallow minima in the likelihood function and a remeasurement usually eliminates this minimum or changes it drastically. The next strongest subjective test is an independent determination of the particle

FIGURE 23: P_n DISTRIBUTION (NO RESTRICTIONS)
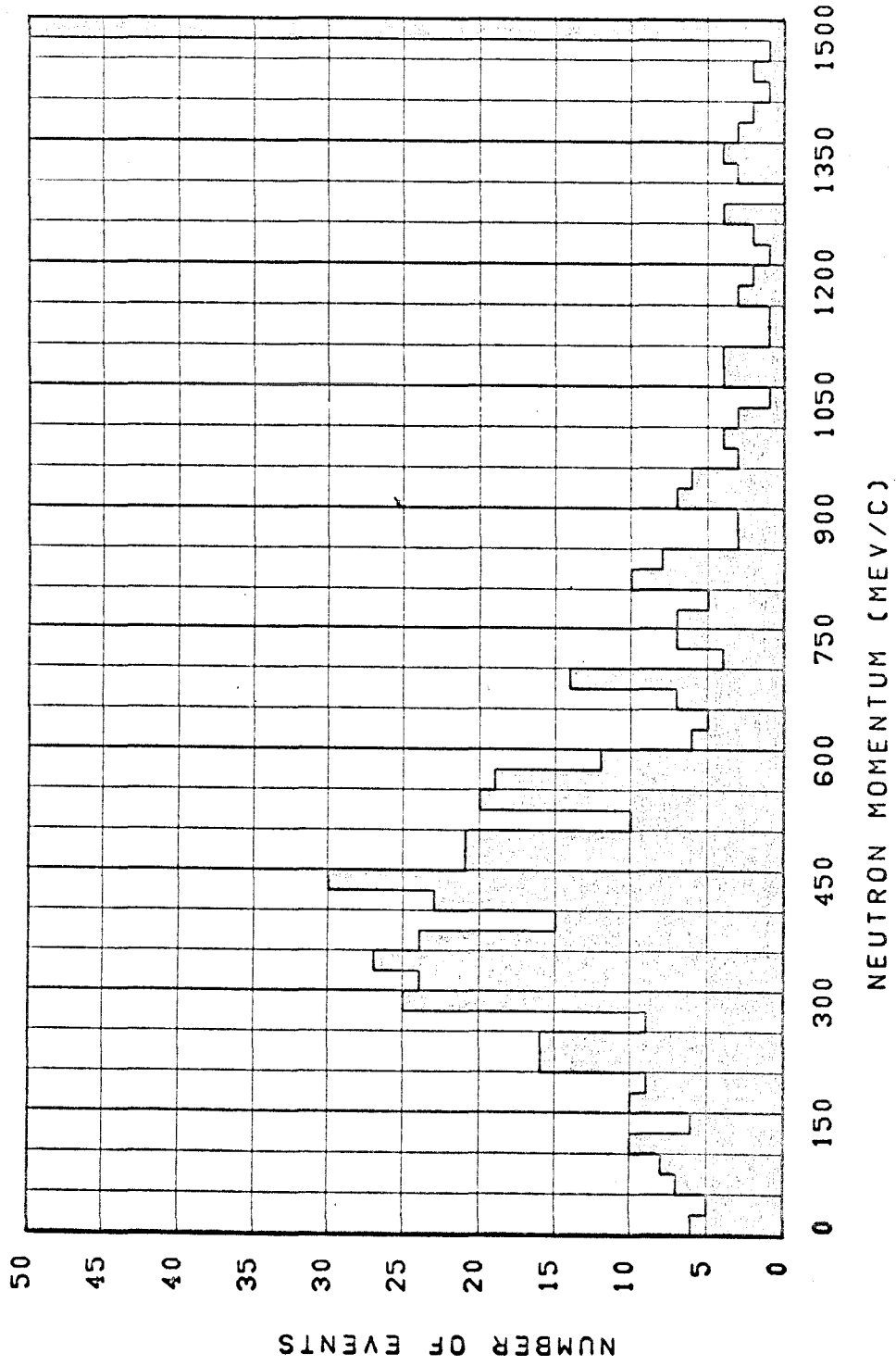
FIGURE 24: P_n DISTRIBUTION (ALL RESTRICTIONS)
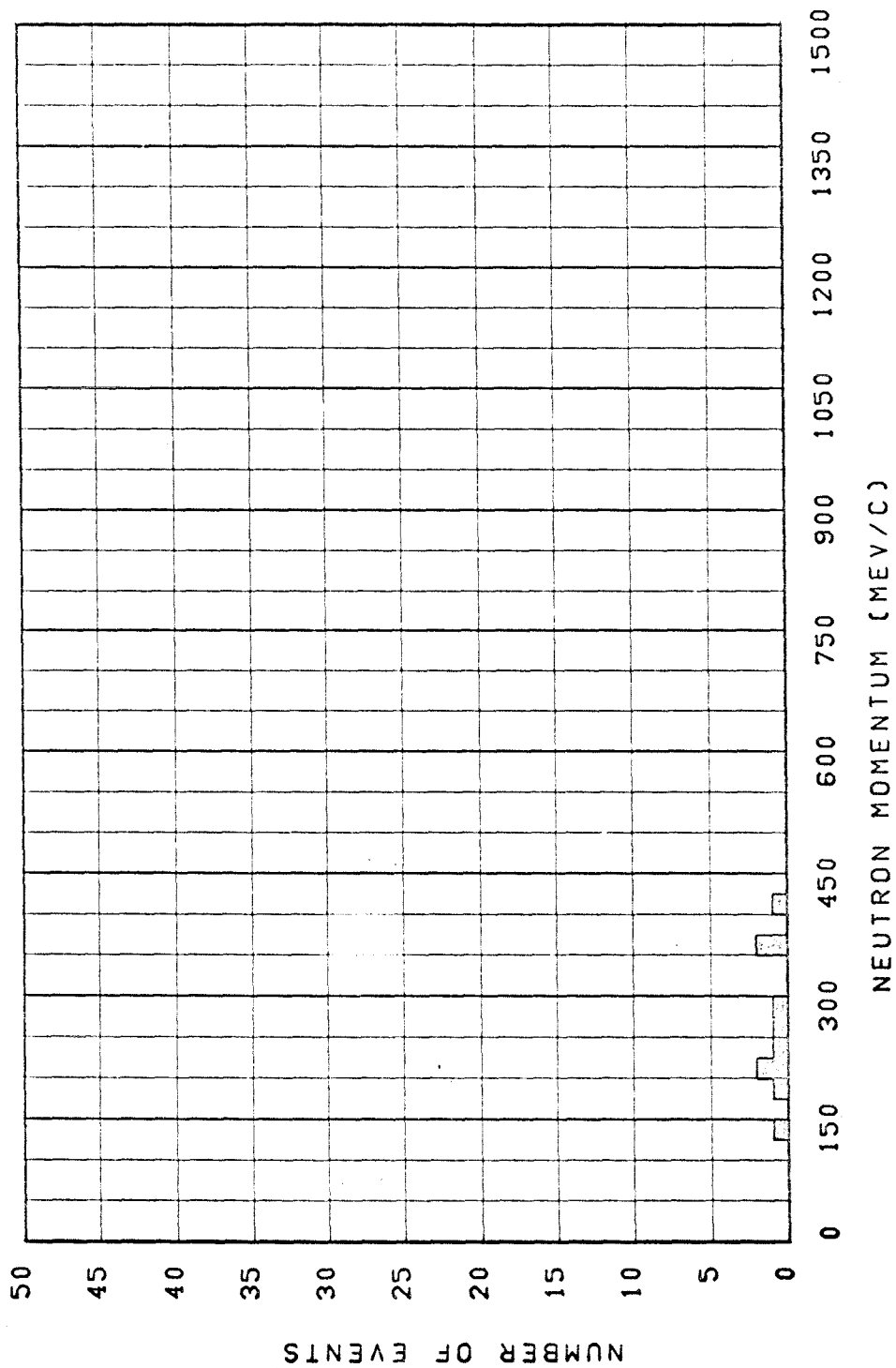
FIGURE 25: DATA DISTRIBUTION (NO RESTRICTIONS)
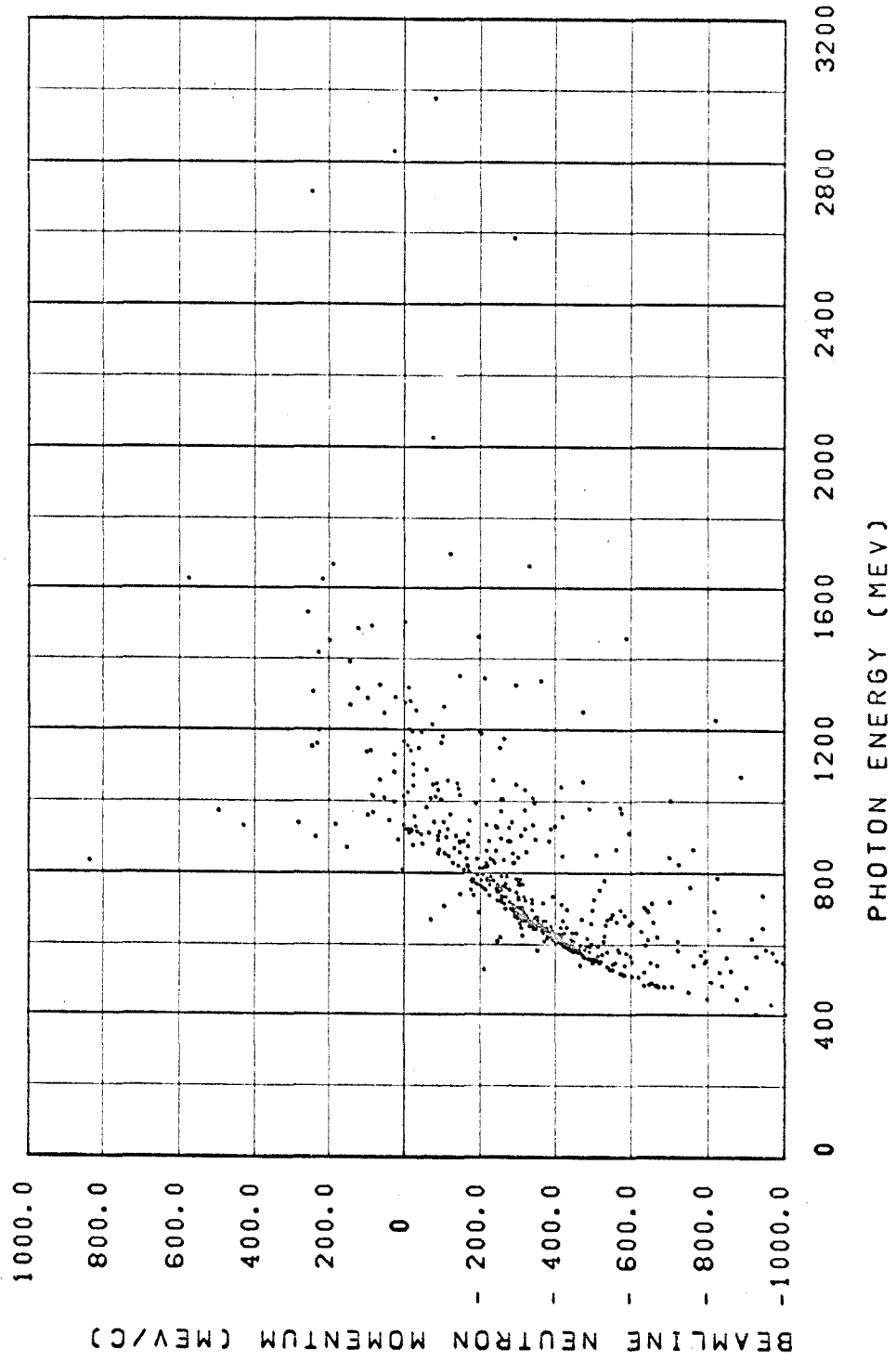
FIGURE 26: DATA DISTRIBUTION (ALL RESTRICTIONS)
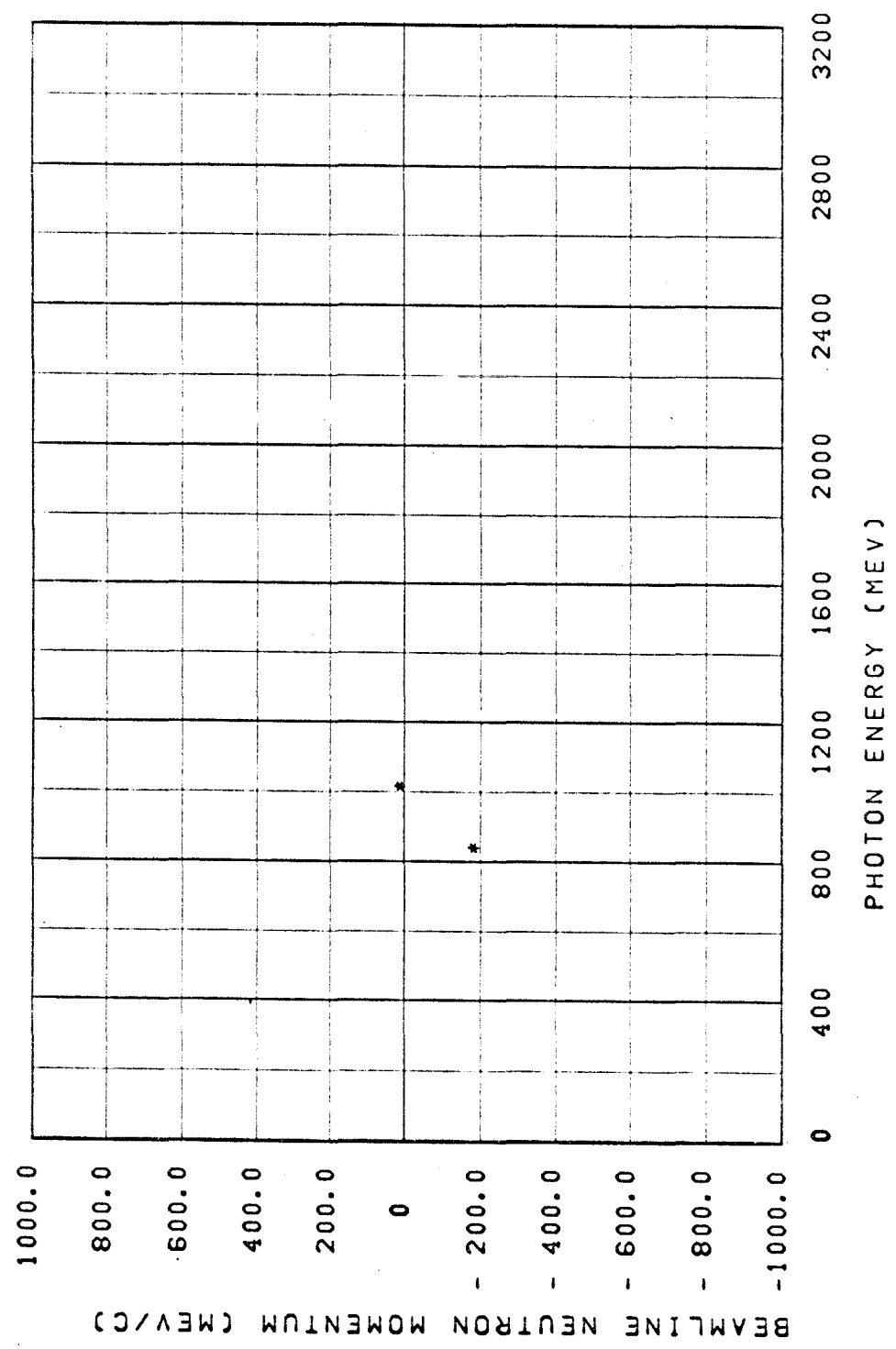
Table 3

Properties of Surviving "Events"

Test and Explanation		Event A $(\overline{W_\gamma = 842})$		Event B $(\overline{W_\gamma = 1014})$	
1. Repeatability (out of 7 analyses, was accepted N times, and probability P that this would happen to a true event)		N = 1 P = 1.5%		N = 1 P = 1.5%	
		MS	Program	MS	Program
2. Multiple Scattering (compares energy (MeV) from scattering of π's and p with that found in program)	π_1 π_2 π_3 p	22 ± 47 218 ± 133 117 ± 21 39 ± 22	116 225 76 26	58 ± 15 30 ± 15 59 ± 139 large	171 65 14 355
3. Visual appearance		Particle I.D. best as stated, but changes to p O.K. Event A has a likely electron pair			
4. Self-consistency of solution (max. deviation from initial angles)		48°		24°	
(implied Λ angle/observed Λ angle)		12°/21°		3°/8°	
(observed decay distance/ expected decay distance of K and probability P of this result)		18.2/2.4 P < .1%		21/.7 P < .1%	
(same as above for Λ)		9.6/6 P consistent		14/6	

momentum by multiple scattering measurements[34] to see if it agrees within errors with the computer solution. It can be seen that no event is subjectively reasonable, all having highly unphysical characteristics. This is not true of Monte Carlo generated events, which normally have all characteristics simultaneously reasonable.

The objective and subjective conclusions are thus in agreement and state that no events of either $K\Lambda$ or $K\Sigma$ were seen in this experiment.

2. Probability Statement of Result

Appendix III describes in detail how the expected number of events N^* and its error σ is generated from the average cross sections, measured beam flux, and calculated efficiencies. The result for this experiment, and its uncertainty, are given by

$$N^* = 0.712\,\bar\sigma_\Lambda + 0.327\bar\sigma_\Sigma$$

$$\sigma = \sqrt{1.466\bar\sigma_\Lambda^{\,2} + 0.415\,\bar\sigma_\Sigma^{\,2} + 0.878\,\bar\sigma_\Lambda\bar\sigma_\Sigma}\cdot 10^{-1}$$

For the nominal cross sections assumed in Part I, this gives

$$N^* = 5.15 \pm .82$$

Following Appendix III, the strongest statement of probability is: The probability that m valid events or less would be seen if the average cross sections are $\bar\sigma_\Lambda$ and $\bar\sigma_\Sigma$ is $W(m\,|\,N^*(\bar\sigma_\Lambda,\bar\sigma_\Sigma),\sigma(\bar\sigma_\Lambda,\bar\sigma_\Sigma))$.

The probability contours of W for this experiment (m = 0,1) are given in Figures 27, 28. While any conclusions are dependent on the
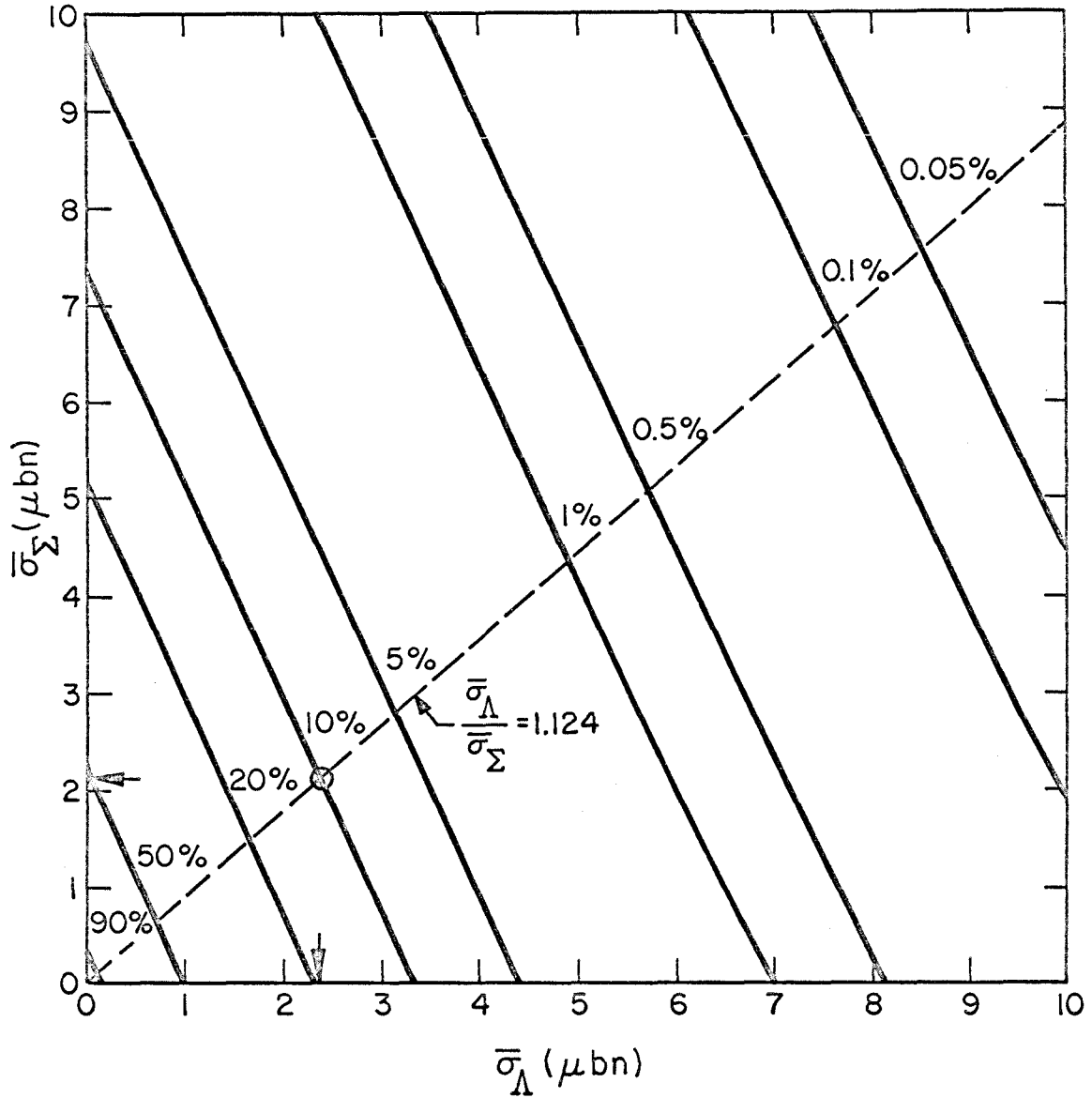
FIGURE 27: THE PROBABILITY THAT NO EVENTS ARE SEEN
IF TRUE CROSS SECTIONS ARE $\overline{\sigma}_{\Lambda}$ AND $\overline{\sigma}_{\Sigma}$
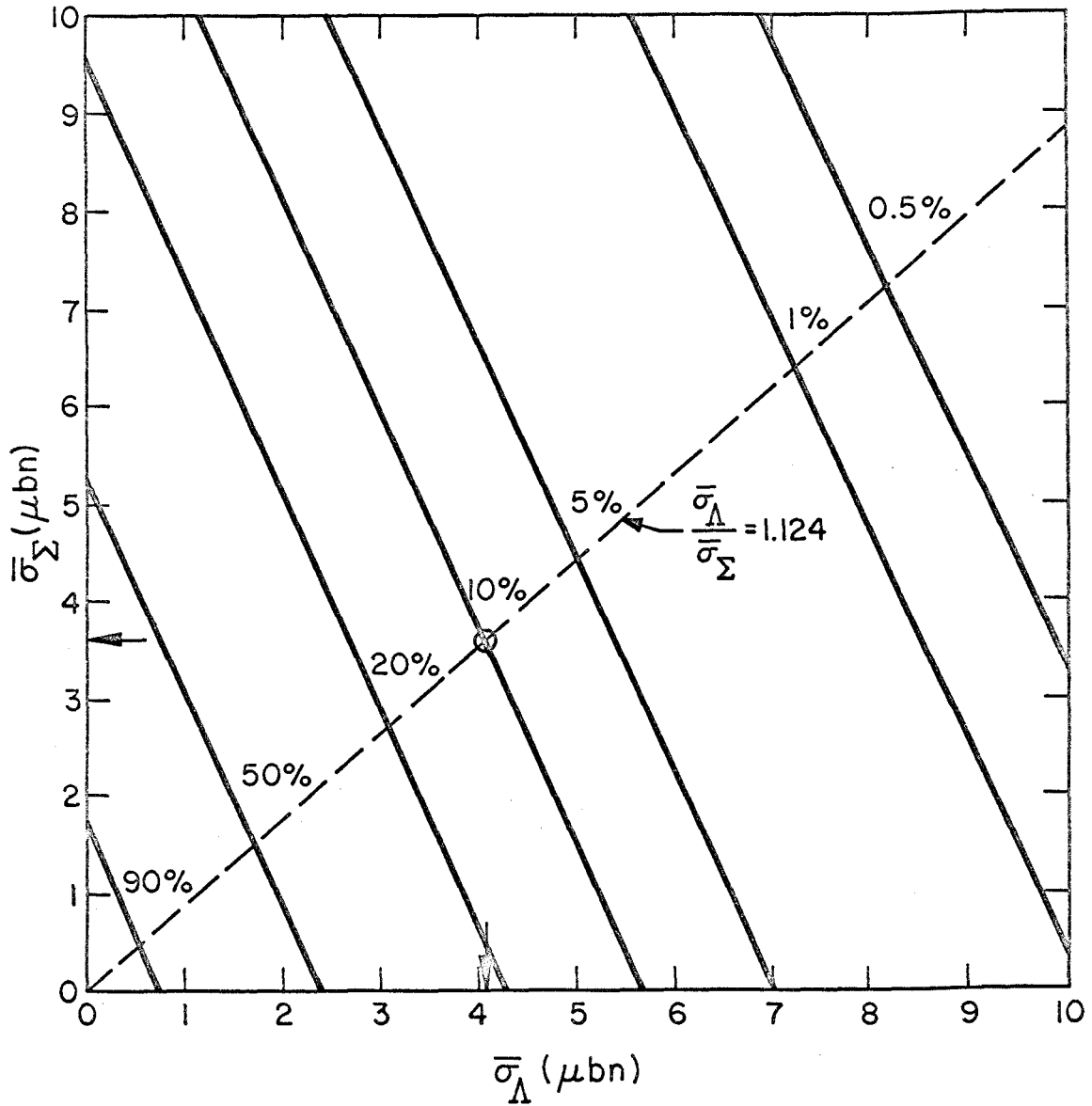
FIGURE 28: THE PROBABILITY THAT ONE EVENT OR LESS IS
SEEN IF TRUE CROSS SECTIONS ARE $\overline{\sigma}_\Lambda$ AND $\overline{\sigma}_\Sigma$

"confidence level" desired, we can pick the 10% probability level and state the resulting upper limits:

If $\bar{\sigma}_\Sigma = 0$ $\qquad$ $\bar{\sigma}_\Lambda \leq 3.34$ µb

If $\bar{\sigma}_\Lambda = 0$ $\qquad$ $\bar{\sigma}_\Sigma \leq 7.35$ µb

If $\bar{\sigma}_\Lambda/\bar{\sigma}_\Sigma = 1.124$ $\quad$ $\bar{\sigma}_\Lambda \leq 2.37$ µb, $\bar{\sigma}_\Sigma \leq 2.11$ µb .

3. Conclusions

The upper limits on $\bar{\sigma}_\Lambda$ and $\bar{\sigma}_\Sigma$ found in this experiment suggest that both the hypothesized values and the previous experimental values (from a subtraction) are high. This is the expected direction of error if the theories are simply balancing many big terms to fit the data. It is also the correct direction if the previous experiments did not have as clean background separation as hoped.

In particular, this result disagrees with the unbroken SU(3) prediction for dominanace of the third πN resonance, because if $K^o \Sigma^o$ and $K^o \Lambda^o$ are taken in the dictated proportions, we get for the ratios on page 11,

$$2 : 2 : .65 : 3 .$$

If these neutral cross sections are really this low, there is grave doubt as to whether it is wise to try to utilize them to accumulate the "clean" information on details of the KY system, as discussed in Part I. Only a radically different and superior technique will be able to gather significant amounts of data.

The Peck speculation[23] has thus been again confirmed.

APPENDIX I.

MONTE CARLO SIMULATION OF EVENTS AND CHAMBER

Many key factors of this experiment, such as the efficiency for seeing $K\Lambda$ and $K\Sigma$ events in our chamber, and the reliability of any analysis system acting on seen "events" are derivable in practice only by a detailed Monte Carlo calculation. By this we mean a step-wise generation of the events in which every physical alternative (decay modes, production angles, etc.) is picked randomly from its correct probability distribution. The chamber geometry is simulated by inequalities. A statistically significant sample of events is then generated, and any physical questions answered by simply tabulating the results.

A program for the IBM 7094 computer was written involving the steps A through M, shown in the block diagram in Figure 29. A brief description of the non-trivial aspects of this program follows:

A. The absolute count rate (all events generated) per picture is determined by the usual combination of factors.

$$N = W \cdot \rho \cdot \ell \int_{k_{min}}^{k_{max} = E_o} \frac{B(k, E_o)}{k} \sigma(k) \; d(\frac{k}{E_o})$$

W = total energy of photon beam/pulse

ρ = density of neutron target particles

ℓ = length of target
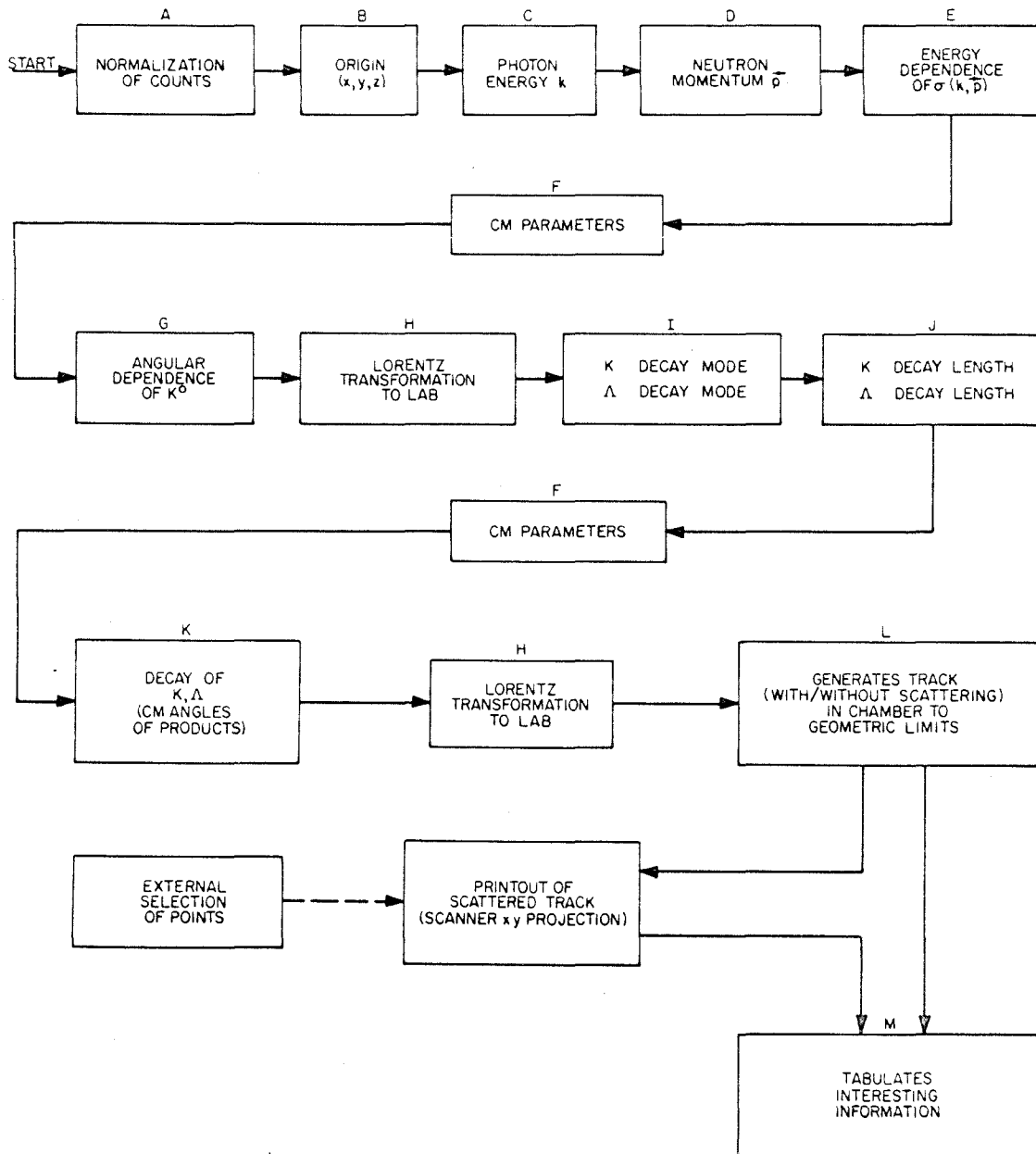
FIGURE 29: BLOCK DIAGRAM OF MONTE CARLO
EVENT SIMULATOR PROGRAM

$B(k)$ = bremsstrahlung distribution function

k = photon energy

$\sigma(k)$ = cross section

E_o = endpoint energy

This formulation does not include the slight change in N when the neutron Fermi momentum distribution is folded into the integral. The uncertainty in the energy dependence of $\sigma(k)$ is much greater than this correction arising from the dependence.

B. The primary interaction (origin) was selected randomly from a flat distribution over a cylinder centered on the known beamline. The diameter of the cylinder was .26 cm., determined from x-ray pictures, and the cylinder was truncated at one end by the entrance window to the target, and at the other by the exit point from the chamber.

C. The photon energy was selected randomly from a distribution $B(k)/k$, with $B(k)$ for our experimental aperture size and shape given by F. B. Wolverton's BPAK program[35]. The "unhardened" distribution which was used differs little in shape from the hardened one (see Figure 30) in the region of interest. The scale change due to hardening is accounted for in W. The distribution was truncated at the maximum γ-energy and also below 600 MeV for economy in generation. This lower limit excludes photons which could be effectively increased to the 915 MeV/c threshold if they met a neutron of Fermi momentum > 400 MeV/c
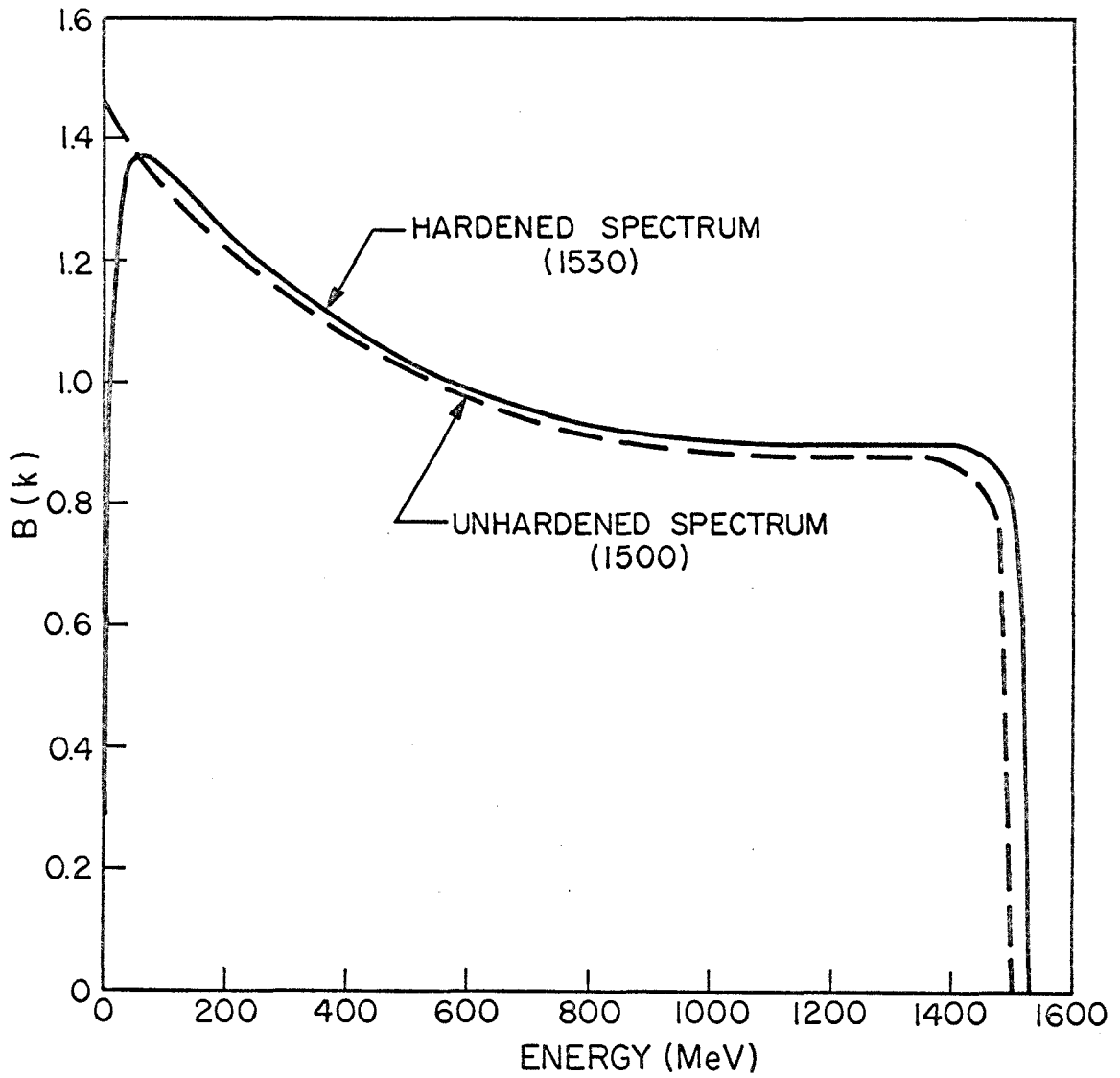
FIGURE 30: SPECTRAL DISTRIBUTION FUNCTIONS

head on. The number of such neutrons is negligible (see Figure 13).

D. The neutron Fermi motion was simulated by choosing the parameters p (momentum), θ (polar angle with beam line in forward direction as pole) and ϕ (azimuthal angle). While ϕ has a flat distribution, there is an enhancement in the number of interactions with large θ (neutrons are more likely to meet the photon head-on rather than tail-end). The resulting distribution is just

$$P(\beta, \theta) \quad = \quad \frac{1 - |\beta|\cos \theta}{2}$$

with β = velocity of neutron.[36] Since $\beta \approx 0.1$ for neutrons, this is a small change from isotropy. Then p was chosen from the distribution given by the momentum-space wave function for the neutron inside a deuteron. This is obtained by Fourier transforming the Hulthén s-state spacial wave function[37]

$$U_o(r) = \frac{A}{r} (e^{-\alpha r} - e^{-\beta r})$$

$$\alpha = .231 \cdot 10^{13} \; 1/cm$$

$$\beta = 1.41 \cdot 10^{13} \; 1/cm$$

The D-wave contribution (7%) does not alter the answer significantly, as is seen from comparison with the Gartenhaus formulation which includes both.[37] The transform is easily carried out as seen in the bracketed part following:

$$P(p_n)\, dp_n \propto p_n^2 \left[\iiint U_0(r)\, e^{-i\vec{p}_n \cdot \vec{r}/\hbar}\, d\vec{r} \right]^2 dp_n$$

a) $\quad P(p_n)\, dp_n \propto \dfrac{p_n^2\, dp_n}{(\alpha^2\hbar^2 + p_n^2)^2\, (\beta^2\hbar^2 + p_n^2)^2}$.

This can also be expressed (for later use) as

b) $\quad P(p_{n_x},\, p_{n_y},\, p_{n_z})\, dp_{n_x}\, dp_{n_y}\, dp_{n_z}$

$$\propto \frac{dp_{n_x}\, dp_{n_y}\, dp_{n_z}}{(\alpha^2\hbar^2 + p_{n_x}^2 + p_{n_y}^2 + p_{n_z}^2)^2\, (\beta^2\hbar^2 + p_{n_x}^2 + p_{n_y}^2 + p_{n_z}^2)^2}$$

where the apparent difference is because a) is being used as a one-dimensional distribution, and b) is for use as a three-dimensional distribution, and thus neglects the small θ dependence described above.

E. The energy dependence of the cross section was based on the estimates from Part I-2. The cross section is given as a function of total center-of-momentum energy, so the selection of events took place after choosing k, p_n, θ_n.

F, H. Center-of-mass parameters for each step of the generation, and Lorentz transformations are standard and will not be discussed.

G. The option of different angular distributions of the K^0 in $\gamma + n \rightarrow K^0 + Y^0$ was included (up to F-states). Since no

physical information is available on this distribution, and the theories are unreliable a priori, the distribution was taken to be isotropic.

I. The variety of decay modes

$$K^0 \nearrow K_S \nearrow \pi^0 + \pi^0 \\ \longrightarrow \pi^+ + \pi^- \\ \searrow \text{negligible 3-body}$$

$$\searrow K_L \longrightarrow \text{3-body} \\ \searrow \text{negligible 2-body}$$

$$\Lambda^0 \rightarrow \begin{array}{c} \pi^0 + n \\ \pi^- + p \end{array}$$
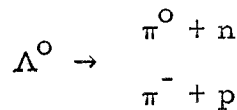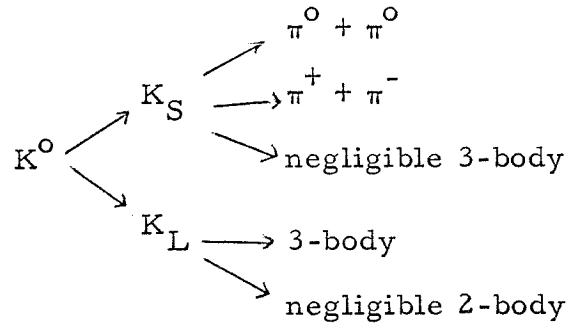
could be chosen in the correct experimental[38] proportions or the desired signature

$$K^0 \rightarrow K_S \rightarrow \pi^+ + \pi^-$$
$$\text{and } \Lambda^0 \rightarrow \pi^- + p$$
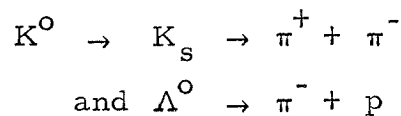
forced with corresponding correction in the count rates.

J. Decay lengths were found from the exponential distributions of the known[39] lifetimes of K_S and Λ, combined with the usual relativistic time dilitation appropriate in each case.

K. Decay angles of the π's and p in the K or Λ decay were taken to be isotropic in the center-of-momentum system. For the Λ this assumes no gross polarization as a result of the primary

reaction. Again, this had to be a starting point in the face of no experimental knowledge.

L. The parameters of the final state particles were then used to generate tracks in the simulated chamber. Included were the energy loss as the particle progressed through various media (D_2, steel, Freon) and detailed information of the visibility of the particle. No multiple Colomb scattering was included at this stage. The visible portion of the real chamber was checked by tests on fiducial lines, and two limits of visibility established: a " maximum" volume corresponding to what we really got as lighted volume from the tests, and a "fiducial" volume which was absolutely sure to be well lighted. These two diameters at beamline depth were 24 cm and 20 cm respectively. The real useable volume of the chamber is oddly shaped, and the numbers above are limits on its effective size. The best experimental figure (discussed later) came out between these two limits and an interpolation was used to get the efficiency.

For 2-vee events occuring in Freon, the multiple scattering of the final states, together with a dot-plot of the projected image as it would appear on the scanner, were included. This type of plot is shown on the following page. The persons doing measurement on real data could then select points on the Monte Carlo events in a manner which included the same human biases as on real data. This external human decision would then be linked into the computation and would influence the future results. The

multiple scattering is based on the double distribution in angle and
displacement given by Rossi[40].
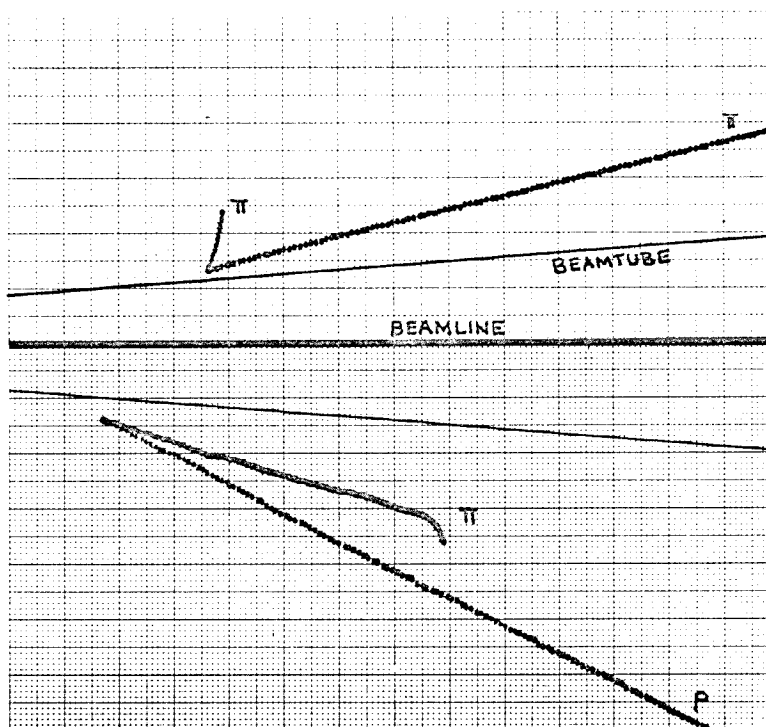
M. Tabulation of results of a long Monte Carlo run included every

reasonably interesting physical manifestation of a $K\Lambda$ event.

Absolute count rates per picture were then available. Finally,

the entire calculation was generalized to include the $K^0\Sigma^0$ mode,

with

$$\Sigma^0 \longrightarrow \Lambda^0 + \gamma$$
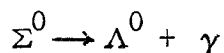
and with only the materialization point of the γ being randomly

chosen (no electron pair generation) from the distribution given

by Rossi for pair production [41].

Testing of this entire system was carried out in appalling, but necessary, proportions. Not only individual calculations were checked, but statistically significant distributions of every random choice made were compiled. The bewildering complexity of possibilities and the desire not to test with "special cases" made this necessary. Conversion of many of our personnel from scanners to fledgling mathematicians made the testing feasible.

APPENDIX II. ANALYSIS PROGRAMS

Data gathered in this experiment were analyzed two ways:
by an admittedly imperfect but trivial direct calculation, and by a
ponderous but reliable kinematic fitting program. These are de-
scribed below. (All events analyzed as KΛ.)

1. Direct Calculation :

If we are given the decay vertex of both K and Λ, plus one point
on the track of each π and p resulting from the decay, plus the
a priori knowledge of all masses and the beamline location, we
can determine the event uniquely except for input errors. Using
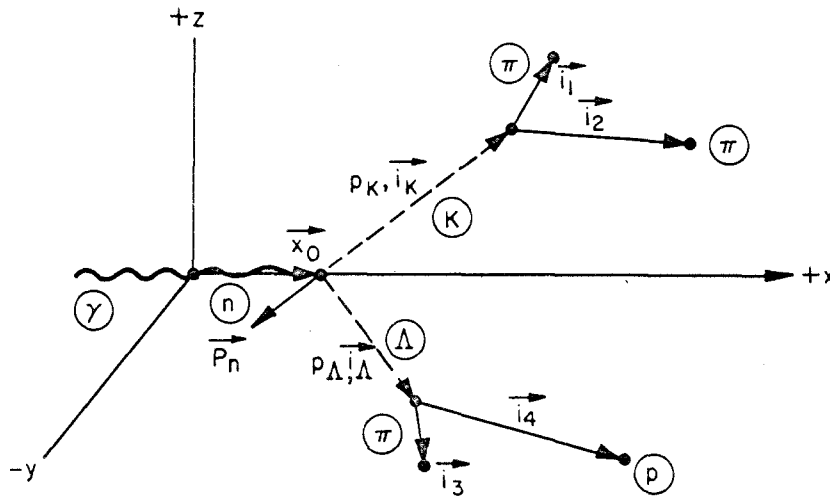
the notation defined by the drawing immediately above, we have
for each decay (for instance, K)

$$\vec{i}_{\perp K} \equiv U(\vec{i}_1 \times \vec{i}_2)$$

U means unitize this vector

p means momentum

$$i_{\perp \Lambda} \equiv U(\vec{i}_3 \times \vec{i}_4)$$

W means total energy

$$p_K = p_1 \vec{i}_1 \cdot \vec{i}_K + p_2 \vec{i}_2 \cdot \vec{i}_K$$

$$0 = p_1 (\vec{i}_{\perp K} \cdot \vec{i}_K \times \vec{i}_1) + p_2 (\vec{i}_{\perp K} \cdot \vec{i}_K \times \vec{i}_2)$$

$$W_K = W_1 + W_2$$

leading to a quadratic solution for p_K^2, only one root of which is positive. Since p_Λ may be similarly found, the equation

$$\vec{P}_n + \vec{P}_\gamma = p_\Lambda \vec{i}_\Lambda + p_K \vec{i}_K$$

$$W_n + p_\gamma = W_\Lambda + W_K$$

then determine the original 2-body reaction. Note that for all these equations, all $\vec{i}$'s are considered known. This means $\vec{i}_K$ and $\vec{i}_\Lambda$ must be found from the intersection of their decay planes with the (line) beamline. If the vertex of a decay is

$$\vec{v} \equiv (v_x, v_y, v_z)$$

and

$$\vec{i}_\perp \equiv (A, B, C) \quad ,$$

a short calculation gives the production point of the strange particle to be

$$x_o = V_x + \frac{B}{A} V_y + \frac{C}{A} V_x \quad ,$$

determining $\vec{i}_K$ or $\vec{i}_\Lambda$. These origins are not necessarily the same because of errors. The event is mathematically translated to make them coincide. At times the errors in the data make the calculation patently inconsistent, or it may be so when dealing with background data; at these times the candidates are flatly rejected. Inconsistency means that unphysical results, such as roots of negative numbers, or geometries leading to momentum-energy nonconservation, occurred. All candidates are analyzed with each particle successively being taken to be the proton, and the best result (closest to the physically possible region of γ-energy, neutron momentum, direction of neutron momentum) chosen. The results of this program operating on Monte Carlo events and real data are shown in Parts IV-2-B and V-I-A respectively, and demand the more exact treatment described in the next paragraphs.

2. <u>Kinematic Fitting</u>:

To include all available physical information in the analysis, and to have some figure of merit for the answers obtained, the method of maximum likelihood[33] was used. A set of independent variables {V} sufficient to predict any physical observable is chosen, and the probability function that a set of real data {D} would be obtained from a reaction with {V} is calculated. Actually, the problem at hand is the inverse: what is the probability of {V} given {D}? This, unfortunately, involves knowledge of the a <u>priori</u> probability of {V} as manifested by Bayes Theorem

$$P(\{V\}\mid \{D\}) \equiv P(\{V\} \text{ given } \{D\}) = P(\{D\} \text{ given } \{V\}) \cdot \frac{(\text{a priori})P(\{V\})}{(\text{a priori})P(\{D\})}$$

and is the ultimate limitation of the maximum likelihood method .

See Annis et al. for detailed study of this question[42]. In

practice, the right-hand side above is maximized with respect to $\{V\}$

with $P\{V\}$ taken constant by assumption when not known, and $P\{D\}$

legitimately taken constant. The correctness of such a step, if

$P\{V\}$ is unknown, can be justified only by checking the results of the

analysis where the right answers are available.

A. Choice of input data.

$\{D\}$ was taken to be the reconstructed x, y, z coordinates

of the points shown in the figure below; the rest of the points

on the track being used for other inputs (like range measurements).

X = REAL POINT (INCLUDING SCATTERING)
O = MEASURED POINT

SMALL NUMBERS ij REFER TO
REAL POINT Vij OR
MEASURED POINT Vij*
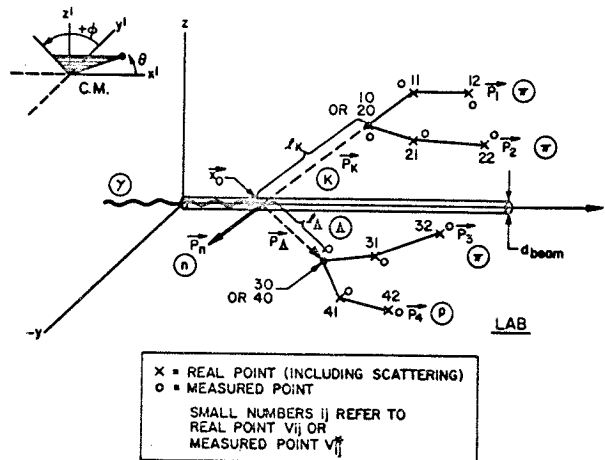
The vertices of the decay $\vec{v}_{10}^{*}$ and $\vec{v}_{30}^{*}$ are obvious choices.

Taking a single point out on each track would determine the

angle in space of the decay product, with an accuracy shown by the top curve in Figure 31. This curve was found using a simple 2-dimensional formulation (constant measurement error and Gaussian scattering as given by Rossi[40]). If too close to the vertex, measurement error ruins the angular accuracy; if too far, multiple scattering builds up and ruins it. The "best point" is expressible in terms of the scattering of the particular track (and for our system is when the deviation on the scanner from initial direction is .5 mm). If this best point is misestimated, the errors can be much worse. A formulation using two points bracketing the best point assuming they combine like independent measurements, gave the result, shown by the bottom curve in Figure 31, that this method was much less sensitive to errors in judgement by the person analyzing. This was the method then used in all data collection: the first point was 2/3 the optimum, the second, 4/3 the optimum.

B. Choice of independent variables:

It was desirable to create a system for $K\Lambda$ analysis only, postponing the $K\Sigma$ analysis until it was seen whether $K\Lambda$ analysis used on generated $K\Sigma$ events could separate them. This will be the only system described, since it was found that the reactions do not separate.

Many sets of independent variables are possible, but only one set had the property of no algebraic ambiguities (double-
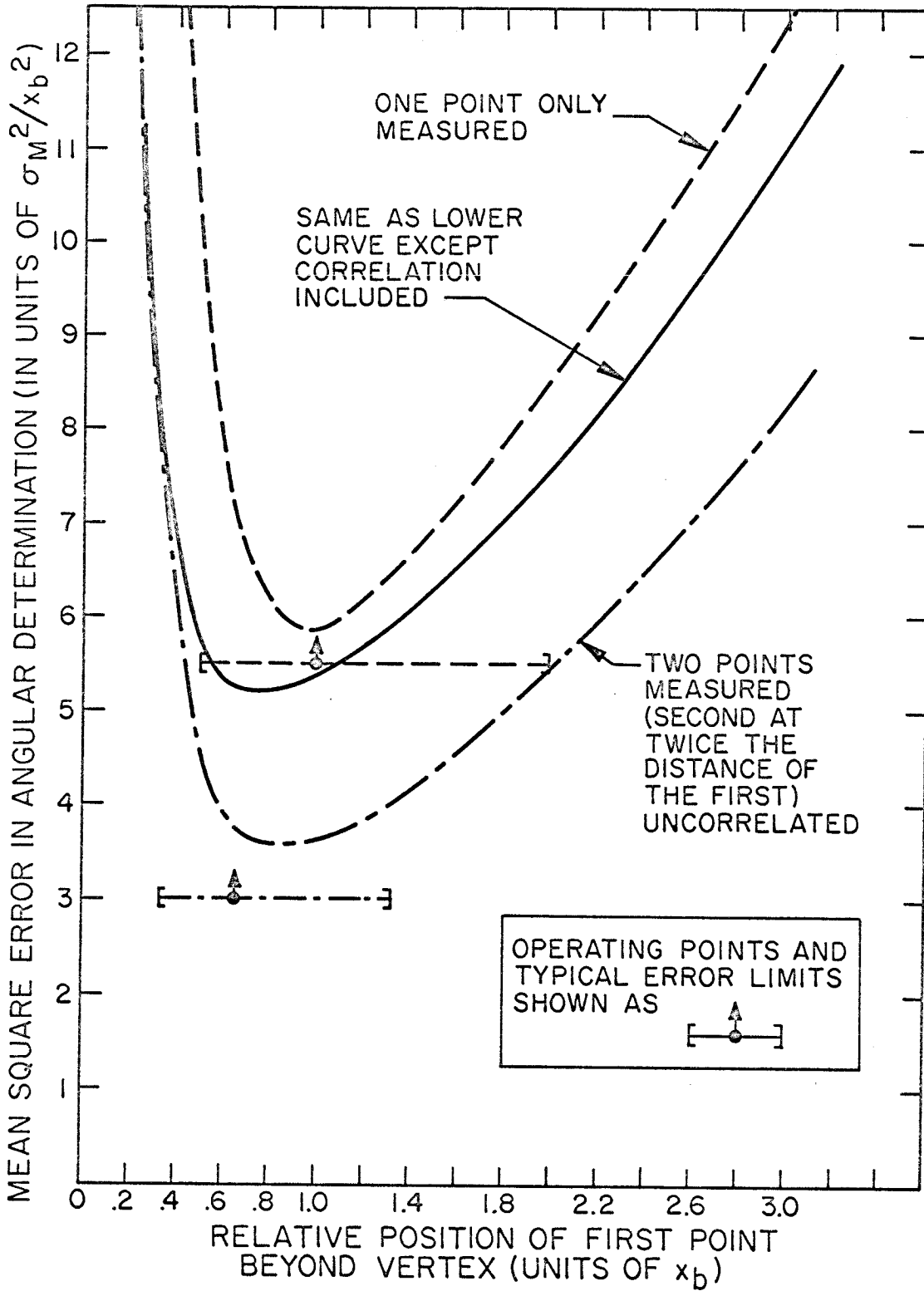
FIGURE 31: SENSITIVITY OF ANGULAR ERRORS TO MEASUREMENT SCHEME

valued results of calculations). This set is closely allied

to the set of probability distributions used in the Monte Carlo

simulation program. Referring to page 84, we have

$$\{V\}_{17} = \left\{ \vec{x}_o = (x_o, y_o, z_o), \text{ the primary interaction point} \right.$$

$\vec{p}_K$, the K momentum

$\vec{p}_n$, the n Fermi momentum

m_K, the K mass

m_Λ, the Λ mass

ℓ_K, the K origin-to-decay point length

ℓ_Λ, the Λ origin-to-decay point length

$(\theta_2, \phi_2)_c$, the polar and azimuthal angles of
decay particles 2 (pion) and 4 (pro-
$(\theta_4, \phi_4)_c$ ton) in the C. M. system of their
respective parents, with the $(xyz)_{C.M.}$
system aligned with the $(xyz)_{lab}$
system $\left. \vphantom{\int} \right\}$

The data is $\{D\} = \vec{v}_{ij}^*$, $i = 1, 4; j = 1, 2$

C. Formulation of probability element (exact):

We want

$$d^{17}D = P(\{V\} \mid \{D\}) \, d^{17} \{V\}$$

$$\propto P \{V\} P(\{D\} \mid \{V\})$$

The known parts of the a priori distribution of $\{V\}$ are the

beamlike constraint, the Fermi momentum of the neutron

constraint, and the constraint of any independent range energy or multiple scattering measurement made on a visible particle. We call these parts L_o, L_N, and L_i (for the ith particle) respectively.

$$L_o = \frac{1}{2\pi\sigma_b^2} \exp\left[-\left(\frac{(y_o - y_o^*)^2}{2\sigma_b^2} + \frac{(z - z_o^*)^2}{2\sigma_b^2}\right)\right]$$

$$L_N = \frac{A_o^2 \quad B_o^2}{\left[A_o + p_n^2\right]^2 \quad \left[B_o + p_n^2\right]^2}$$

$$L_i = f_n \frac{(\theta_s^2 - \theta_s^{2*})^2}{2\sigma_n^2} + \frac{f_s (\theta_s^2 - \theta_{so}^2)^2}{2\sigma_s^2}$$

with

σ_b = the beamline "width" as determined from x-ray pictures and the experiment of L. J. Fretwell.[30]

$y_o^* = z_o^* = 0$ The location of the beamline[30]

$A_o = .2077.10^4$ (MeV/c)^2 See Smythe[37]

$B_o = 7.74 \cdot 10^4$ (MeV/c)^2

f_n = 1 or 0 if an external multiple scattering measurement was or was not made.

f_s = 1 or 0 if the particle did or did not stop, giving a range energy measurement. (f_s was forced to 1 if the particle momentum was becoming less than that necessary to produce the seen length; this prevented an unreal condition).

$$\theta_s^2 = \frac{19.11}{p_i^4} (p_i^2 + m_i^2) \text{ the mean square angle of multiple}$$

scattering/unit length as given by Rossi[40].

θ_s^{2*}, σ_n the multiple scattering measurement of θ_s^2, and

its error.

$\theta_{s_o}^2$, σ_s the range-energy determination of θ_s^2, and its

error.

All other a priori constraints are so gross as to not warrant

inclusion.

Continuing with the rest of the probability element

$$P(\{D\} \mid \{V\}) = \int_{\vec{v}_{ij}} B(\vec{v}_{10}^* \cdots \vec{v}_{42}^* \mid \vec{v}_{10} \cdots \vec{v}_{42})$$

$$\cdot S'(\vec{v}_{10} \cdots \vec{v}_{42} \mid \{V\}) \, d\vec{v}_{10} \cdots d\vec{v}_{42}$$

where B and S' are probability functions and $\vec{v}_{ij}$ are the real

positions of the track as distinguished from the measured

positions $\vec{v}_{ij}^*$. Since the points $\vec{v}_{ij}^*$ are measured inde-

pendently,

$$B = \prod_{i,j} E_{ij}(\vec{v}_{ij}^* \mid \vec{v}_{ij})$$

where

$$E_{ij}(\vec{v}_{ij}^{\;*}\;\vec{v}_{ij}) = \frac{1}{(2\pi)^{3/2}\,\sigma_{x_{ij}}\,\sigma_{y_{ij}}\,\sigma_{z_{ij}}}\;\exp\;-\left[\sum_{x=x,y,z}\frac{(x_{ij}-x_{ij}^{*})^2}{2\sigma_{x_{ij}}^{\;2}}\right]$$

where $(\sigma_x,\,\sigma_y,\,\sigma_z)_{ij}$ are the measurement (and other) errors in the data points.

Now

$$S' = S_0(\vec{v}_{10},\,\vec{v}_{30}\,|\,\{V\})\cdot S(\genfrac{}{}{0pt}{}{\text{rest of}}{\vec{v}'s}\,|\,\{V\},\,\vec{v}_{10},\,\vec{v}_{30})$$

and

$$S_0 = S_{10}(\vec{v}_{10}\,|\,\{V\})\;S_{30}(\vec{v}_{30}\,|\,\{V\})$$

(the latter by virtue of $\vec{v}_{30}$ being determined by V independently from $\vec{v}_{10}$).

and

$$S = \prod_{i=1}^{4} S_i(\vec{v}_{i1}\,\vec{v}_{i2}\,|\,\{V\},\,\vec{v}_{10},\,\vec{v}_{30})$$

(for similar reasons)

(e.g., S_1 is the probability of getting to $\vec{v}_{i1}$ and $\vec{v}_{i2}$ when the particle starts from $\vec{v}_{10}$ with parameters $\{V\}$.) We can do the integrals over $\vec{v}_{10}$ and $\vec{v}_{30}$ easily because S_{10} and S_{30} are delta-functions:

$$S_{10} = \sigma(\vec{v}_{10} - \left[\vec{x}_0 + \vec{i}_K\,\ell_K\right])$$

$$S_{30} = \sigma(\vec{v}_{30} - \left[\vec{x}_0 + \vec{i}_\Lambda\,\ell_\Lambda\right])$$

where

$$\vec{i}_K = \vec{p}_K / p_K \qquad \vec{i}_\Lambda = \frac{\vec{p}_\Lambda(\{V\})}{p_\Lambda(\{V\})}$$

Defining

$$\vec{c}_K \equiv \vec{c}_1 \equiv \vec{c}_2 \equiv \vec{x}_o + \vec{i}_K \, \ell_K$$

$$\vec{c}_\Lambda \equiv \vec{c}_3 \equiv \vec{c}_4 \equiv \vec{x}_o + \vec{i}_\Lambda \, \ell_\Lambda$$

the integration yields

$$P(\{D\}\{V\}) = L_K \, L_\Lambda \, \prod_{i=1}^{4} \, H_i$$

where

$$L_K = \frac{1}{(2\pi)^{3/2} \, \sigma_{x_{10}} \, \sigma_{y_{10}} \, \sigma_{z_{10}}} \, \exp \, -\left[\sum_{x=x, y, z} \frac{(x_{10}^* - c_{K_x})^2}{2 \, \sigma_{x_{10}}^2} \right]$$

$$L_\Lambda \qquad \text{analogous with } 10 \ \rightarrow \ 30$$
$$K \ \rightarrow \ \Lambda$$

$$H_i = \int_{\vec{v}_{i1}} \int_{\vec{v}_{i2}} E_{i1}(\vec{v}_{i1}^* | \vec{v}_{i1}) \, E_{i2}(\vec{v}_{i2}^* | \vec{v}_{i2})$$

$$S_i(\vec{v}_{i1}, \vec{v}_{i2} \mid \{V\}, \vec{c}_K, \vec{c}_\Lambda) \, d\vec{v}_{i1} \, d\vec{v}_{i2}$$

Note the dependence of S_i on $\vec{c}_K$, $\vec{c}_\Lambda$.

D. Breakdown of "Exact" analysis:

At this point the "exact" calculation becomes unmanageable

in all respects: algebraic complication, cost of analysis,

and checkability. There are two main reasons for this:

(a) The proper multiple scattering functions S_i correlates

the points $\vec{v}_{i1}$ and $\vec{v}_{i2}$, leading to hard integrals.

(b) If the measurement errors σ_x, σ_y, σ_z are to reflect

real anisotropies in the chamber, then S_i must be formu-

lated in 3-dimensions and H_i then integrated. This

demands some length variables (analogous to ℓ_K, ℓ_Λ)

to be integrated over, and the algebra is impossible in

practice. If S_i is formulated in 2-dimensions, some

"effective" σ_x, σ_y must be used, and any tractable

method results in approximations.

After the creation of simple models to see if needful ap-

proximations let any physical content survive, the following

formulation was decided on.

(a) Break S_i into the product $S_{i1} S_{i2}$, where these are the

individual uncorrelated probabilities to multiple scatter

to points 1 and 2 on the track. Then by comparing the

middle curve of Figure 31 (giving the error in angle for

correlated points, as derived from an isotropic 2-di-

mensional model) with the bottom curve (uncorrelated error)

it is seen that we can roughly compensate for this

approximation by increasing the squared errors on

expected deviations of the points (from the initial direction) by a factor $F = 1.4$.

(b) Isotropize the measurement errors σ_x, σ_y, σ_z for a given point by taking

$$\sigma^2_{effective} = 1/3\,(\sigma_x^2 + \sigma_y^2 + \sigma_z^2)$$

In terms of Fretwell's chamber reconstruction program, we have for each point the two-dimensional error

$$\epsilon = \sqrt{(\delta^2 + \epsilon_{c_x}^2) + (\delta^2 + \epsilon_{c_y}^2)}$$

with δ the one-dimensional point measured error due to setting errors, ϵ_c the similar error due to reconstruction of the point.

$$\sigma_x = \sigma_y = \epsilon/\sqrt{2}$$

$$\sigma_z \approx 4\epsilon/\sqrt{2} \quad \text{(measured anisotropy in z-direction)}$$

giving

$$\sigma_{eff_{ij}} = \sqrt{3}\;\epsilon_{ij}\;.$$

Now we return to the integration of H_i.

E. Formulation of Approximate Probability Element:

We now have

$$H_i = \left[\int_{\vec{v}_{i1}} E_{i1}\,S_{i1}\,d\vec{v}_{i1}\right]\left[\int_{\vec{v}_{i2}} E_{i2}\,S_{i2}\,d\vec{v}_{i2}\right] \equiv H_{i1}\,H_{i2}$$

Using a coordinate system (x_{ij}, y_{ij}, z_{ij}) (Figure 32), with x_j along the initial direction of particle i, we have from Rossi[40]

$$S_{ij} = \left[\frac{\sqrt{3}}{\pi} \frac{1}{\theta_{s_i}^{3/2} \ell_{ij}^{3/2}} \exp - \frac{3 y_{ij}^2}{\theta_{s_i}^2 \ell_{ij}^3} \right] \left[\text{similar term in } z_{ij} \right]$$

Where ℓ_{ij} is approximated by $\vec{v}_{ij} - \vec{v}_{io}^*$

The appropriate error is

$$E_{ij} = \exp - \left[\frac{(y_{ij} - y_{ij}^*)}{2 \sigma_{eff_{ij}}^2} + \frac{(z_{ij} - z_{ij}^*)}{2 \sigma_{eff_{ij}}^2} \right]$$

Giving, in the system where $(xyz)_j$ is rotated to make $z_j^* = 0$,

$$H_{ij} = \frac{\exp - \left[\frac{y_{ij}^{*2}}{2F(\sigma_{eff}^2 + \sigma_{ms}^2)} \right]}{2 \pi F(\sigma_{eff_{ij}}^2 + \sigma_{ms_{ij}}^2)}$$

where $\sigma_{ms_{ij}}^2 = \frac{\theta_s^2}{3} \ell_{ij}^3$, and F has been introduced to compensate for the correlation of points.

Returning to a vector formulation,

$$y^{*2} = \ell_{ij}^2 \left[1 - \left(\frac{\vec{v}_{ij}^* - \vec{c}_{io}}{|\vec{v}_{ij}^* - \vec{c}_{io}|} \cdot \frac{\vec{p}_i}{p_i} \right)^2 \right]$$

with the same small angle approximation made in the multiple scattering formulation. The dot product, instead of being
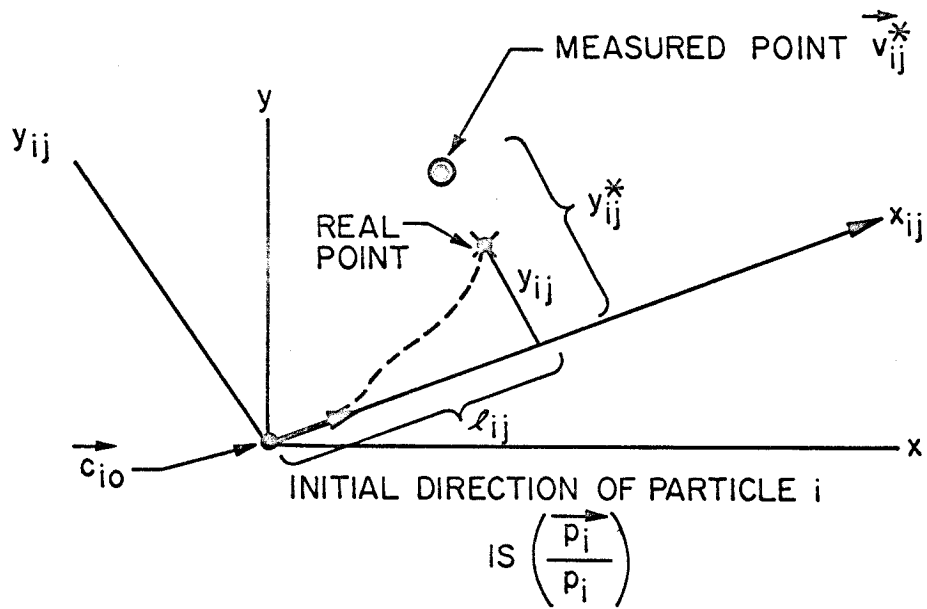
FIGURE 32: xy PROJECTION OF COORDINATE
SYSTEM FOR MULTIPLE SCATTERING

squared, is actually taken times its absolute value. This trick[30] avoids the possibility that $\vec{p}_i$ will be the negative of the correct value.

This completes the formulation of the probability element in terms of familiar variables of the problem.

$$d^{17}P = L_o L_N \left(\prod_{i=1}^{4} L_i \right) L_K L_\Lambda \underbrace{\prod_{\substack{i=1,4 \\ j=1,2}} H_{ij} d^{17} \{V\}}$$

Straightforward kinematics gives all dependent variables in terms of the independent set $\{V\}$:

$$(p_\Lambda)_y = (p_n - p_K)_y$$

$$(p_\Lambda)_z = (p_n - p_K)_z$$

$$(p_\Lambda)_x = \left[\frac{(p_\Lambda)_y^2 + (p_\Lambda)_z^2 + m_\Lambda^2 - K^2}{2K} \right]$$

$$K = \underbrace{\sqrt{m_n^2 + \vec{p}_n^2}}_{W_n} - \underbrace{\sqrt{m_K^2 + \vec{p}_K^2}}_{W_K} - (p_n)_x + (p_K)_x$$

$$\vec{p}_1 = \vec{p}_K - \vec{p}_2$$

$$\vec{p}_3 = \vec{p}_\Lambda - \vec{p}_4$$

$$\vec{P}_2 = \vec{P}_2' + \vec{P}_K \left\{ \frac{1}{2} + \frac{\vec{P}_K \cdot \vec{P}_2'}{m_K(W_K + m_K)} \right\}$$

$$\vec{P}_4 = \vec{P}_4' + \vec{P}_\Lambda \left\{ \frac{1}{2} - \frac{(m_\pi^2 - m_p^2)}{2m_\Lambda^2} + \frac{\vec{P}_\Lambda \cdot \vec{P}_4'}{m_\Lambda(W_\Lambda + m_\Lambda)} \right\}$$

$$\vec{P}_2' = P_{c_K}(\cos\theta_{2_c}, \sin\theta_{2_c}\cos\phi_{2_c}, \sin\phi_{2_c}\sin\phi_{2_c})$$

$$\vec{P}_4' = P_c(\cos\theta_{4_c}, \sin\theta_{4_c}\cos\phi_{4_c}, \sin\phi_{4_c}\sin\phi_{4_c})$$

$$P_{c_K} = \frac{1}{2}\sqrt{m_K^2 - 4m_\pi^2}$$

$$P_{c_\Lambda} = \frac{1}{2}\sqrt{m_\Lambda^2 - 2(m_\pi^2 + m_p^2) + \frac{(m_\pi^2 - m_p^2)^2}{m_\Lambda^2}}$$

F. Optimization of {V} :

If we choose $W \equiv -\ln L$, and if L is composed of Gaussian terms only, we are minimizing the well-known $\chi^2/2$. The final value of 2W should distribute itself as χ^2, and thus be a figure of merit for each candidate. For non-Gaussian terms such as L_n, and variable normalization "constants," the simple theory breaks down and no trivial distribution of χ^2 is available; recourse to the use of Monte Carlo events to check the distribution is then necessary.

The mean value of χ^2 for a given term is the number of constraints (N) that term contributes. The RMS devi-

ation of χ^2 from its mean is $\sqrt{2N}$. These facts were used to determine N exactly for all terms other than L_N. The improper normalization constants were taken to be slowly varying, and thus dropped from χ^2. A detailed calculation by A. T. Chen of the moments of the term L_N gave

$$\langle \chi^2 \rangle = 5.98 \implies N \cong 6 \text{ (if Gaussian } N = 3)$$

$$\Delta\chi^2_{RMS} = 4.44 \implies N \cong 10$$

showing the effects of a long non-Gaussian tail of the wave function. N was taken as 6, but somewhat more spreading in χ^2 would be expected than for this figure.

Term	N	
L_o	2	
L_N	6	
L_i	1	for each non-zero f_n, f_s
L_K	3	
L_Λ	3	
H_{ij}	2	each

The number of degrees of freedom for a fit is the number of constraints minus the number of parameters. Thus the maximum and minimum degrees of freedom (D.O.F.) would be

L_o	L_N	L_i	L_K	L_Λ	H_{ij}	D.O.F.
2	6	8	3	3	16	21
2	6	0	3	3	8	5

The typical number is like 14. (Note that if only one point
is measured on a short track, one H_{ij} disappears along with
2 constraints.)

G. Computer Utilization:

The foregoing analysis was programmed for the IBM 7094
computer, with the variable metric minimization routine[43]
MIN as its software core. The program MIN was both tested
to learn its pitfalls (literally) and revised to avoid them.
A clear understanding of its behavior on known 2-dimensional
terrain proved useful in 17-dimensions. In particular, it
was learned that the RMS errors derived by MIN tend to be
repeatable to only about 30% for this experiment.

Starting values for the set {V} were estimated from crude
scattering or good range energy measurements, simple
kinematics and approximate geometry as measured.
In practice, it was found necessary to run in the mode with
m_K and m_Λ assumed (add +2 to number of degrees of free-
dom), because background events would force m_K and m_Λ
into energy non-conserving regions that trapped the solution
immediately. The resulting 15 dimensional minimum-hunt

was given 250 steps in this space to converge, and usually did so in about 30 seconds of execution time.

Extensive testing of this program using Monte Carlo and human generated events completely confirmed its reliability. The most important of these tests are discussed in Section IV-2-C of this thesis.

APPENDIX III.   DETAILS OF QUANTITATIVE ANALYSIS

(CROSS SECTIONS)

1. Prediction of Total Counts

The chief theoretical unknowns in this problem are the cross

sections $\sigma(k)$ of $\gamma n \rightarrow K\Lambda$ and $\gamma n \rightarrow K\Sigma$ as functions of energy and

angle.   Using the functions as described in Part I-2 of this thesis,

and introducing scale factors f_Λ and f_Σ, we have for the total number

of real counts expected:

$$N = \int_t W(t)\, \rho_N(t) \int_{\epsilon_{threshold}}^{1.0} \frac{B_H(\epsilon, E_0')}{k}$$

$$\left[\int_\Lambda \left[\frac{\sigma_\Lambda(k)}{f_\Lambda} \right] C_\Lambda(k, \Lambda)\, A_\Lambda(k, \Lambda)\, S_\Lambda(t, k, \Lambda)\, P(\Lambda) d\Lambda \right.$$

$$\left. + \int \left[\frac{\sigma_\Sigma(k)}{f_\Sigma} \right] C_\Sigma(k, \Sigma)\, A_\Sigma(k, \Sigma)\, S_\Sigma(t, k, \Sigma)\, p(\Sigma)\, d\Sigma \right] d\epsilon\, dt$$

with subscripts Λ and Σ denoting those reactions, and

C = chamber efficiency for seeing event

A = net analysis efficiency

S = scanning efficiency

t = time (or picture number)

k = photon energy

E_0 = endpoint photon energy

ϵ = $k/E_0{}'$

ϵ_{thresh} = threshold ϵ for $K\Lambda$ production

Λ = all other parameters needed to uniquely specify

     a Λ-event

Σ = all other parameters for Σ-events

$W(t)$ = total beam energy through chamber/unit time

     (or pulse)

$\rho_N(t)$ = target density of neutrons

$B_H(\epsilon, E_0{}')$ = spectral distribution of photons for endpoint

     $E_0{}'$ = 1530 and beam "hardened" by lithium hydride.

The bulk of the work of integrating this expression is accomplished by running the Monte Carlo chamber simulator (Appendix I) until statistically sound values emerge. This simulator produces

$$I_\Lambda = \rho_{N_0} W_0 \int_\Lambda \int_{\epsilon_{thresh}}^1 \frac{B(\epsilon, E_0)}{k} \sigma_\Lambda(k) \; C_\Lambda(k, \Lambda) \; P(\Lambda) \; d\epsilon d\Lambda$$

where ρ_{N_0} = density at 30°C and 50 atm

    W_0 = $5 \cdot 10^8$ MeV/pulse

    E_0 = 1500 MeV

  $B(\epsilon, E_0)$ = unhardened spectral distribution function, and similarly gives I_Σ.

Using the discreet information available on beam monitoring and scanning efficiency, and the integral information I, we form the best

approximation to N,

$$N = \sum_{\substack{\text{monitor} \\ \text{points}}} \frac{\left[N_i W_i(t) \right]}{W_0} \left[\frac{\rho_N(t)}{\rho_{N_0}} \right] \left[S_0(t) \right]_i$$

(AIII-1)

$$\cdot \left[\frac{I_\Lambda}{f_\Lambda} \bar{S}_{s\Lambda} H_\Lambda \bar{A}_\Lambda + \frac{I_\Sigma}{f_\Sigma} \bar{S}_{s\Sigma} H_\Sigma \bar{A}_\Sigma \right]$$

where either we record these quantities in period i, or average over

all events (bar). We have broken S into $S_0(t) \bar{S}_{s\Lambda}$ for Λ and

$S_0(t) \bar{S}_{s\Sigma}$ for Σ, with the second factor representing the efficiency

loss because of very short tracks. Also included is the approximate

correction

$$H = \frac{\int_\epsilon \frac{B_H(\epsilon, E_0')}{k} \sigma(k) \, d\epsilon}{\int_\epsilon \frac{B(\epsilon, E_0)}{k} \sigma(k) \, d\epsilon}$$

representing a small change arising from differences in the experi-

mental and Monte Carlo photon distributions.

2. Numerical Evaluation

    The experiment coordinated data from 13,832 pictures, together

with beam monitoring information and the integral results from running

the Monte Carlo calculation on about 9000 $K\Lambda$ events and the same

number of $K\Sigma$ events. Sources of the numbers and errors are given

in the following paragraphs, and a summary of the numerics of

Eq. AIII-1 referred to is given in Table 4 .

A. $N_i W_i(t)$ is derived from the recorded ion chamber and scaler readings from the system described briefly in Part III-2. The numerous corrections for temperature, pressure, premature dump, counter saturation, accidentals, absorptions before monitoring have been ably described by Fretwell[30], and since the runs for this experiment and that were contiguous, the same corrections and calibrations are used. (Fretwell's F_6, the absorption in the polyethylene target, was a large correction. It was derived independently and checked within the theoretical uncertainty.) He gives

$$N_i W_i(t)/10^{10} = 4.225 \frac{T}{P} \frac{F/S_c \cdot I}{1 + .0036 \ F/S_c}$$

with error

$$E = \left[.001586 + \frac{1}{F} + \frac{1}{S_c} \right]^{1/2}$$

with T = absolute temperature at ion chamber ($^{\circ}$C)

P = pressure at ion chamber (mm Hg)

F = counts on fast scaler

S_c = counts on slow scaler

I = ion chamber integrated current.

B. The factor $\left(\frac{N^{(t)}}{N_0} \right)_i$ is just the relative density of neutrons, corrected for the gauge inaccuracies, temperature and pressure of the target. Target purity was found spectroscopically[44] to be 99.65%.

Table 4

NUMERICS OF AIII-1

Roll	Number of Pictures	Final Scan Efficiency	Effective Flux/Pulse (units of $5 \cdot 10^8$ MeV/pls)
71	500	.722	.989
71	860	.625	.989
71	1275	.625	.963
72	1310	.722	.913
72	821	.722	.857
72	500	.775	.857
70	1503	.722	1.066
70	497	.722	1.045
70	635	.609	1.045
56	1004	.609	1.085
56	271	.476	1.085
56	175	.476	1.115
56	49	.609	1.115
56	501	.476	1.115
56	634	.476	1.115
57	500	.829	1.049
57	438	.476	1.049
57	562	.547	1.049
57	52	.476	1.049
57	118	.422	1.049
57	146	.422	1.058
57	184	.336	1.058
57	636	.422	1.058
55	256	.564	1.172
55	90	.476	1.172
55	205	.476	1.210
55	369	.476	1.223

Using $\bar{S}_{s\Lambda} = .95 \pm .02$ $\bar{S}_{s\Sigma} = .90 \pm .06$

$H_\Lambda = 1.052$ $H_\Sigma = 1.076$

$I_\Lambda = .478 \pm .048$ $I_\Sigma = .214 \pm .024$

$\bar{A}_\Lambda = .876 \pm .036$ $\bar{A}_\Sigma = .824 \pm .071$

C. H_Λ and H_Σ were determined by numerical integration of the appropriate expressions, using for $B(k, E_0)$ and $B_H(k, E_0')$ the curves found from F. Wolverton's spectrum calculator BPAK (see Figure 30, page 74). The hardened spectrum was found (using BPAK) by Fretwell, aided by P. Nilsson and A. T. Chen. Errors in H are negligible.

D. The integrals I_Σ and I_Λ emerged from the generation of 18,000 events which were forced to have charged-mode decays (for economy). This non-randomness was corrected for using the following branching ratios[38]

$$\frac{K_S \to \pi^+ + \pi^-}{K_S \to \text{all}} = .70$$

$$\frac{\Lambda \to \pi^- + p}{\Lambda \to \text{all}} = .665.$$

Errors listed are due only to statistics of counting (700 events with desired signature are obtained) and not to any uncertainty in $\sigma(k)$ or $\sigma(\Theta)$. The natural question that arises here is the following: what is the sensitivity of the integrals I_Σ and I_Λ to the unknown energy and angle dependences? Since the portion of the CM sphere which is outside the beam tube includes $0.8 \le \cos \Theta_{CM} \le - 0.9$, the average differential cross section would have to be quite peaked to have much effect. For the energy dependence effect, a linear ramp having the same average cross section was tried, and the count rate increased by $\sim 10\%$. The shape dependence is thus not too severe.

E. The analysis efficiencies A_Λ and A_Σ combine the loss of events because of restrictions imposed at the scanning machine with the loss during the kinematic fitting process from Monte Carlo calculations. Note that A_Σ is less than A_Λ, but hardly differs within the statistical error. This reflects the fact that these Σ's, being analyzed as Λ events, are not separable within the accuracy of this experiment. The efficiencies listed are for the most stringent set of requirements for acceptance, as discussed in Part IV-2-C.

F. The time-independent portion of the scanning efficiency, $S_{s\Lambda}$ or $S_{s\Sigma}$, represents the complete cut-off of scanning efficiency because of short tracks. Whereas Fretwell[30] arrived at a cut-off in "seeability" at .4 cm., the short track in that case was relatively isolated, whereas for vees it will appear as a kink at the end of a much longer track. Also, we do not know the a priori distribution of lengths of our background tracks, as they approach zero; thus we cannot look for an experimental cut-off. The large percentage of very short (2-3 bubbles or less) "kinks" found implies they are not impossible. Most of the 700 Monte Carlo events mentioned in (E) were checked for tracks of length less than .1 cm in real space. It was found that this ruled out about 2.5% for Λ and 6% for Σ. However, projection of 140 of these 700 events onto graphs, so that the true visual aspect could be subjectively checked (Appendix I), resulted in a greater loss (based on the collective pessimistic opinion of the scanners). Measurements on these dubious events often resulted in correct analyses anyway, but to be conservative these

events were assigned 0% scanning efficiency and deleted <u>before</u> the

A_Λ and A_Σ were calculated. The final attenuations by $S_{s\Lambda}$ and $S_{s\Sigma}$

are thus greater than the computer values and of greater uncertainty.

G. The time-dependent (in theory) scanning efficiencies constitute

the greatest source of error in this experiment, true to bubble-

chamber form. The final results shown in the table are derived

using the treatment explained in detail in Section 3.

3. <u>Scanning Efficiencies</u>

This experiment is characterized by probable low scanning

efficiencies (difficult pictures), probable high correlations between

scanners (great variation in quality of signatures) and a low or

vanishing number of real events (small cross section). The usual scanning

experiment has almost diametrically opposite features; usually small

demands are made on the sophistication of a model to combine the

efficiencies. Below are discussed some of the approximate possible

approaches to the insoluble problem (strictly speaking), and the

numerics of their application to this experiment.

A. <u>Postulate:</u> One vee of an event is uncorrelated with the other vee

as far as scanning efficiency is concerned. Recall that in this

experiment scanners are asked to record all vees, singly or multiply.

Coupled with the fact that vees occur at a rate of ~4/picture,

eliminating any tendency to look harder for a second vee, only a

physical reason causing vees to occur in easily-seen pairs or difficult-

to-see pairs violates the above postulate. (If in reality, a hard-to-

see vee correlates with a hard-to-see mate, our efficiency under the above postulate will be underestimated, and if it correlates with an easy-to-see mate, our efficiency will be overestimated. A weaker postulate would be that such correlations occur and cancel.) This means that if we deal with the single vee efficiency E_S, then the desired efficiency is just E_S^2 with a _correlated_ relative error $\simeq 2 \cdot \Delta E_S / E_S$. This error is a deviation from the efficiency averaged over all events; the efficiencies for particular classes of events may have considerable spread about E_S^2. In the discussion below, "event" designates a single vee.

B. _Extrapolation Model._ We have available two scan comparison regions, in which 5 to 8 people covered the same film independently, compared to the 4 usually on a region. If we plot net number of events found vs. number of people covering the region, and extrapolate the curve to an upper limit, then this represents the total number of events that could be found in this region. There could exist an undetectable class of events with zero efficiency, and thus any result can be invalid. This method assumes that all such classes have been accounted for (such as $S_{s\Lambda}$ above) and that the extrapolation is not unwarranted. The figure below shows this extrapolation for our experiment and Table 5 shows the corresponding combination efficiencies attained by the same sets of people actually doing the rest of the scanning.

Table 5

Scanning Efficiencies in the Preferred Subset of Events

Combination of Scanners	Extrapolation Model Efficiencies (single v)	Pairwise Model Predicted Efficiencies and Errors (single v)	Corrected Extrapolation Model Efficiencies (single v)	Final 2-V Efficiency and Error *
ABCDH	.920	.856 ± .038	.88	.775 ± 6.6%
ABCD	.890	.830 ± .040	.85	.722 ± 7.4%
BDGH	.728	.756 ± .050	.69	.476 ± 10.6%
BDFH	.728	.695 ± .055	.69	.476 ± 10.6%
BDEH	.728	.683 ± .057	.69	.476 ± 10.6%
ABDH	.816	.804 ± .045	.78	.609 ± 9%
BCEH	.680	.688 ± .056	.65	.422 ± 11.4%
BE^{2}H	.612	.628 ± .061	.58	.336 ± 12.4%
ABD	.826	.811 ± .044	.79	.625 ± 8.8%
BCDH	.777	.720 ± .053	.74	.547 ± 9.8%
BCDEH	.786	.774 ± .047	.75	.564 ± 9.6%
ABCDEFGH	.970	.907 ± .031	.91	.829 ± 5.2%

* Error is statistical only; the approximately 10% systematic error in N_T^2 is added later.
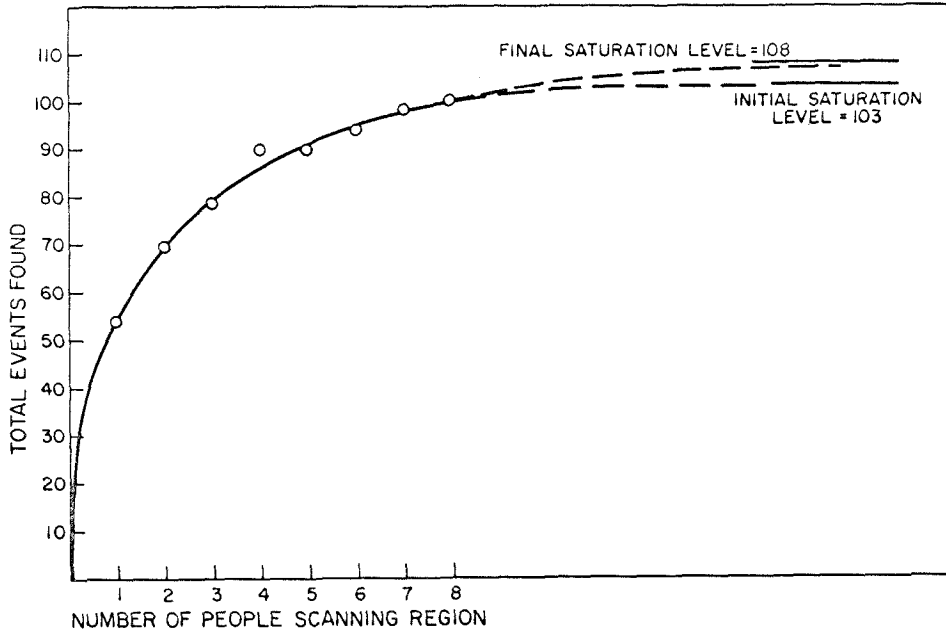
C. <u>Difficulties of rigorous model.</u> Suppose m scanners cover a region

of film with real average efficiencies e_i, i = 1, m, but find only N_F

of N_T events because of correlations[*]. The individual efficiencies

based on N_F we call E_i, i = 1, m. Experimentally we have these

E_i's, N_F, and all such conditional probabilities as

$P(A|B)$ (Probability that A finds the event given
                that B found it)

$P(A|BC)$

$P(A|BCD)$

Is this enough information to determine N_T, and thus e_i (or equi-

valently, to correct any combination efficiencies by N_F/N_T) ?

Irrespective of the algebraic complication (which itself would render

this scheme impractical), reflection shows infinitely many solutions

---

[*] "Correlations" may be taken to mean that the efficiency for one
class of events is appreciably different from the average effici-
ency over all classes.

exist to the above set of data.

For simplicity and eventual application, consider the combination of only two scanners (designated "1" and "2"). They will be ordered such that $e_1 \geq e_2$. In the limit of independent scanning, 2 will find a fraction e_2 of what 1 finds. The physical meaning of the opposite case, which we term "100% correlated scanning" is that while e_2 and e_1 may be different, the events 2 finds are a subset of those 1 finds. (See below.)
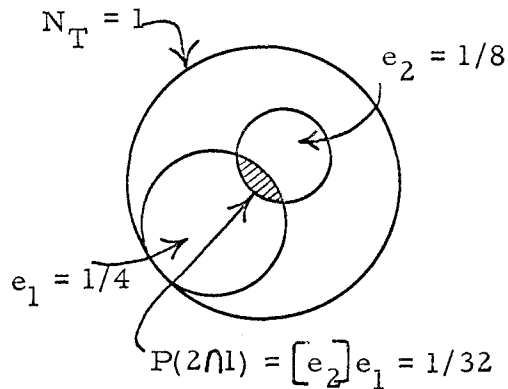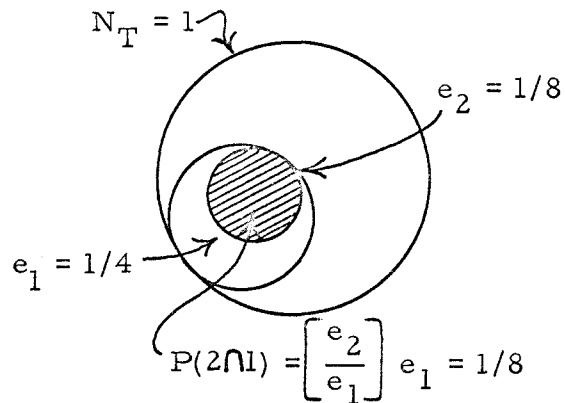
NO CORRELATION   COMPLETE CORRELATION

Keeping in mind that the efficiencies must be ordered as above, define an effective correlation C by

$$P(2\,|\,1) = \frac{e_2}{e_1} \, C + (1 - C) \, e_2 \qquad\qquad \text{(AIII-2)}$$

or

$$P(2 \cap 1) = P(2\,|\,1)\, P(1)$$

$$= e_2 C + (1 - C) \, e_2 e_1.$$

When C = 0 (no correlation) $P(2 \cap 1) = e_1 e_2$

C = 1 (100% correlation) $P(2 \cap 1) = e_2$,

the correct probabilities for those cases.

Since

$$N_F = 1 \cup 2 = 1 + 2 - 1 \cap 2$$

or

$$N_F = N_T(e_1 + e_2 - P(2 \cap 1))$$

we get

$$E_S = \frac{N_F}{N_T} = \underbrace{e_1 + e_2 - e_1 e_2}_{\substack{\text{uncorrelated} \\ \text{efficiency}}} + e_2 C(e_1 - 1)$$

If expressed in terms of the E's;

$$E_S = \frac{E_1 - 1 + E_2(1 - C)}{E_1 E_2(1 - C)} \quad .$$

A simple calculation shows that the measured $P(2|1)$ adds no new information to the problem because

$$P(2|1) = \frac{E_2 + E_1 - 1}{E_1} \quad .$$

Thus C is not determinable from $P(2|1)$ and E's (remember that e's are unknown). Thus no unique solution exists, although the E_S found above is correct.

The correlation of efficiencies can be made evident in spite of these quantitative troubles. If for a region with many scans, we

.take $e_i = E_i$, we can use AIII-2 to roughly determine C. If there are

unseen events, e_i must decrease and C increase, (for $P(2|1)$ experi-

mentally constant) as seen from the figure below. Thus a lower

bound on C is established. This experiment gives correlations ranging

from C = 0 to C = .8 on this basis.
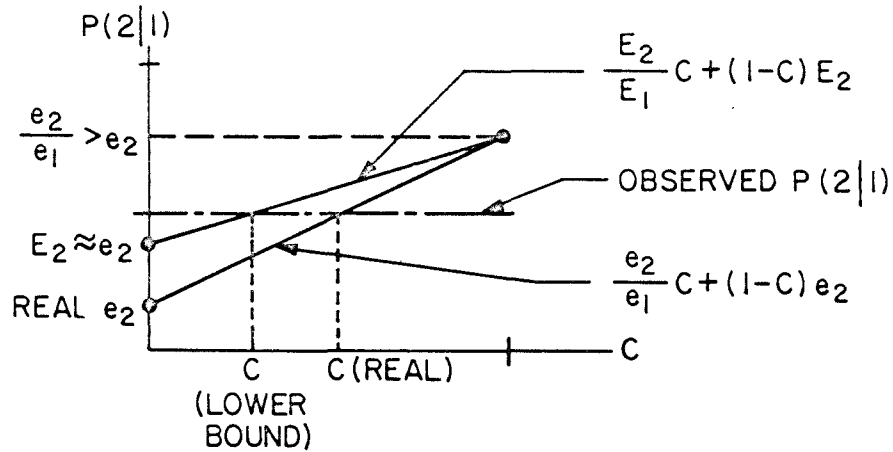
.D. <u>Pairwise Model.</u> If we use an approximate C, e and AIII-2 to

calculate E_S, such as just explained, we can then generate the

combination efficiencies by combining scanners pairwise, using the

experimental C appropriate to that combination. When combining a

pair with another pair, we can use the same formula, realizing that

this constitutes a model not necessarily real. The C used is the

average of the possible C's relating any two scanners in the group,

excluding those pairs already used. (See following.)

a) Form $1 \cup 2$

c) Form

$$1 \cup 2 \cup 3 \cup 4$$

using

$$\bar{C} = 1/4$$
$$(C_{13} + C_{14} + C_{23} + C_{24})$$

b) Form $3 \cup 4$
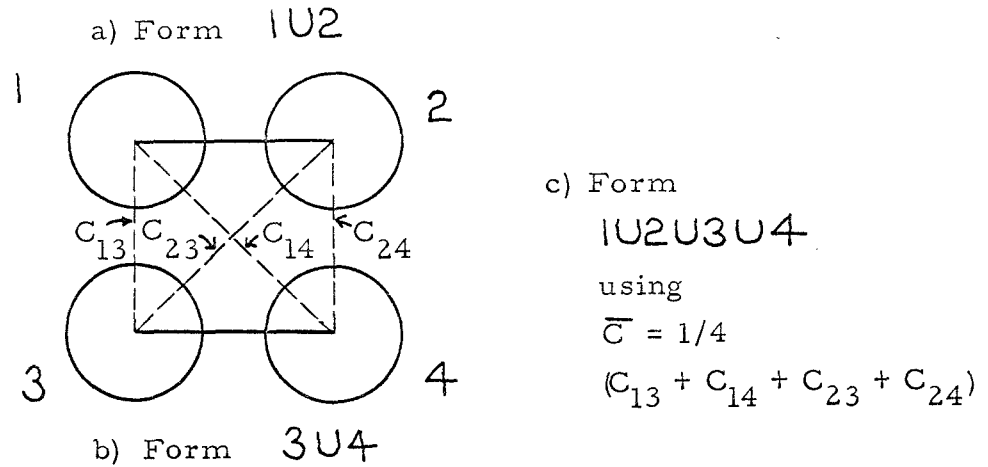
(It corresponds to deriving $P(1 \mid 2, 3)$ or $P(1 \mid 2, 3, 4)$ from lower terms like $P(1 \mid 2)$ etc.) The justification would be that if this could match the observed 4-combination of scanners, it might predict approximately how many events were not found after 8 scans, though clearly $P(1 \mid 2345678)$, etc., are to be reckoned with.

If the extrapolation model is applied first, then except for errors in the extrapolation and statistical error in the inputs, the starting point for the pairwise model should be almost correct. Thus it should return the results input to it, and predict the correct combination efficiencies in addition.

E. <u>Numerics of Scanning Efficiencies.</u> Data is available from two scan comparison regions ($\sim 3\%$ statistics) and a subset of one of these regions ($\sim 10\%$ statistics). The subset was generated by a 1:1 matching of the pictorial Monte Carlo events to the total pool of vees in one scanning region. The match was made with respect to lengths of tracks, positions of vertices, and opening angles. Data from this subset should more accurately represent the scanning efficiencies

and correlations for real vees. Individual efficiencies (E's) for single vees in this region ranged from 30% to 50%, figures similar to the range for the total region of preferred and non-preferred vees.

The scheme outlined in E was carried out on a good statistics region (but unrepresentative of real efficiencies). The following typical agreements were found:

Scanning Combinations	Predicted Efficiencies	Observed
BCDH	.822 ± .011	.818
ABD	.798 ± .012	.780
BEH	.757 ± .014	.742
BCEH	.793 ± .012	.790
ABDH	.820 ± .011	.814
BCE	.777 ± .013	.760
ABCDH	.857 ± .011	.876
BCDEH	.881 ± .010	.905

Continuing this process up to 8 scanners gave the result that the extrapolated number N_T was low by about 6%. Such a procedure carried out on the Monte Carlo-matched region has large uncertainties, but gave a systematic indication that the extrapolated value $N_F = 103$ was also too low. Replacement of this value by $N_F = 108 \pm 6$ then gave efficiencies deemed self-consistent with the calculated ones. The numerical results for all of these tests are shown in Table 5.

Plots were made of the time dependence of the individual

scanning rates, and except in one case they were time-independent to within these admittedly poor statistics. Therefore the most significant efficiency corrections were taken to be those of the representative subset; the poor statistics incurred are the cost of doing an experiment with no reasonable set of accepted events with which to check efficiencies.

The squares of these efficiencies, together with a correlated error equal to twice the original relative error, are the final efficiencies for two V's used in this experiment. (Table 5.)

4. Probabilistic Interpretation of Results

Using each $f = \bar{\sigma}_0/\bar{\sigma}$, where $\bar{\sigma}$ is the average cross section from threshold to endpoint energy, and $\bar{\sigma}_0$ represents the input value of $\bar{\sigma}$, we can arrange the numerics of 2. and 3. to give

$$N^* = 0.712\,\bar{\sigma}_\Lambda + 0.327\,\bar{\sigma}_\Sigma$$

with error

$$\sigma = \sqrt{1.466\,\bar{\sigma}_\Lambda^{\,2} + 0.415\,\bar{\sigma}_\Sigma^{\,2} + 0.878\,\bar{\sigma}_\Lambda\,\bar{\sigma}_\Sigma} \cdot 10^{-1}.$$

This includes values of $\bar{\sigma}_0$ found by analytic integration of the theoretical curves given in Part I-2.

$$\bar{\sigma}_{\Lambda_0} = 5.10\ \mu b \quad (.406\ \mu b/sr)$$

$$\bar{\sigma}_{\Sigma_0} = 4.55\ \mu b \quad (.364\ \mu b/sr).$$

If m events are found in an experiment, and $N^* \pm \sigma$ are expected, what is the probability

$$W(m \mid N^*(\bar{\sigma}_\Lambda, \bar{\sigma}_\Sigma), \ \sigma(\bar{\sigma}_\Lambda, \bar{\sigma}_\Sigma))$$

to have seen this number or less? If the expected number were exactly N, then the above probability would be

$$I(m \mid N) = \sum_{n=0}^{m} \frac{N^n e^{-N}}{n!},$$

the partial sum of the Poisson distribution. The probability that N is the true value if $N^* \pm \sigma$ is calculated will be approximated by

$$G(N \mid N^*, \sigma) = A \exp - \frac{(N - N^*)^2}{2\sigma^2} \quad N, N^* \geq 0.$$

This truncated Gaussian has

$$A = \frac{1}{\sqrt{2\pi} \ \sigma} \ \frac{2}{\left[1 + \mathrm{Erf}(N^*/\sqrt{2} \ \sigma) \right]} \ .$$

The answer is then given by

$$W(m \mid N^*, \sigma) = \int_0^\infty I(m \mid N) \ G(N \mid N^*, \sigma) \ dN.$$

This integral is carried out by completing the square, expanding the resulting binomial series, and relating term-by-term to the incomplete gamma function

$$\Gamma(a, x) = \int_x^\infty e^{-t} t^{a-1} \ dt.$$

One arrives at

$$W(m \mid N^*, \sigma) = \frac{A}{2} \sum_{n=0}^{m} \sum_{i=0}^{n} \binom{n}{i} \frac{B_n}{n!} (-b_0)^i \, \Gamma\left(\frac{n-i+1}{2}, \, b_0^2\right)$$

with

$$B_n = (\sqrt{2}\,\sigma)^{n+1} \exp -\left[N^* - \sigma^2/2\right]$$

$$b_0 = \frac{\sigma}{\sqrt{2}} \left(1 - \frac{N^*}{\sigma^2}\right).$$

This formidable formula is quite easy to use, since

$$\Gamma\left(\frac{1}{2}, \, b_0^2\right) = \sqrt{\pi} \, (1 - \mathrm{Erf}(b_0))$$

and

$$\Gamma(1, \, b_0^2) = \exp - b_0^2$$

and

$$\Gamma(a+1, \, b_0^2) = a \, \Gamma(a, b_0^2) + b_0^{2a} \exp - b_0^2 .$$

In particular, for m = 0

$$W(0 \mid N^*, \sigma) = \frac{1 + \mathrm{Erf}\left(\frac{N^*}{\sqrt{2}\,\sigma} - \frac{\sigma}{\sqrt{2}}\right)}{1 + \mathrm{Erf}\left(\frac{N^*}{\sqrt{2}\,\sigma}\right)} \exp -\left[N^* - \sigma^2/2\right]$$

(Note that as $\sigma \to 0$, $W \to \exp - N^*$ as it should.)

For m = 1,

$$
\begin{aligned}
W(1 \mid N^{*}, \sigma) = \Bigg\{ & \frac{1 + \mathrm{Erf}\left(\dfrac{N^{*}}{\sqrt{2}\,\sigma} - \dfrac{\sigma}{\sqrt{2}}\right)}{1 + \mathrm{Erf}\left(\dfrac{N^{*}}{\sqrt{2}\,\sigma}\right)} \left[1 + N^{*} - \sigma^{2}\right] \\
& + \frac{\sqrt{\dfrac{2}{\pi}}\,\sigma}{1 + \mathrm{Erf}\left(\dfrac{N^{*}}{\sqrt{2}\,\sigma}\right)} \exp - \left[\frac{\sigma^{2}}{2}\left(1 - \frac{N^{*}}{\sigma^{2}}\right)^{2}\right]\Bigg\} \exp - \left(N^{*} - \frac{\sigma^{2}}{2}\right)
\end{aligned}
$$

(Note that as $\sigma \to 0$, $W \to (1 + N^{*}) \exp - N^{*}$.)

This form of exhibiting the results (see contour map of W vs. $\bar{\sigma}_\Lambda$ vs. $\bar{\sigma}_\Sigma$ in Part V) has been chosen because, except for the truncated G, there are no ambiguities. The usual method of finding confidence levels for $\bar{\sigma}$ involves the ordinary problems of the probability distribution inversion discussed in Appendix II, and adds nothing to the result. It may be carried out by double integration of the individual Poisson terms with respect to $\bar{\sigma}_\Lambda$ and $\bar{\sigma}_\Sigma$.

Usually, experimenters let σ (the error in N^{*}) go to zero. The confidence level integrals are then trivial. Taking m = 0 for an example, this approximation breaks down badly if $\sigma/N^{*} \gtrsim .5$, where a stated "best upper limit" on the cross section will be low by $\geq 40\%$. For this experiment, where $\sigma/N^{*} \approx .17$, there is only a 4% change in the stated "best limit" caused by σ, but in the region of the predicted cross section, the probability curve with error σ folded in is 165% of

the one without, and in the region of very low probability (.1%) the same ratio is 1000%. (See Figure 33).
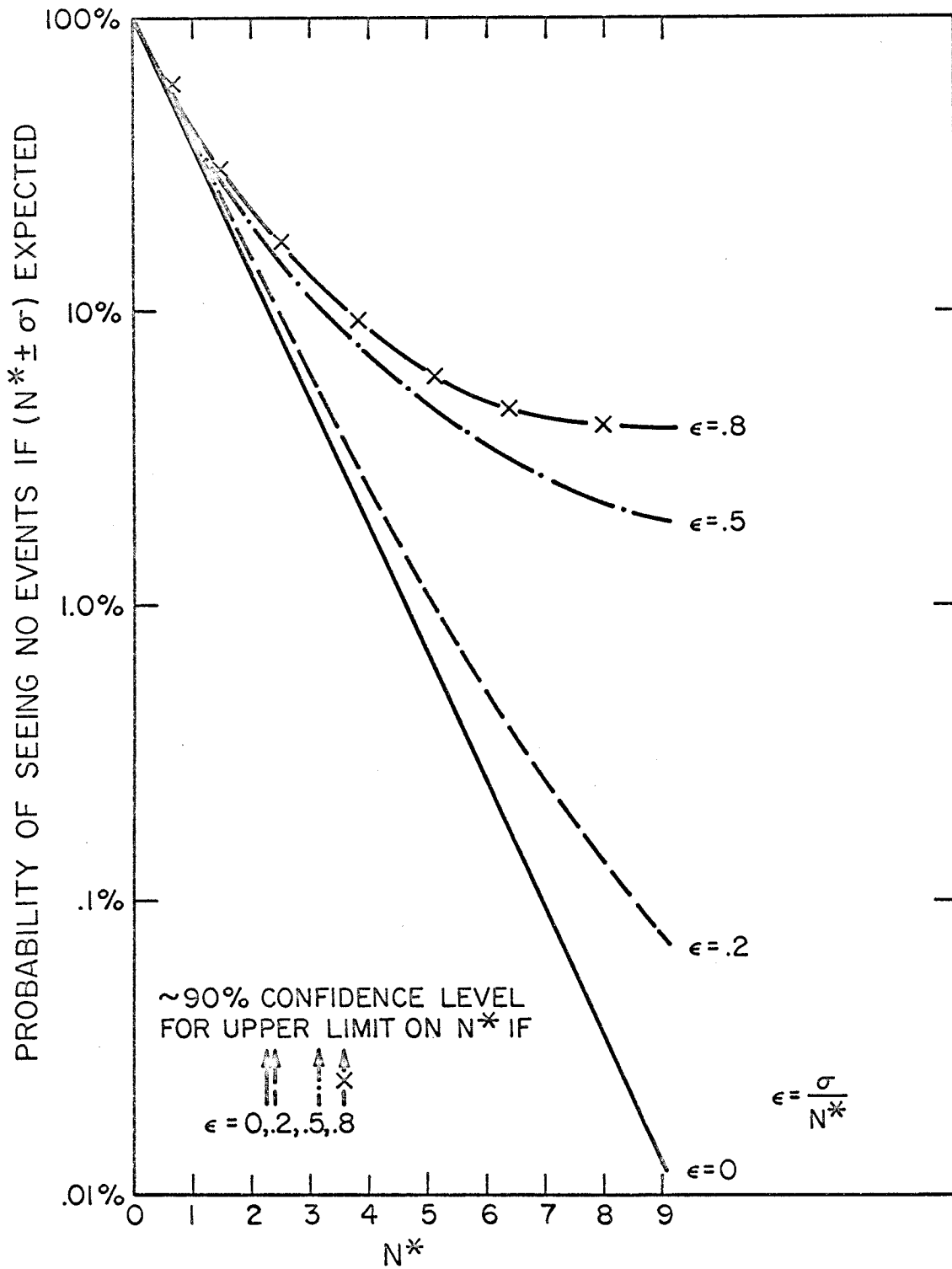
FIGURE 33: EFFECT OF EXPERIMENTAL ERROR ON PROBABALISTIC
INTERPRETATION OF EXPERIMENT

REFERENCES

1. M. Kawaguchi and M.J. Moravcsik, Phys. Rev. 107, 563 (1957).

2. R.H. Capps, Phys. Rev. 114, 920 (1959).

3. A. Fujii and R.E. Marshak, Phys. Rev. 107, 570 (1957).

4. L. Bertanza, P.L. Connolly, B.B. Culwick, F.R. Eisler,
    T. Morris, R. Palmer, A. Prodell, and N.P. Samios,
    Phys. Rev. Letters 8, 332 (1962).

5. P.L. Donoho and R.L. Walker, Phys. Rev. 112, 981 (1958);
    B.D. McDaniel, A. Silverman, R.R. Wilson, and
    G. Cortellessa, Phys. Rev. 115, 1039 (1959;
    H.M. Brody, A.M. Wetherell, and R.L. Walker, Phys. Rev.
    119, 1710 (1960).

6. R.L. Anderson, E. Gabathuler, D. Jones, B. McDaniel, and
    A.J. Sadoff, Phys. Rev. Letters 9, 131 (1962).

7. A.J. Sadoff, R.L. Anderson, E. Gabathuler, and D. Jones,
    Bull. Am. Phys. Soc. 9, 34 (1964).

8. H. Thom, E. Gabathuler, D. Jones, B.D. McDaniel, and
    W.M. Woodward, Phys. Rev. Letters 11, 433 (1963).

9. E.D. Alyea, Jr., Ph.D. Thesis, California Institute of
    Technology, 1962.

10. A.D. MacInturff and C.E. Roos, Phys. Rev. Letters 13, 246 (1964).

11. A. Kanazawa, Phys. Rev. 123, 993 (1961).

12. G.T. Hoff, Phys. Rev. Letters 12, 652 (1964).

13. Ye. V. Kuznetsov, Ya. Ya. Shalamov, A.F. Grashin, and
    Ye. D. Kuznetsov, Physics Letters 1, 314 (1962).

14. M. Rimpault, Thesis, Bordeaux (1962).

15. T.P. Wangler, A.R. Erwin, and W.D. Walker, Phys. Rev.
    137, B414 (1965).

16. R.K. Adair, Phys. Rev. 111, 632 (1958).

17. T.K. Kuo, Phys. Rev. $\underline{129}$, 2264 (1963).

18. N.A. Beauchamp and W.G. Holladay, Phys. Rev. $\underline{131}$, 2719 (1963).

19. S. Hatsukade and H.J. Schnitzer, Phys. Rev. $\underline{128}$, 468 (1962).

20. Fayyazuddin, Phys. Rev. $\underline{134}$, B182 (1964).

21. M. Gourdin and J. Dufour, Nuovo Cimento $\underline{27}$, 1410 (1963).

22. D.E. Groom, Ph.D. Thesis, California Institute of Technology, 1965.

23. C.W. Peck, Ph.D. Thesis, California Institute of Technology, 1964.

24. C.A. Levinson, H.J. Lipkin and S. Meshkov, Physics Letters $\underline{7}$, 81 (1963).

25. L. Holloway and A. Fujii, Nuovo Cimento $\underline{28}$, 1517 (1963).

26. K.C. Tripathy, Phys. Rev. $\underline{141}$, 1350 (1966).

27. J.H. Mullins, E.D. Alyea, Jr., and J.M. Teem, Proc. Conf. Instrumentation for High-Energy Physics at Berkeley, Interscience Pub. (New York, 1960) p. 106.

28. H.R. Crouch, Jr., et al. Phys. Rev. Letters $\underline{13}$, 636 and 640 (November 1964).

29. D.G. Coyne, Proposal for a Heavy Liquid Bubble Chamber Experiment; California Institute of Technology Synchrotron Laboratory, 1962 (unpublished).

30. L.J. Fretwell, Jr., Ph.D. Thesis, California Institute of Technology, 1967.

31. J.H. Mullins, Ph.D. Thesis, California Institute of Technology, 1959.

32. L.J. Fretwell, Jr., and R. Gomez, private communication.

33. J. Orear, UCRL-8417 (1958) (unpublished).

34. P.J.A. Nilsson, F. Beuger, P. Anderson, private communication. The use of multiple scattering measurements for momentum determination in a CF_3Br chamber will be described further in a CTSL internal report.

35. F. Wolverton, Manual for BPAK I, Thick Radiator
    Bremsstrahlung Computer Program, (unpublished).

36. W. R. Smythe, Ph. D. Thesis, California Institute of
    Technology, p 69, 1957.

37. op. cit., p. 67.

38. M. Chretien et al., Phys. Rev. 131, 2208 (1963).

39. F. S. Crawford, Proceedings of the 1962 International
    Conference on High-Energy Physics at CERN (CERN, Geneva,
    1962), p. 839.

40. B. Rossi, High-Energy Particles (Prentice-Hall, Inc., New
    York, 1952), p. 69.

41. op. cit., p. 79.

42. M. Annis, W. Cheston, and H. Primakoff, Rev. Mod. Phys.
    25, 818 (1953).

43. W. C. Davidon, ANL-5990 Rev. (1959) unpublished.

44. Mass Spectrometer Analysis by Petroleum Analytical Research
    Corporation, Houston (October 6, 1964).

45. M. Gell-Mann, Phys. Rev. 125, 1067 (1962).

46. R. F. Dashen, Y. Dothan, S. C. Frautschi, and D. H. Sharp,
    (to be published in Phys. Rev.) AEC Research and Development
    Report CALT-68-78. (1966).